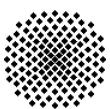


**Application of a new resonance  
formalism to Pressurized Water  
Reactors**

Philipp Oberle





## **Application of a new resonance formalism to Pressurized Water Reactors**

von der Fakultät Energie-, Verfahrens-  
und Biotechnik der Universität Stuttgart  
zur Erlangung der Würde eines  
Doktor-Ingenieurs (Dr.-Ing.)  
genehmigte Abhandlung

vorgelegt von

**Dipl.-Ing. Philipp Oberle**  
geboren in Singen a. H.

Hauptberichter:  
Prof. G. Lohnert, Ph.D.

Mitberichter:  
Prof. Dr.-Ing. V. Heinzl

Tag der mündlichen Prüfung: 02.03.2010





# Abstract

## Application of a new resonance formalism to Pressurized Water Reactors

In the presented study a new neutron scattering formalism is integrated into an established deterministic simulation system. With this energy- and temperature dependent scattering approach a more accurate form of the energy dependent neutron flux form can be determined. The neutron flux form is needed as weighting function for the calculation of effective multi group cross sections. The new scattering approach leads to an improved energy discretization in multi group calculations and therefore to more accurate results of nuclear reactor simulations.

The impact of the improved description of the scattering process is demonstrated in the results. The new model takes account for neutron up scattering. The up scattering and the energy dependent scattering kernels are causing changes in the neutron flux form in the energy region of resonances.

The validation of the implementation of the energy- and temperature dependent scattering approach into the KAPROS [16] fine flux module ULFISP [16] has been applied by pressurized water reactor pin cell comparison calculations with the existing solution of the Monte Carlo code MCNPX [58]. The used scattering model in MCNPX is based on an analog method. For both solutions absorption- and reactivity changes as well as changes of the safety relevant fuel Doppler coefficient are compared. Good agreement between both methods was observed

An additional new method which combines the standard and the new scattering model has been developed to analyze which specific isotopes lead to significant changes in the neutron flux form when the new approach is applied. For the most relevant isotopes an analysis of the reasons for their importance is included. A special significance was determined for the isotopes uranium-238 and oxygen-16.

The long term impact of the new scattering approach to the fuel inventory and for this reason to burnup dependent reactivity changes are shown by fuel pin cell and fuel assembly burnup calculations. The vectors of some important isotopes changed significantly during burnup. The application of the new scattering approach leads to a 1% higher fission material fuel inventory in a UO<sub>2</sub> pin cell burnup simulation at 80 MWd/kg HM burnup. The relevance of the new scattering approach for complete reactor core simulations is investigated for a UO<sub>2</sub>/MOX reactor core benchmark of the OECD/NEA. For this purpose a new interface module has been developed between KAPROS and the core simulator PARCS [36]. For the reactivity results compensating effects were observed while the absolute value of the safety relevant negative Doppler coefficient rises for 9 %.



# Kurzfassung

## Anwendung eines neuen Resonanzformalismus auf Druckwasserreaktoren

In der vorliegenden Arbeit wird ein neues Neutronenstreumodell in ein bestehendes neutronenphysikalisches deterministisches Simulationssystem integriert. Mit diesem energie- und temperaturabhängigen Streumodell kann eine genauere Form des energieabhängigen Neutronenflusses im epi-thermischen Resonanzbereich bestimmt werden. Die Neutronenflussform wird dann in der Berechnung der effektiven Wirkungsquerschnittsgruppenkonstanten als Wichtungsfunktion verwendet. Über die verbesserte Energiediskretisierung bei der Gruppenkonstantenberechnung führt das neue Streumodell zu genaueren Ergebnissen von Kernreaktor Simulationen.

Die Auswirkungen der genaueren Beschreibung des Streuprozesses werden anhand der Ergebnisse veranschaulicht. In dem neuen Modell wird die energetische Aufwärtsstreuung der Neutronen berücksichtigt. Diese Aufwärtsstreuung sorgt zusammen mit den energieabhängigen Streukernen für Änderungen der Neutronenflussform im Energiebereich der Resonanzen.

Zur Validierung der Implementierung des energie- und temperaturabhängigen Streumodells in das KAPROS [16] Feinflussmodul ULFISP [16] werden Vergleichsrechnungen mit der bestehenden Monte Carlo Lösung in MCNPX [58] anhand von Druckwasserreaktor-Einheitszellen durchgeführt. Das angewandte Streumodell in MCNPX beruht dabei auf einem analogen Verfahren. Anhand von Absorptions- und Reaktivitätsänderungen, sowie Änderungen des sicherheitsrelevanten Doppler Brennstoffreaktivitätskoeffizienten wurden die beiden Lösungsverfahren verglichen und eine gute Übereinstimmung zwischen beiden Verfahren festgestellt.

Durch eine weitere neuartige Methode, die das herkömmliche Modell mit dem neuen Streumodell Isotopenweise kombiniert, wird analysiert, welche Isotopen zu Änderungen in der Neutronenflussform durch die Anwendung des neuen Streumodells führen. Eine Ursachenuntersuchung für die sehr unterschiedlichen isotopenbedingten Änderungen ist für die wichtigsten Isotope enthalten. Eine besondere Bedeutung wurde hierbei für die Isotope Uran-238 und Sauerstoff-16 ermittelt.

Langzeiteinflüsse des neuen Streumodells auf das Brennstoffinventar und damit verbundene Änderungen der abbrandabhängigen Reaktivität werden an Brennstab- und Brennelementabbrandrechnungen dargestellt. Für einige Brennstoffisotope wurden hierbei bedeutende Änderungen beobachtet. So führt die Anwendung des verbesserten Streumodells für eine  $\text{UO}_2$ -Brennstababbrandsimulation (bis zu einem Abbrand von 80 MWd/kg SM), zu einem etwa 1% erhöhtem Spaltstoffanteil. Die Bedeutung des neuen Streumodells für Gesamtkernrechnungen wird am Beispiel eines  $\text{UO}_2/\text{MOX}$  Gesamtkern Benchmarks der OECD/NEA untersucht. Hierfür wurde ein neues Kopplungsmodul zwischen KAPROS und dem Kernsimulator PARCS [36] entwickelt. Bei den Reaktivitätsergebnissen zeigen sich kompensierende Effekte, während der Betrag des sicherheitsrelevanten negativen Dopplerkoeffizienten um 9% steigt.

# Table of Contents

<b>1</b>	<b><i>Introduction</i></b> .....	<b>1</b>
1.1	Nuclear reactor simulations .....	1
1.2	The new scattering formalism.....	3
1.3	Previous research .....	4
1.4	Approach and outline of the presented work .....	5
<b>2</b>	<b><i>Theory and codes</i></b> .....	<b>7</b>
2.1	<b>Group cross section calculation and resonance treatments</b> .....	<b>7</b>
2.1.1	Multigroup cross section calculation.....	7
2.1.2	Narrow-, wide- and intermediate resonance treatment .....	8
2.1.3	Nordheim integral method .....	9
2.1.4	The fine flux method .....	10
2.1.5	Derivation of the slowing down equation .....	10
2.2	<b>The energy- and temperature dependent scattering formalism</b> .....	<b>15</b>
2.2.1	The energy- and temperature dependent scattering kernel.....	15
2.2.2	Modification of the code DOUBLE2 .....	17
2.3	<b>Implementation of the energy- and temperature dependent scattering kernel...</b>	<b>18</b>
2.3.1	Modification of the KAPROS module ULFISP.....	18
2.3.2	Implementation of the single differential scattering kernel .....	19
2.3.3	The hybrid method .....	24
2.4	<b>Code descriptions</b> .....	<b>26</b>
2.4.1	The lattice code KARBUS and it's extended version KARBUSE .....	28
2.4.2	The fine flux module ULFISP.....	30
2.5	<b>The Monte Carlo method</b> .....	<b>35</b>
2.5.1	Some principal aspects of the Monte Carlo method .....	35
2.5.2	Different scattering treatments used in this work with MCNPX .....	36
<b>3</b>	<b><i>Pin Cell Application</i></b> .....	<b>38</b>
3.1	<b>Pin cell results</b> .....	<b>38</b>
3.1.1	Problem specifications .....	38
3.1.2	Fine flux calculation results .....	40
3.2	<b>First validation of ULFISP using MCNPX</b> .....	<b>44</b>
3.2.1	Scattering treatments in ULFISP and MCNPX.....	44
3.2.2	PWR pin cell calculations with ULFISP.....	46
3.2.3	Comparison calculations between ULFISP and MCNPX.....	48
3.3	<b>Pin cell burnup results</b> .....	<b>53</b>
	UO <sub>2</sub> pin cell burnup results .....	53
	MOX pin cell burnup results .....	55

<b>3.4 Sensitivity of specific isotopes to the new scattering formalism.....</b>	<b>58</b>
3.4.1 Validation of the hybrid method .....	58
3.4.2 Sensitivity of specific isotopes for UO <sub>2</sub> fuel.....	59
3.4.3 Sensitivity of specific isotopes for MOX fuel.....	61
<b>4 Fuel Assembly and Reactor Core Application.....</b>	<b>63</b>
<b>4.1 MOX/UO<sub>2</sub> core benchmark specifications.....</b>	<b>63</b>
<b>4.2 Fuel assembly burnup calculations.....</b>	<b>65</b>
4.2.1 Burnup step sensitivity study .....	65
4.2.2 Reactivity comparison between different fine flux options in ULFISP.....	68
4.2.3 UO <sub>2</sub> fuel assembly burnup results.....	69
4.2.4 MOX fuel assembly burnup results.....	71
<b>4.3 Reactor core calculations.....</b>	<b>73</b>
4.3.1 Comparison with benchmark participants at hot zero power .....	75
4.3.2 Hot full power.....	78
<b>5 Summary.....</b>	<b>80</b>
<b>References.....</b>	<b>83</b>

# Nomenclature

## Latin symbols

A	-	Mass number
C	-	Dancoff factor
E	eV	energy
F	1/cm <sup>3</sup>	collision density
HM	kg	heavy metal
k	eV/K	Boltzmann constant $k= 8.617343E-05$ eV/K
k <sub>eff</sub>	-	effective reactivity (system respects leakage)
k <sub>inf</sub>	-	reactivity for an infinite system
l	cm	length
m	kg	atomic mass
n	-	number of materials
M <sup>T</sup>	-	temperature dependent velocity spectrum
T	K	temperature
P <sub>e</sub>	-	neutron escape probability
P <sub>m</sub>	-	standardized neutron transfer probability
R	-	reaction rates
t	sec	time
u	-	lethargy
v	m/s	neutron velocity
w	m/s	target nucleus velocity
V	m <sup>3</sup>	volume
wt	kg	weight
XS	barn	cross section

## Greek symbols

$\alpha_T$	pcm/K	fuel Doppler reactivity coefficient
$\Delta$	-	difference
$\lambda$	-	ratio between microscopic elastic scattering and total cross section
$\Lambda$	-	ratio between macroscopic elastic scattering and total cross section
$\lambda_r$	-	resonance width describing parameter
$\mu$	-	cosine angle
$\nu$		number of neutrons per fission
$\Phi$	$1/\text{cm}^2$	neutron flux density
$\phi$		neutron flux
$\sigma$	barn	microscopic cross section
$\sigma_{\text{pot}}$	barn	potential cross section
$\Sigma$	$1/\text{cm}$	macroscopic cross section
$\nabla$	-	Nabla-operator
$\sigma_g$	barn	microscopic group cross section constant
$\Sigma_t$	$1/\text{cm}$	macroscopic group cross section constant
$\Gamma_p$	eV	practical resonance width
$\Omega$	-	angular direction

## Indices

a	absorption
b	bound
c	capture
F	fuel
M	moderator
pot	potential
e	elastic
t	total

## List of abbreviations

ARO	All Rods Out
BOL	Begin Of Life
BWR	Boiling Water Reactor
EOL	End Of Life
GRS	Gesellschaft für Anlagen- und Reaktorsicherheit = Society for Facility- and Reactorsafety
HFP	Hot Full Power
HTGR	High Temperature Gas cooled Reactor
HTR	High Temperature Reactor
HZP	Hot Zero Power
IFBA	Integral Fuel Burnable Absorber
LWR	Light Water Reactor
MOX	Mixed Oxide
NEA	Nuclear Energy Agency
NS&E	Nuclear Science and Engineering
OECD	Organization for Economic Co-operation and Development
PWR	Pressurized Water Reactor
UO <sub>2</sub>	Uranium-Dioxide
URR	Unresolved Resonance Region
RRR	Resolved Resonance Region
SSF	Self Shielding Factor
WABA	Wet Annular Burnable Absorber
XS	Neutron Cross Section

# 1 Introduction

## 1.1 Nuclear reactor simulations

The design of nuclear power reactors aims at two main objectives. First the safety requirements need to be obeyed and second the operation of the reactor should be as economic as possible. For several decades reactor design is supported by computer simulations. Like all computer simulations, nuclear reactor calculations can only be approximations of the reality. This fact is respected by safety margins in nuclear engineering as well as in all other engineering fields. Setting up these safety margins in nuclear reactor design is a very ambitious task which has to be guided by conservatism. Big efforts have always been undertaken to reduce uncertainties in nuclear application simulations and thereby to be able to increase safety and economic reliability at the same time. In the beginning of computational reactor simulation huge restrictions had to be accepted because of the relatively small computational power and memory. In return for the steadily increasing computing capabilities, nuclear reactor simulations could be improved permanently. Not only can the existing simulation approaches be executed more precisely, but simulations can also be expanded by new, more accurate but also more computational expensive physical modeling. This dissertation report deals with the implementation of a more accurate physical model into an existing nuclear reactor simulation system. This implementation will be described and the influence on both safety and economics will be investigated.

Nuclear simulations usually start from the Boltzmann Transport equation which is used to determine the distribution of neutrons of a system in space, angle, energy and time. To solve the transport equation in deterministic codes these variables have to be discretized which, of course, induces uncertainties to the results. This work examines the discretization of energy. Figure 1.1 shows the energy discretization of the total cross section of uranium-238. The red curve demonstrates a quasi continuous point wise illustration of the total cross section while the black step function represents 69 (WIMS-69 [3] energy group structure) discretized constants, so called “multigroup” constants, of the same uranium-238 total cross section.

The multigroup constants have to be calculated from their point wise representation by appropriate weighting. This means that inside one energy group every point value is connected to an importance. The importance is directly connected to the energetic neutron flux distribution of the investigated system and therefore strongly problem dependent. The basics for group constant calculation are summarized in chapter 2.1. Obviously an accurate multigroup constant calculation is much more difficult in the resolved resonance energy region (between 4 and 10000 eV in figure 1.1) than for example in the thermal energy region. Since the beginning of nuclear engineering in the 1940s numerous different physical models have been developed for best estimate weighting of resonance cross sections. Some of the most common ones are shortly introduced in chapter 2.1.

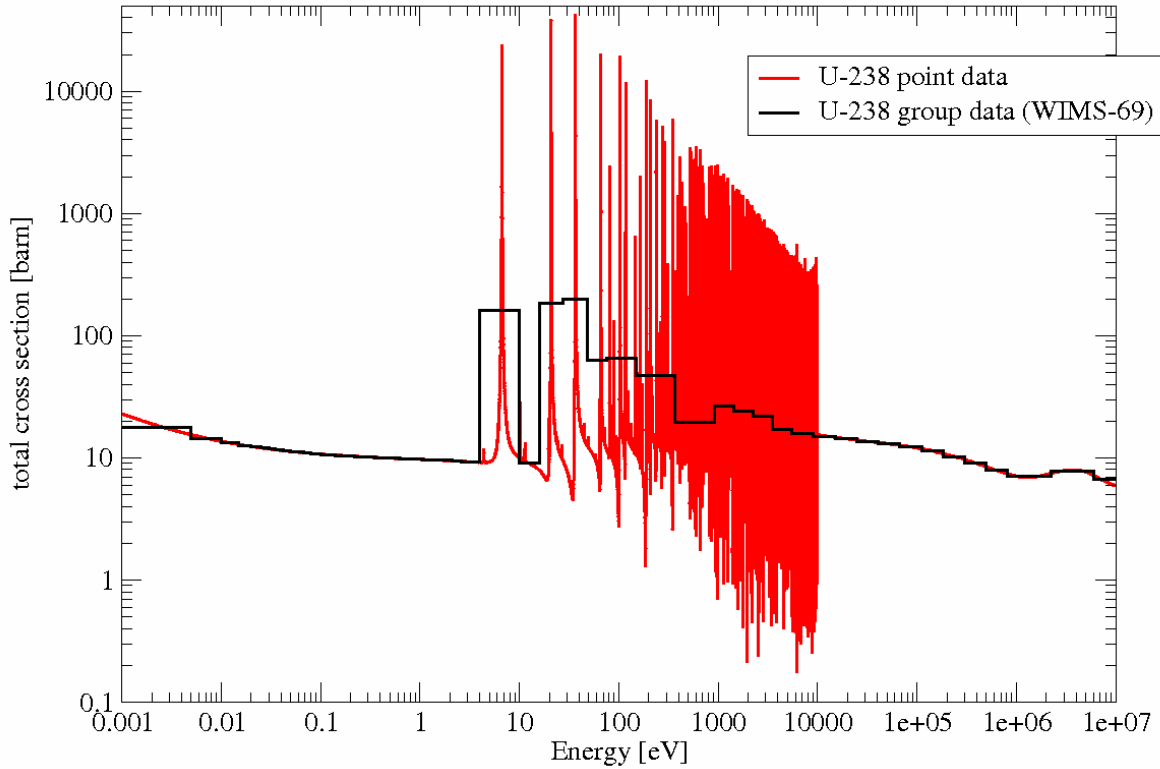


Figure 1.1.: Total cross section of U-238 in point wise and group wise (WIMS-69 group structure [3]) representation at temperature  $T = 0$  K

An accurate calculation of effective cross sections in the resonance region can be performed by the fine flux approach. In the fine flux approach a problem-specific neutron flux shape with an acceptable energy resolution is determined by solving the slowing down equation:

$$V^j \cdot \Sigma_t^j(E) \cdot \Phi(E) = \sum_{i=1}^k V^i \cdot P^{ij}(E) \int_{E'=E'_{\min}}^{E'_{\max}} \Sigma_s^i(E' \rightarrow E) \cdot \Phi^i(E') dE' \quad (1.1)$$

Equation (1.1) is derived in chapter 2.1 (equation (2.17)) from the Boltzmann transport equation and explained in detail. The left side of the equation describes the total number of neutron reactions in volume  $V^j$  at energy  $E$ . On the right side, the neutron transfer from all other volumes  $V^i$  to the investigated volume  $V^j$  of energy  $E$  and all neutrons which scatter from other energies  $E'$  to the considered energy  $E$  are counted. The calculation of the transfer probabilities from volumes  $V^i$  to volume  $V^j$  is described in detail in chapter 2.4. The determination of the neutron scattering from other energies  $E'$  to energy  $E$  depends on a specific scattering law. The major task of this study is the replacement of the standard scattering law, which is used widely in many deterministic code systems (e.g. KAPROS ULFISP [16], SCALE CENTRM [21]), by a more precise representation. The better description of the neutron flux shape in the resonance energy region will lead to more accurate effective multigroup cross sections and to more accurate integral results. The impact of these more precisely determined group cross sections on nuclear reactor simulations will be analyzed in chapter 3 and chapter 4.

## 1.2 The new scattering formalism

The standard and the more accurate scattering method are visualized in figure 1.2 by showing the corresponding scattering kernels. The kernels (blue and red curve) belong to the left linear ordinate (with normalized transfer probabilities  $P_m$ ) while the uranium-238 scattering cross section belongs to the right logarithmic ordinate. In figure 1.2 we assume that a neutron of energy  $E' = 36.4$  eV has an elastic scattering reaction with an uranium-238 nucleus of temperature  $T = 800$  K. The blue and the red scattering kernels represent probabilities to which energy  $E$  the neutron will be scattered. The blue curve stands for the asymptotic scattering kernel which offers the neutron the possibility to be scattered to energies between  $E = 35.8$  eV and  $E = 36.4$  eV. The probabilities to which specific energy a single neutron will be scattered are constant for all possible energies. Obviously a neutron can only be down-scattered with this scattering treatment. This means that the target nucleus does not perform any movement from thermal agitation. Although it has been implied that the uranium-238 nucleus is at temperature  $T = 800$  K, it will be handled by the asymptotic scattering treatment as being at rest or in other words as being at temperature  $T = 0$  K. Furthermore in the standard kernel the elastic scattering cross section  $\Sigma_s^i(E')$  is constant as well, which means that only the potential scattering cross section is taken into account and scattering resonances are neglected.

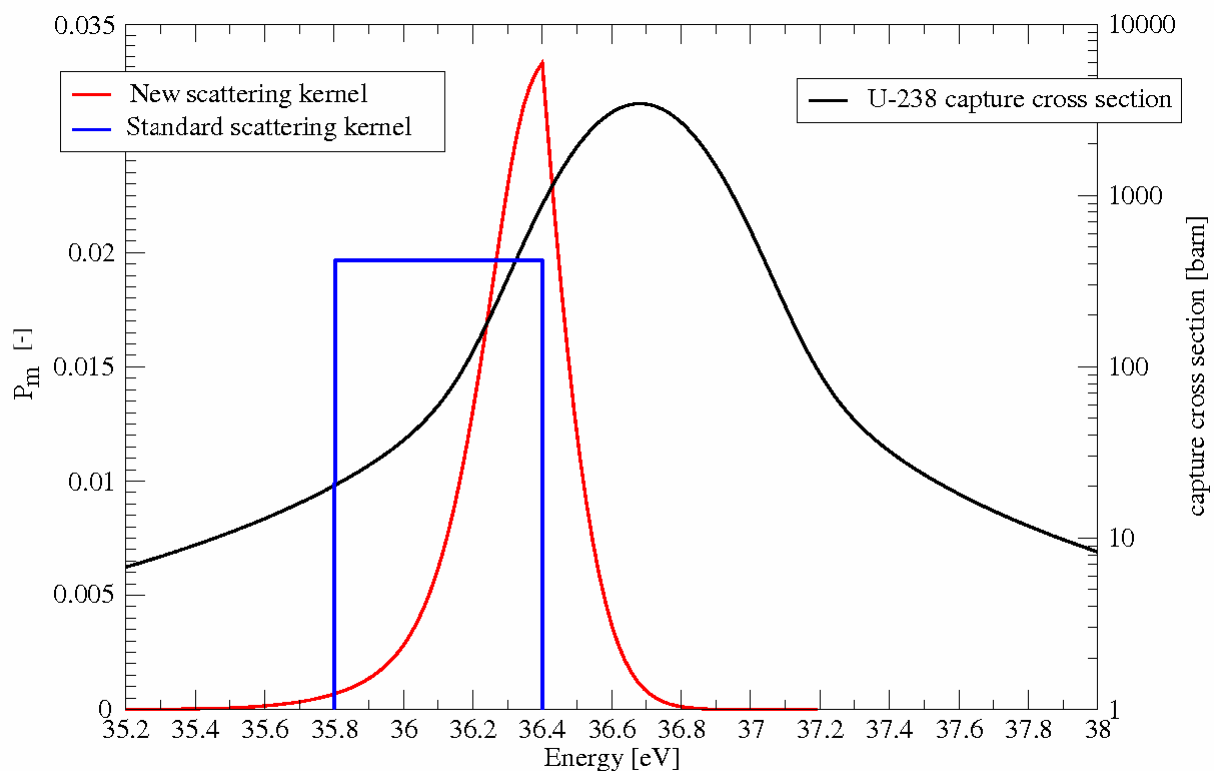


Figure 1.2: Scattering kernels for a neutron of  $E = 36.4$  eV having an elastic scattering reaction with a U-238 nucleus at  $T = 800$  K and the third large resonance of U-238 (black curve)

The red curve represents the new, so called single differential energy- and temperature dependent scattering kernel, which is explained in detail in chapter 2.2. In contrary to the double differential scattering kernel, the single differential scattering kernel neglects the information of any flight directions of the scattered neutron and takes into account only the

energetic changes. This scattering kernel respects the movement of the target nucleus which can lead to acceleration (up scattering) of the neutron in case of a scattering event. Moreover this model takes the energy dependence of the scattering cross section  $\Sigma_s^i(E')$  into account (cross section resonances are respected). The neutron energy  $E$  after scattering is not restricted to a certain energy region like in the asymptotic approach. Instead the neutron probability  $\Sigma_s^i(E' \rightarrow E)$  of being scattered to far energies is asymptotically approaching to infinite small values (compare with red curve in figure 1.2 at  $E > 37$  eV or  $E < 35.4$  eV).

The black curve in figure 1.2 shows the third s-wave resonance of uranium-238 which is characterized by a huge capture probability. For the scattered neutron at energy  $E = 36.4$  eV the energy- and temperature dependent scattering kernel offers a high probability (33.6 %) to be up scattered into the energy region where the resonance absorption is huge due to the resonance. This possibility is neglected by the asymptotic scattering approach. Therefore the new scattering treatment will lead to a higher absorption of neutrons in uranium-238 which will change the reactivity and, in long term observation, the inventory of a system. Moreover, it will be shown that the effect of the higher neutron absorption increases at higher temperatures which affects the fuel Doppler coefficient as well.

### 1.3 Previous research

In the past, several theoretical and practical developments and analysis have been investigated concerning the energy- and temperature dependent scattering treatment. Wigner and Wilkins [90] already used a two-body kinematics model for potential scattering and developed an isotropic temperature dependent scattering kernel. Brown and John [18] extended this approach by introducing energy dependent cross section by utilizing an exponential function for the scattering cross section of heavy water. Blackshaw and Murray [12] looked further on energy dependent cross sections for a Maxwellian monatomic gas. The single differential scattering kernel was first derived by Ouisloumen and Sanchez [69]. They developed an exact form of the single differential scattering cross section for elastic scattering in an isotropic media with a Maxwellian velocity distribution. Their theory is the basis for the practical implementation of the single differential energy- and temperature dependent scattering treatment into the fine flux code ULFISP which is performed in this work.

Dagan implemented the single differential scattering treatment into the fine flux code OZMA [70] in his thesis [27]. OZMA can be used for resonance integral analysis for different fine flux scattering treatments. The usage of the energy- and temperature dependent scattering treatment in OZMA is restricted to uranium-238 for specific energy groups in the epi-thermal energy region. Results of Dagan and Rothenstein [26] showed an increase of neutron absorption in the resonances of about 1% at  $T = 1200$  K for the pressurized water reactor (PWR)  $\text{UO}_2$  pin cell of Tellier [85] which contains pure uranium-238. The negative Doppler coefficient at this temperature was increased by 12%. Bouland, Kolesov and Rowlands [14] presented similar results with 1% increased resonance absorption in uranium-238 and a negative increased Doppler coefficient of 9% at light water reactor operating temperatures.

The double differential scattering treatment respects the energy distribution and the spatial direction of the scattered neutron. Rothenstein and Dagan developed [79] and implemented the double differential scattering treatment into the NJOY [54] system and introduced it through  $s(\alpha, \beta)$  tables [28] into the Monte Carlo code MCNP [57]. The impact of the double differential scattering kernel was determined by Dagan et al. [29] in 2007 to a negative increased Doppler coefficient of 13% for a typical light water reactor pin cell. In a burnup calculation at temperature  $T = 1200$  K they determined the increase of the plutonium-239 inventory to 2% at 50 MWd/kg HM. For a burnup simulation of a high temperature gas

cooled reactor (HTGR) pebble bed unit cell at temperature  $T= 1800$  K a plutonium-239 inventory increase of almost 5% at 60 MWd/kg HM was found.

With the Monte Carlo approach of Rothenstein and Dagan, Becker [5] recently investigated, for a pressurized water reactor assembly system at temperature  $T= 800$  K, a negative Doppler coefficient increase of 14%. At the end of cycle at 80 MWd/kg HM burnup he determined the increase of the simulated plutonium-239 inventory to 1.4 %. In a similar study for a high temperature reactor (HTR) unit cell [7], Becker investigated spectrum specific changes of the Doppler coefficients between 8.8% and 11%. In corresponding burnup calculations at temperature  $T= 1200$  K he achieved enrichment specific plutonium-239 inventory increases of 1.5% to 2.25% at 90 MWd/kg HM burnup.

Recently, Lee, Smith and Rhodes [52] implemented an exact form of the single differential scattering kernel into the Monte Carlo code MCSD [52]. MCSD solves the slowing down equation and is incorporated into the resonance treatment of CASMO-5 [76] which is used in their study to analyze the effects of various scattering kernels. For a pressurized water reactor  $UO_2$  pin cell from the Doppler benchmark of Mosteller [59], they investigated an increase of the negative fuel Doppler coefficient of 9-10%. The reactivity difference between the asymptotic and the single differential scattering kernel was determined to  $\Delta k = 211$  pcm at  $T= 900$  K.

## 1.4 Approach and outline of the presented work

The new development in this thesis is the implementation of the single differential scattering kernel into a deterministic code system which allows complete reactor core analysis. The new algorithm operates continuously in the epi-thermal energy region and can be used for an arbitrary number of fuel isotopes. The implementation is described in chapter 2.3. The implementation is based on Dagan's work for OZMA. However, the realization of the application is much more generalized. Detailed analysis for a pressurized water reactor pin cell is presented in chapter 3.1. A comparison with the Monte Carlo approach of Dagan and Rothenstein follows in chapter 3.2.

The absolute number of isotopes which can be covered by the new algorithm is only restricted by the available computer memory. In practice, burnup calculations have been performed utilizing the energy- and temperature dependent scattering kernel for 80 important fuel isotopes (actinides, fission products and oxygen). The results from these burnup calculations are summarized in chapter 3.3.

In order to reduce the requirements for computation power resources for many zones reactor core simulations, a modified algorithm allows the isotope-wise scattering treatment. This new procedure called "hybrid method" is explained in chapter 2.3 and validated in chapter 3.4. The hybrid method was applied for the analysis on the sensitivity of the energy- and temperature dependent scattering method on specific isotopes which is documented in chapter 3.4. Chapter 4 deals with the utilization of the algorithm for a PWR reactor core application. A well documented OECD/NEA benchmark [49] has been chosen to quantify the impact of the energy- and temperature dependent scattering treatment on a reactor core simulation. Chapter 4.1 introduces the benchmark. Chapter 4.2 presents fuel assembly burnup calculations for MOX and  $UO_2$  assemblies which include burnable poisons as well. Chapter 4.3 compares the reactor core results to results of other benchmark participants for hot zero power conditions. Simplified hot full power simulations conclude chapter 4.

Two major aims are followed up by this report. First is the confirmation of the fully functional new scattering approach in ULFISP. Second aim is to show the impact of the energy- and temperature dependent scattering treatment on reactivity, Doppler coefficient and

fuel inventory of pressurized water reactors at the different simulation scales pin cell, fuel assembly and reactor core.

## 2 Theory and codes

The energy- and temperature dependent scattering kernel will be transferred into reactor calculations via effective multi group cross sections. In this chapter first the basics for multigroup cross section calculation will be introduced. The new scattering kernel has its strongest influence in the region of resolved cross section resonances. It is implemented into a fine flux method which represents resonance cross sections most precise. Other commonly used resonance treatments are described briefly. The fine flux method relies on the slowing down equation which will be derived from the transport equation because of its high importance of being the starting position of this work. Further on the energy- and temperature dependent scattering kernel will be introduced by its basic equations.

The program DOUBLE3 which calculates single differential scattering kernels and its further developments from its predecessor DOUBLE2 [27] will be introduced. The implementation of the energy and temperature dependent scattering treatment into the fine flux module ULFISP which is the main objective of this work is specified. Chapter 2.4 describes the deterministic codes which play a major role in this work and explains the proceeding of deterministic reactor core calculations as applied in most industrial and scientific applications as well as in this work. The Monte Carlo application which is used for validation of the new ULFISP scattering approach in chapter 3.2 is introduced in chapter 2.5.

### 2.1 Group cross section calculation and resonance treatments

#### 2.1.1 Multigroup cross section calculation

For deterministic calculations the energy dependence of neutron cross sections has to be simplified to a certain number of discrete values, so called group constant cross sections. The main issue of group constant calculation is the conservation of reaction rates before and after discretization. In a region with volume  $V$  with a neutron flux  $\Phi(\vec{r}, E)$  and a neutron cross section  $\sigma_k(E)$  for a material  $k$  the reaction rate  $R_k$  is:

$$R_k = \int_V \int_E \sigma_k(E) \phi(\vec{r}, E) d\vec{r} dE \quad (2.1)$$

For the mean value  $\langle \sigma \rangle_g^k$  (group constant) of energy group  $g$ , equation (2.2) is valid per definition:

$$\langle \sigma \rangle_g^k \cdot \int_V \int_{E(g)} \phi(\vec{r}, E) d\vec{r} dE = \int_V \int_{E(g)} \sigma_k(E) \phi(\vec{r}, E) d\vec{r} dE \quad (2.2)$$

or

$$\langle \sigma \rangle_g^k = \frac{\int \int_{V E(g)} \sigma_k(E) \phi(\vec{r}, E) d\vec{r} dE}{\int \int_{V E(g)} \phi(\vec{r}, E) d\vec{r} dE} \quad (2.3)$$

For solving equation (2.3) the neutron flux  $\phi(\vec{r}, E)$  needs to be known. The problem is that the calculation of the flux is one of the final aims of a reactor calculation and it is unknown at the moment of group cross section calculation. So an approximation of the flux has to be done. Having a look at the total cross section of uranium-238 in figure 1.1, it is obvious that the resolved resonance energy region is quiet difficult to characterize mathematically compared to the thermal and fast energy region. Especially for this description of the resonance energy region several different approaches for providing weighting fluxes have been developed in nuclear reactor calculation history. Before looking at different resonance treatment methods we will separate the spatial and the energy flux dependence. Therefore we make the assumption of dividing the spatial and the energy flux dependence like in equation (2.4):

$$\phi(\vec{r}, E) = R(\vec{r}) \cdot \varphi(E) \quad (2.4)$$

Inserting equation (2.4) in (2.3) eliminates the spatial dependence and leads to:

$$\langle \sigma \rangle_g^k = \frac{\int \sigma_k(E) \varphi(E) dE}{\int_{E(g)} \varphi(E) dE} \quad (2.5)$$

For the weighting of the group cross section calculation only needed now is the weighting flux  $\varphi(E)$  which can be determined through various approximations. This energy dependent flux needs special treatments in the range of the complex structures of cross section resonances. Therefore in the following several common resonance treatments are introduced.

### 2.1.2 Narrow-, wide- and intermediate resonance treatment

The following short introduction to the narrow-, wide-, and intermediate resonance treatment is mainly taken from a nuclear science and engineering paper of R. Goldstein and E.R. Cohen [42] but can be found in numerous reactor theory literatures e.g. [9]. In the narrow resonance approximation, it is assumed that the resonance width is so narrow with respect to the average neutron energy loss per collision that a single collision allows a neutron to leave the resonance region. The other extreme is described by the wide resonance approximation, which assumes that the neutron needs a large number of collisions to cross the resonance energy region. The choice between these approximations can be made by the usage of the “practical width” first introduced by Wigner [89]. The practical width  $\Gamma_p$  [40] is the distance of the potential energies  $E_p$  left and right of the resonance peak (at energy  $E_r$ ), at which the microscopic resonance cross section is equal to the microscopic potential scattering cross section:

$$\Gamma_p = 2|E_p - E_r| \quad (2.6)$$

If the practical width is larger than the maximum energy loss on collision, the resonance is considered “wide”. If the practical width is small compared to the maximum energy change, the resonance is considered “narrow”. Because of this definition only for “extreme” resonances will the narrow resonance and the wide resonance approximations give accurate results. Goldstein and Cohen suggested the intermediate resonance treatment to solve this problem. They introduced a resonance dependent parameter  $\lambda_r$  with which the neutron flux in the resonance region can be represented as:

$$\varphi(E) = \frac{\sigma_0 + \lambda_r \cdot \sigma_{pot}}{\sigma_0 + \sigma_a(E) + \lambda_r \cdot \sigma_s(E)} \cdot \frac{1}{E} \quad (2.7)$$

with:

$\varphi(E)$	neutron flux density
$\sigma_0$	constant microscopic moderator cross section
$\sigma_{pot}$	constant microscopic potential cross section
$\sigma_a$	energy dependent microscopic absorption cross section
$\sigma_s$	energy dependent microscopic scattering cross section
$0 \leq \lambda_r \leq 1$	resonance dependent IR-parameter

For the limit value  $\lambda_r=1$  formula (2.7) provides the narrow resonance approximation, for  $\lambda_r=0$  it provides the wide resonance approximation. To use the intermediate resonance approximation correctly it is necessary to compute  $\lambda_r$  for every resonance of every isotope as e.g. applied in HELIOS [43]. This results in bigger administration work for complex problems. Instead of it is possible to calculate isotopic average parameters as used e.g. in WIMS/D [3].

### 2.1.3 Nordheim integral method

Another resonance treatment is the Nordheim integral method as developed by Nordheim [63]. As e.g. applied in the module NITAWL [61] of the SCALE [81] system, Nordheim's approach solves the integral equation via a direct numerical solution. A quasi fine flux is rebuild from resonance parameters like the resonance energy, the neutron-, gamma-, and fission width of the resonance [62] which have to be provided from cross section libraries. The neutron flux density can then be computed by equation (2.8) where the two integrals on the right side represents the source term due to scattering in the fuel and in the moderator. On the left side the flux multiplied the total macroscopic fuel cross section represents the total removal rate.  $\Sigma_t$  and  $\Sigma_s$  are the macroscopic total and scattering cross sections.

$$\varphi(E)\Sigma_t^F(E) = \frac{1}{\alpha^F} \int_E^{E/(1-\alpha^F)} \varphi(E')\Sigma_s^F(E') \frac{dE'}{E'} + \frac{1}{\alpha^M} \int_E^{E/(1-\alpha^M)} \varphi(E')\Sigma_s^M(E') \frac{dE'}{E'} \quad (2.8)$$

with

$$\alpha = \left( \frac{A-1}{A+1} \right)^2 \quad (2.9)$$

with mass number A of the target nucleus.

A complete description of this method can be found at reference Nordheim [62].

### 2.1.4 The fine flux method

The best way to describe neutron cross section resonances is via the fine flux method which is mainly used in this work. The basis of fine flux calculations is the “slowing down equation” which can be derived from the Boltzmann Transport equation. The slowing down equation will then be simplified for solving two-zone models, a precisely calculated fuel zone and an approximated moderator zone which includes the impact of cladding through a Dancoff-correction.

Similar to the quasi fine flux treatment of the nordheim integral method is the fine flux method as applied e.g. in ULFISP [16] or CENTRM [21]. In contrast to Nordheim’s method the cross sections in fine flux methods do not have to be reconstructed from resonance parameters but have to be available as point cross sections precalculated from raw ENDF-files [25]. These point cross sections represent especially the resonance region most precisely but require huge computer memory and computation time.

The fine flux method is used in this study for implementation of a new scattering treatment and is therefore presented in more detail here. The theoretical basis of the fine flux method is the slowing down equation which is a simplification of the Boltzmann-Transport equation. The slowing down equation is used for the calculation of the neutron spectrum in the epithermal resonance region. In the following its derivation is presented. During derivation following simplifications have to be done:

1. neutron sources from inelastic scattering, (n,xn)-processes, fission and external sources are neglected
2. up scattering is neglected (what is changed in this work)
3. anisotropic scattering is neglected

### 2.1.5 Derivation of the slowing down equation

The movement and energy change of neutrons can be described with the Boltzmann-Transport equation. For numerical solutions the Transport equation has to be discretized in time, space, angle and energy. The energy discretization has central relevance in this study. Therefore the slowing down equation which is used in fine flux methods for most precise energy discretization is derived from the Boltzmann-Transport equation in the following. Equation (2.10) shows a simplified linearized Boltzmann equation. The derivation is described in various literatures e.g. references [37] and [92].

$$\begin{aligned} & \frac{1}{v} \frac{\partial \Phi(E, r, \Omega, t)}{\partial t} + \Omega \nabla \Phi(E, r, \Omega, t) + \Sigma_t(E, r, \Omega, t) \Phi(E, r, \Omega, t) \\ & = \int_{\Omega'} \int_0^{\infty} \Sigma(E', \Omega' \rightarrow E; \Omega) \Phi(E', r, \Omega', t) d\Omega' dE' + S(E, r, \Omega, t) \end{aligned} \quad (2.10)$$

The slowing down equation is a special simplification of the Boltzmann transport equation. For our purpose we consider a stationary system:

$$\frac{\partial \Phi}{\partial t} = 0 \quad (2.11)$$

Furthermore, any other neutron source is neglected:

$$S(E, r, \Omega, t) = 0 \quad (2.12)$$

Anisotropy is neglected through integration over all directions  $\Omega$  as well,

$$\int_0^{2\pi} \Omega d\Omega = 1 \quad (2.13)$$

which leads to the slowing down equation (2.14):

$$\nabla \Phi(E, r) + \Sigma_t(E, r)\Phi(E, r) = \int_0^{\infty} \Sigma(E' \rightarrow E)\Phi(E', r)dE' \quad (2.14)$$

To simplify even further we create  $k$  homogeneous regions with volumes  $V^k$ , where the flux  $\Phi$  is constant:

$$\frac{\partial \Phi}{\partial r} = 0 \quad (2.15)$$

In region  $i$  the space dependence of the flux and the cross sections is eliminated via

$$\Phi^i(E) = \frac{1}{V^i} \int_{V^i} \Phi(r, E) dV \quad (2.16)$$

and

$$\Sigma^i(E) = \frac{1}{V^i} \int_{V^i} \Sigma(r, E) dV \quad (2.17)$$

This leads to equation (2.18) where on the right side the total number of reactions in region  $j$  is given as:

$$V^j \Sigma_t^j(E) \Phi(E) = \sum_{i=1}^k V^i P^{ij}(E) \int_{E'=E'_{\min}}^{E'_{\max}} \Sigma_s^i(E' \rightarrow E) \Phi^i(E') dE' \quad (2.18)$$

Where  $P^{ij}$  is the probability that a neutron born at energy  $E$ , through collision in region  $i$ , will undergo its the next collision in region  $j$ . The derivation of equation (2.19) is neglected here. It can be found e.g. in reference [92].

$$P_{ij}(\Phi_i, E) = \frac{\int_{V_i} \int_{V_j} \Phi(r', E) P(E; r' \rightarrow r) dr' dr}{\int_{V_i} \Phi(r', E) dr'} \quad (2.19)$$

In an infinite system for all  $i$ ,  $P^{ij}$  needs to be:

$$\sum_{i=1}^N P_{ij}(E) = 1 \quad (2.20)$$

For isotropic scattering in the center of mass system the simplified asymptotic scattering kernel is:

$$\Sigma_s^i(E' \rightarrow E) = \Sigma_s^i(E') \frac{1}{(1-\alpha)E'} \quad (2.21)$$

with

$$\alpha = \left( \frac{A-1}{A+1} \right)^2 \quad (2.22)$$

where  $A$  is the mass number of the target nucleus.

With this scattering law  $E'_{\min}$  in equation (2.21) becomes  $E'_{\min} = E$  and  $E'_{\max}$  becomes  $E'_{\max} = E/\alpha$ . For  $n^i$  materials of zone  $i$ , equation (2.23) is valid:

$$V^j \cdot \Sigma_t^j(E) \cdot \Phi(E) = \sum_{i=1}^k V^i \cdot P^{ij}(E) \int_{E'=E}^{E/\alpha} \Sigma_s^i(E') \frac{1}{(1-\alpha^{i,n_i})E'} \cdot \Phi^i(E') dE' \quad (2.23)$$

Because of homogeneous material mixtures inside one region, equation (2.23) becomes:

$$V^j \cdot \Sigma_t^j(E) \cdot \Phi(E) \sum_{n_j=1}^{n_{j,\max}} \Sigma_t^{j,n_j}(E) = \sum_{i=1}^k V^i \cdot P^{ij}(E) \sum_{n_i=1}^{n_{i,\max}} \left[ \int_{E'=E}^{E/\alpha} \Sigma_s^{i,n_i}(E') \frac{1}{(1-\alpha^{i,n_i})E'} \cdot \Phi^i(E') dE' \right] \quad (2.24)$$

Usually equation (2.24) is transformed from energy to lethargy. Because the standard version of ULFISP works with lethargies this transformation is done here as well. It is mainly taken from reference [16]. Lethargy is defined as:

$$u = \ln \frac{E_{\max}}{E} \quad (2.25)$$

where  $E_{\max}$  is an arbitrary energy above the resonance energy region where the spectrum shows an asymptotic  $\Phi(E) = \frac{1}{E}$  characteristic. For isotropic scattering equation (2.26)

$$\Sigma_s^i(u' \rightarrow u) = \Sigma_s^i(u') \frac{e^{u'-u}}{(1 - \alpha^{i,n_i})} \quad (2.26)$$

is valid. With equation (2.26) equation (2.24) becomes:

$$V^j \cdot \Sigma_t^j(u) \cdot \Phi(u) \sum_{n_j=1}^{n_{j,\max}} \Sigma_t^{j,n_j}(u) = \sum_{i=1}^k V^i \cdot P^{ij}(u) \sum_{n_i=1}^{n_{i,\max}} \left[ \int_{u - \ln \frac{1}{\alpha^{i,n_i}}}^u \Sigma_s^{i,n_i}(u') \frac{e^{u'-u}}{(1 - \alpha^{i,n_i})} \cdot \Phi^i(u') du' \right] \quad (2.27)$$

Introducing the collision density F:

$$F^j(u) = \Phi^j(u) \cdot \sum_{n_j=1}^{n_{j,\max}} \Sigma_t^{j,n_j}(u) \quad (2.28)$$

thus equation (2.27) becomes:

$$V^j \cdot F^j(u) = \sum_{i=1}^k V^i \cdot P^{ij}(u) \sum_{n_i=1}^{n_{i,\max}} \left( \int_{u - \ln \frac{1}{\alpha^{i,n_i}}}^u \frac{e^{u'-u}}{(1 - \alpha^{i,n_i})} \cdot \frac{\Sigma_s^i(u')}{\sum_{n_i=1}^{n_{i,\max}} \Sigma_t^{i,n_i}(u')} F^i(u') du' \right) \quad (2.29)$$

In ULFISP equation (2.29) is solved for a two zone system, respectively fuel and moderator. Therefore the probability for a neutron having its next collision in the fuel is the probability of a neutron which had its last collision in the fuel and is going to have its next collision in the fuel  $P^{FF}$ , plus the probability of a neutron which had its last collision in the moderator and is going to have its next collision in the fuel  $P^{MF}$ .

$$P^F = P^{FF} + P^{MF} \quad (2.30)$$

With the corresponding probabilities equation (2.29) becomes:

$$\begin{aligned}
F^F(u) = & \\
P^{FF}(u) \sum_{n_F=1}^{n_{F,\max}} & \left( \int_{u-\ln \frac{1}{\alpha^{F,n_F}}}^u \frac{e^{u'-u}}{(1-\alpha^{F,n_F})} \cdot \frac{\sum_s^F(u')}{\sum_{n_F=1}^{n_{F,\max}} \sum_t^{F,n_F}(u')} F^F(u') du' \right) + \\
\frac{V^M}{V^F} P^{MF}(u) \sum_{n_M=1}^{n_{M,\max}} & \left( \int_{u-\ln \frac{1}{\alpha^{M,n_M}}}^u \frac{e^{u'-u}}{(1-\alpha^{M,n_M})} \cdot \frac{\sum_s^M(u')}{\sum_{n_M=1}^{n_{M,\max}} \sum_t^{M,n_M}(u')} F^M(u') du' \right)
\end{aligned} \tag{2.31}$$

For homogeneous cross sections inside a region we can apply the reciprocity theorem from e.g. [40]:

$$V^x \sum_t^x P^{xy} = V^y \sum_t^y P^{yx} \tag{2.32}$$

A good approximation for the moderator spectrum is  $\Phi(E) = 1/E$  or  $\Phi(u) = e^u/E_{\max}$ . Therefore we can simplify the moderator part of equation (2.31) to:

$$\begin{aligned}
\frac{V^M}{V^F} P^{MF}(u) \sum_{n_M=1}^{n_{M,\max}} & \left( \int_{u-\ln \frac{1}{\alpha^{M,n_M}}}^u \frac{e^{u'-u}}{(1-\alpha^{M,n_M})} \cdot \frac{\sum_s^M(u')}{\sum_{n_M=1}^{n_{M,\max}} \sum_t^{M,n_M}(u')} F^M(u') du' \right) = \\
P^{FM}(u) \cdot \frac{e^u}{E_{\max}} \cdot \frac{\sum_{n_F=1}^{n_{F,\max}} \sum_t^{F,n_F}(u)}{\sum_{n_M=1}^{n_{M,\max}} \sum_t^{M,n_M}(u)} & \cdot \left( \sum_{n_M=1}^{n_{M,\max}} \frac{1+\alpha^{M,n_M}}{2} \cdot \sum_s^{M,n_M}(u) \right)
\end{aligned} \tag{2.33}$$

For a two zone model (only one fuel zone) equation (2.34) is valid:

$$P^{FF} + P^{MF} = 1 \tag{2.34}$$

Therefore we can rewrite equation (2.32) with equation (2.33) and equation (2.34) to equation (2.35):

$$\begin{aligned}
F^F(u) = & \\
(1 - P^{FM}(u)) & \sum_{m_F=1}^{m_{F,\max}} \left( \int_{u - \ln \frac{1}{\alpha^{F,m_F}}}^u \frac{e^{u'-u}}{(1 - \alpha^{F,m_F})} \cdot \frac{\Sigma_s^F(u')}{\sum_{m_F=1}^{m_{F,\max}} \Sigma_t^{F,m_F}(u')} F^F(u') du' \right) + \\
P^{FM}(u) & \cdot \frac{e^u}{E_{\max}} \cdot \frac{\sum_{m_F=1}^{m_{F,\max}} \Sigma_t^{F,m_F}(u)}{\sum_{m_M=1}^{m_{M,\max}} \Sigma_t^{M,m_M}(u)} \cdot \left( \sum_{m_M=1}^{m_{M,\max}} \frac{1 + \alpha^{M,m_M}}{2} \cdot \Sigma_s^{M,m_M}(u) \right)
\end{aligned} \tag{2.35}$$

Equation (2.35) is a direct solvable integral equation which is implemented for the standard scattering model of ULFISP. Originating from this, other approaches for the calculation of the collision density are available in ULFISP. They are documented in reference [16] but are not used in this work and therefore will not be derived here.

## 2.2 The energy- and temperature dependent scattering formalism

### 2.2.1 The energy- and temperature dependent scattering kernel

The exact form of the differential scattering cross section for elastic scattering in an isotropic media with a Maxwellian velocity distribution was first derived by Ouisloumen and Sanchez [69]. In the following the main equations of the energy- and temperature dependent scattering kernel are presented. More detailed descriptions of the single and double differential scattering kernel are available in references [26], [27], [30], [69], [78].

The effective differential scattering cross section for neutrons of velocity  $v$  in a homogeneous medium that has a temperature  $T$  dependent velocity spectrum  $M^T(V)$  is defined by equation (2.36):

$$\sigma_e^T(v \rightarrow v') = \frac{1}{v} \int_0^\infty v_r \sigma_e(v, w \rightarrow v') \cdot M^T(w) dw \tag{2.36}$$

where

- $v$  : neutron velocity before collision
- $v'$  : velocity of the scattered neutron
- $w$  : velocity of the target nucleus
- $v_r = v - w$  : relative velocity between the neutron and the target nucleus before collision
- $\sigma_e^T(v, w \rightarrow v')$  : differential scattering cross section for an individual collision event
- $T$  : temperature

Here the temperature dependent Maxwell velocity spectrum is defined by equation (2.37):

$$M^T(w) = \left( \frac{Am}{2\pi kT} \right)^{\frac{3}{2}} e^{\left( -\frac{Amw^2}{2kT} \right)} \quad (2.37)$$

with the variables:

- A: mass number
- m: atomic mass
- k: Boltzmann constant

The Maxwellian velocity distribution of the neutron scattering medium is a simplification of the model of Ouisloumen and Sanchez. It assumes that the target nucleus behaves like an ideal gas, as far as its thermal agitation is concerned [26]. Numerous research studies have been performed to develop scattering models which account for the bounding forces of molecules in crystal lattices e.g. the early studies of Lamb [51] or more recent studies of Courcelle and Rowlands [23]. Although it is clear that the ideal gas model is an approximation for solid materials it has been concluded by Shamaoun and Summerfield [82] that: "...at the temperatures and energies of interest in reactor physics, the chemical binding effect can be ignored for both absorption and scattering." A detailed study on this topic has been published recently by Dagan [30].

In their study Ouisloumen and Sanchez derived equation (2.38) which shows the isotropic energy- and temperature dependent scattering cross section in energy dependent form utilizing the Maxwell spectrum of equation (2.37):

$$\sigma_{s0}^T(E \rightarrow E') = \frac{(A+1)^2}{8AEkT} \int_0^\infty \sigma_s(E_r) e^{\left( \frac{A}{A+1} \frac{E_r - E}{kT} \right)} \psi_0(t) dE_r \quad (2.38)$$

$\psi_0(t)$  comprises the error functions and is defined as:

$$\begin{aligned} \psi_0(t) = & H(t_+ - t)H(t - t_-)[\text{erf}(t + \epsilon_{\min}) - \text{erf}(\epsilon_{\max} - t)] + \\ & H(t - t_+)[\text{erf}(t + \epsilon_{\min}) - \text{erf}(t - \epsilon_{\min})] \end{aligned} \quad (2.39)$$

with the Heaviside step function  $H(x)$ :

$$H(x) = \begin{cases} 0 & : x \leq 0 \\ 1 & : x > 0 \end{cases} \quad (2.40)$$

and the error function  $\text{erf}(x)$ :

$$\text{erf}(x) = \frac{2}{\sqrt{\pi}} \int_0^x e^{-t^2} dt \quad (2.41)$$

with

$$t_{\pm} = \frac{\epsilon_{\max} \pm \epsilon_{\min}}{2} \quad (2.42)$$

and

$$\varepsilon_{\max/\min}^2 = \frac{A+1}{kT} \max/\min(E, E') \quad (2.43)$$

the relative Energy  $E_r$  between neutron and nuclide can be expressed as:

$$E_r = t^2 kT \frac{A+1}{A} \quad (2.44)$$

Equation (2.38) is solved analytically by the program DOUBLE2 developed by Rothenstein and Dagan [27]. Following considerations have been applied by Dagan into DOUBLE2:

- the input cross sections have to be at temperature  $T= 0K$ , Doppler broadening is performed by DOUBLE2 as well
- the entire integrand will vanish for  $E_r \gg E$  due to the exponential term. In DOUBLE2 the integrand is set to zero for exponential terms lower than  $10^{-25}$
- For  $E \gg E_r$  the exponent can be extremely large. In this case the term originating from the error function difference (equation (2.39)) tends to vanish faster than the exponent's growth, ensuring a finite converging value of the integral when performing numeric computation. Nevertheless, such multiplication of extremely large numbers by extremely small numbers requires special attention, especially at low temperatures, which increase the exponential term
- the approximated formula for error functions is taken from reference [1] and assures a maximal inaccuracy of  $1,5 \cdot 10^{-7}$

The integral in equation (2.38) is performed using  $10^{\text{th}}$  order Gauss-Legendre integration, using weights for this method from reference [1].

## 2.2.2 Modification of the code DOUBLE2

Dagan implemented the isotropic energy- and temperature dependent scattering treatment in his thesis [27] into the OZMA [70] code. He prepared the scattering kernels with the program DOUBLE2. For the implementation into ULFISP several changes in DOUBLE2 had to be done which made a new version reasonable. In the following the main changes from DOUBLE2 to DOUBLE3 and performance differences between ULFISP and OZMA are pointed out.

Dagan's solution in OZMA applies the single differential scattering treatment for chosen specific energy groups of the MUFT [77] group structure. A group is chosen if large uranium-238 resonances are present. The single differential scattering treatment in OZMA can only be performed for uranium-238.

In ULFISP a much more general solution has been applied. ULFISP utilizes the energy- and temperature dependent scattering treatment continuously from 149 eV to 4 eV for all nuclides. While in OZMA only scattering inside an energy group is possible and scattering across group borders is neglected, in ULFISP the scattering treatment need to be used continuously across group borders. In fact, the specific ULFISP routine has no information about any group structure and is only controlled by scattering starting and ending energy, which have to be given by input. Therefore it is possible to calculate group cross sections with ULFISP for any multigroup structure which is supported by the KAPROS system. According to these differences, DOUBLE3 works completely energy-group independent for any isotope

while DOUBLE2 has been strongly connected to the MUFT group energy structure. Actually, as mentioned previously, DOUBLE3 provides scattering transfer probabilities which are simply calculated by division of the scattering kernel (equation (2.38)) by the sum of all scattering kernels which belong to the same energy. The total value of this sum is the absolute Doppler broadened elastic scattering cross section  $\sigma_s(E)$  in equation (2.45):

$$\sum_j \sigma_s^j(E' \rightarrow E) \cong \int_0^\infty \sigma_s(E' \rightarrow E) dE' = \sigma_s(E) \quad (2.45)$$

The scattering kernels in DOUBLE3 are calculated up to input controlled accuracy. In this work all scattering kernels (from which scattering probabilities have been derived) have been calculated till values of  $\sigma_s^j(E' \rightarrow E) = 10^{-5}$ . This leads to visible inconsistencies at dips of resonance cross sections. Therefore, for all elastic scattering cross sections less than one barn, the scattering kernels have been calculated down to values of  $\sigma_s^j(E' \rightarrow E) = \sigma_s^j(E) \cdot 10^{-5}$ . A new data format has been created for the scattering transfer probabilities as well.

## 2.3 Implementation of the energy- and temperature dependent scattering kernel

### 2.3.1 Modification of the KAPROS module ULFISP

For the present study, first a reactivation of ULFISP in the KAPROS system was necessary. Main issue was the replacement of the old KEDAK cross section format which is not supported anymore. For the new ULFISP data format, the CENTRM [21] point wise data library format has been chosen. CENTRM is a fine flux module of SCALE [81]. For neutron spectra calculations, it offers similar characteristics as ULFISP. These neutron spectra (or neutron flux forms) can then be used as weighting functions for multigroup cross section calculations. The choice of the CENTRM point wise data format enabled the usage of the detailed SCALE point wise cross section libraries in ULFISP. In all ULFISP calculations in this work the point cross sections of the SCALE ENDF/B 6 libraries have been used.

For validation of the reactivated ULFISP module numerous test calculations have been performed. Figure 2.1 shows a comparison of the flux shapes of ULFISP and CENTRM of a UO<sub>2</sub> fuel pin cell (specification in chapter 3.1.1) calculated at temperature T=800 K. The ULFISP calculation was provided by utilizing 49900 energy points between 1 and 10000 eV while CENTRM used 36200 energy points. The common 1/energy progression of the flux in this energy region for a thermal problem is clearly visible. The deep flux depressions result mainly from uranium-238 resonances. The very good agreement between both results is pointed out. For better visualization the neutron flux forms are slightly shifted away from each other.

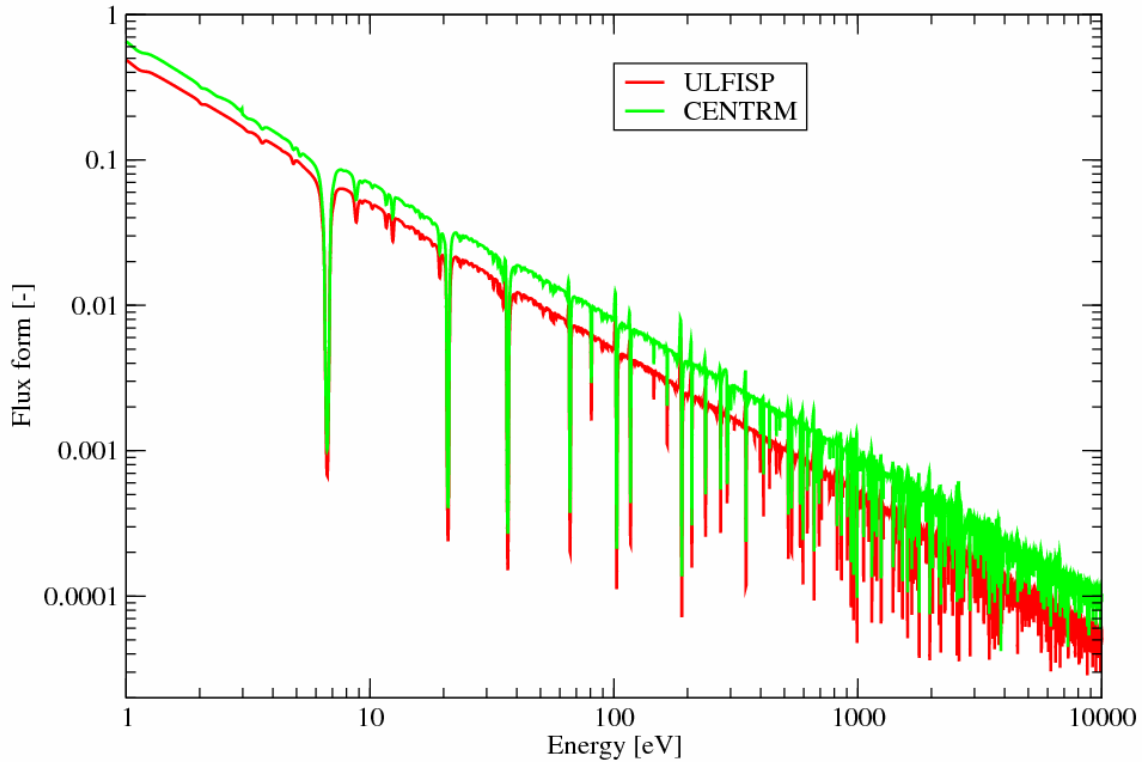


Figure 2.1: Neutron flux form vs. energy calculated by ULFISP and CENTRM for  $\text{UO}_2$  fuel at  $T = 800$  K (slightly shifted away from each other for better visualization)

### 2.3.2 Implementation of the single differential scattering kernel

The slowing down equation was derived from the Boltzmann equation in chapter 2.1.5. Originating from equation (2.35) a new scattering equation, utilizing the energy and temperature dependent scattering treatment was derived by the author and will be presented in the following. The new scattering equation will perform temperature and cross section dependent down scattering and up scattering by using precalculated scattering transfer probabilities. These scattering probabilities have been created with DOUBLE3, a further development of DOUBLE2 written by Dagan and Rothenstein [27]. The temperature and cross section dependent scattering kernel and the DOUBLE3 algorithm are presented in detail in chapter 2.2.2.

The implementation of the new scattering algorithm was performed in the energy domain. Therefore, the slowing down equation (2.35) is changed from lethargy to energy:

$$\begin{aligned}
 F(E) = & (1 - P^{FM}(E)) \sum_{m_F=1}^{m_F, \max} \left[ \int_E^{E/\alpha^{F, m_F}} \frac{1}{(1 - \alpha^{F, m_F}) E'} \frac{\Sigma_s^{F, m_F}(E')}{\Sigma_t^F(E')} \cdot F^F(E') dE' \right] \\
 & + P^{FM}(E) \cdot \frac{\sum_{m_F=1}^{m_F, \max} \Sigma_t^{F, m_F}(E)}{\Sigma_t^M(E)} \cdot \frac{1}{E} \left[ \sum_{m_M=1}^{m_M, \max} \frac{1 + \alpha^{M, m_M}}{2} \cdot \Sigma_s^{M, m_M}(E) \right]
 \end{aligned} \tag{2.46}$$

Equation (2.47) shows the calculation of the collision density with the new scattering approach.

$$\begin{aligned}
F^F(E) = & (1 - P^{FM}(E)) \sum_{m_F=1}^{m_{F,\max}} \left[ \int_{E_{\min}(P_m(E' \rightarrow E))}^{E_{\max}(P_m(E' \rightarrow E))} P_m(E' \rightarrow E) \frac{\Sigma_s^{F,m_F}(E')}{\Sigma_t^F(E')} \cdot F^F(E') dE' \right. \\
& \left. + P^{FM}(E) \cdot \frac{\sum_{m_F=1}^{m_{F,\max}} \Sigma_t^{F,m_F}(E)}{\Sigma_t^M(E)} \cdot \frac{1}{E} \left[ \sum_{m_M=1}^{m_{M,\max}} \frac{1 + \alpha^{M,m_M}}{2} \cdot \Sigma_s^{M,m_M}(E) \right] \right]
\end{aligned} \tag{2.47}$$

The scattering kernel  $\frac{1}{(1 - \alpha_{m_F}^F) E'}$  is replaced by the temperature- and cross section

dependent scattering transfer probability  $P_m(E' \rightarrow E)$  calculated by DOUBLE3.  $P_m$  is described in detail in chapter 2.2. Furthermore the integration limits have been changed and are now a function of the energy- and temperature dependent scattering kernel. In this work the scattering limit, has been set to  $P_{m,\min} = 10^{-5}$ . For energy regions with an elastic scattering cross section lower than one barn, the scattering limit has been set to:  $P_{m,\min} = \frac{P_m}{\Sigma_s} = 10^{-5}$ . In

figure 2.2 the scattering limits (where  $P_{m,\min} = 10^{-5}$ ) have been determined to  $E = 35.4$  eV and  $E = 37.0$  eV.

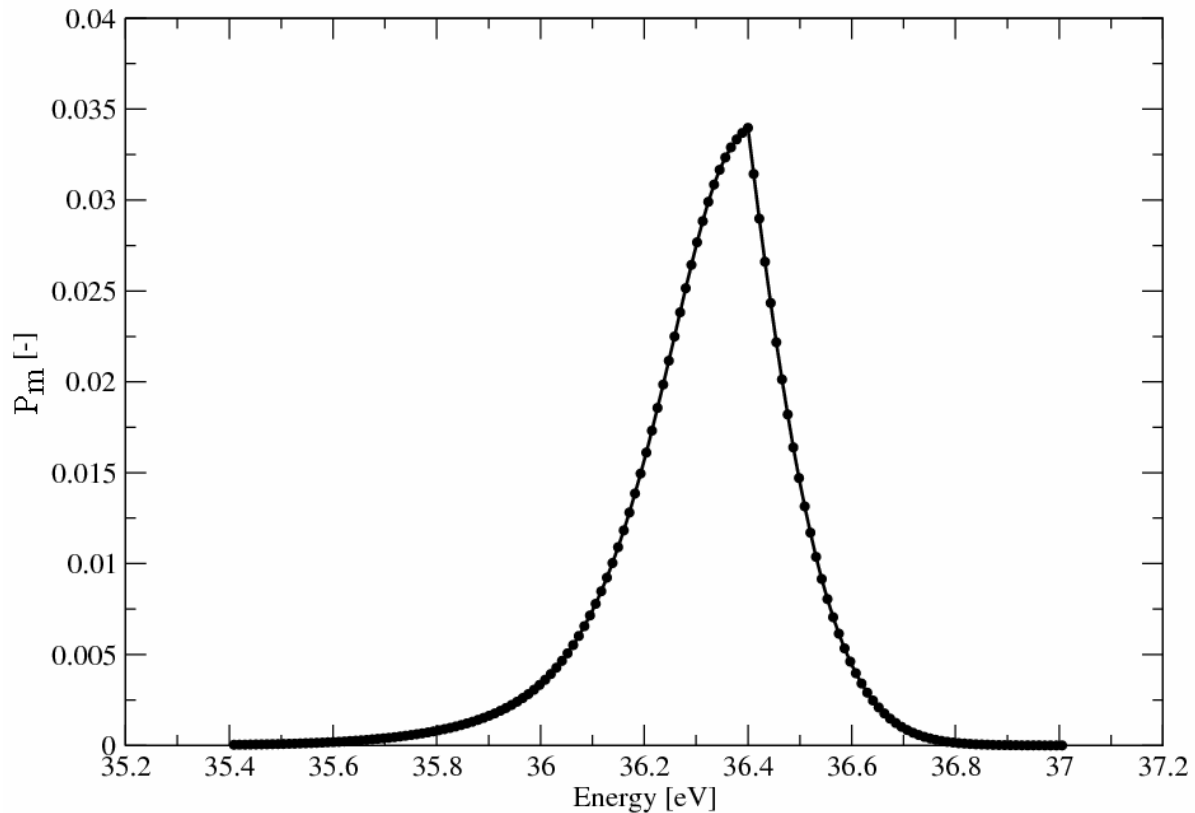


Figure 2.2: Energetic resolution of the scattering transfer probabilities  $P_m$  for a neutron of  $E = 36.4$  eV (energy region of the third U-238 resonance) having an elastic scattering reaction with U-238 ( $T = 800$  K)

Each point in the curve of figure 2.2 represents a discretization point of the scattering distribution  $P_m$ . Per definition the sum of all scattering probabilities  $P_m = 1$ :

$$\left( \sum_i P_m^i \equiv 1 \right) \quad (2.48)$$

The fuel part (first line) of equation (2.47) can be explained very illustratively: We are searching for neutrons which scatter from energy  $E'$  to energy  $E$  forming the collision density  $F^F(E)$  in the fuel. First requirement is that neutrons of energy  $E'$  are available. This is expressed by the relative probability  $F(E')$ . Second these neutrons will have some kind of reaction. The

term  $\frac{\Sigma_s^{F,m^F}(E')}{\Sigma_t^F(E')}$  represents the probability that a neutron will have an elastic scattering reaction instead of any other reaction. Thirdly, the considered neutrons will be scattered to energy  $E$  with the probability of  $P_m(E' \rightarrow E)$ . Last, we take into account that the scattered neutrons have the possibility to have their next collision in the moderator and not in the fuel by the factor  $(1 - P^{FM}(E))$ .

In the asymptotic approach the collision density is calculated from high to low energies. Thereby the actual collision density is calculated from previous ones. For the first calculation points the precalculated moderator spectrum (second line of equation (2.47)) is used and therefore a “spectrum overlap” has to be used to allow the flux form to swing from the first arbitrary considered moderator spectrum value into the real fuel neutron flux form. In all pin cell calculations presented in this chapter the normal fine flux calculation starts at  $E=1300$  eV while the first determined group constant has its upper energy limit at  $E=911,8$  eV. Thus the difference between  $E=1300$  and  $E=911,8$  eV has been taken as “swing into spectrum buffer”. Figure 2.3 illustrates this effect at an example of a  $UO_2$  pin cell (specification chapter 3.1.1). The flux form depicted in red results from a calculation started at  $E=10000$  eV providing a reference solution in the shown energy region. The black line represents a flux form from a calculation which started at  $E=1300$  eV. There the two flux forms show considerable differences. At approximately  $E=1000$  eV the “swing into” is finished and both flux forms give very good agreement.

For the up scattering approach an additional overlap of the flux form at low energies is necessary. In all presented calculations the fine flux forms (normal approach) have been calculated down to  $E= 1.6$  eV. This allows the up scattering from lower energies into the last (27<sup>th</sup>) energy group. The lower energy border of  $E= 1.6$  eV has been chosen due to up scattering of oxygen at  $T=1200$  K. Utilizing either higher temperatures or lighter isotopes might necessitate an adjustment to a lower energy.

Because of up scattering, for the new approach the collision densities have to be assumed before they are calculated. This is worked out by iterating the calculation of the collision density. For the first computation the collision density from the asymptotic approach is taken, which is already a quiet good approximation. After that an arbitrary number of iterations are possible. In practice three iterations have been found to be sufficient.

Figure 2.4 shows iterations of the collision density for the energy region of the third uranium-238 large resonance. The good convergence of the collision density for increasing iteration numbers is clearly visible. The evolving form of the new flux form results from up scattering at the energetic lower shoulder of the resonance and from reduced down scattering at the energetic higher shoulder of the resonance. This effect is analyzed in more detail in chapter 3.2.

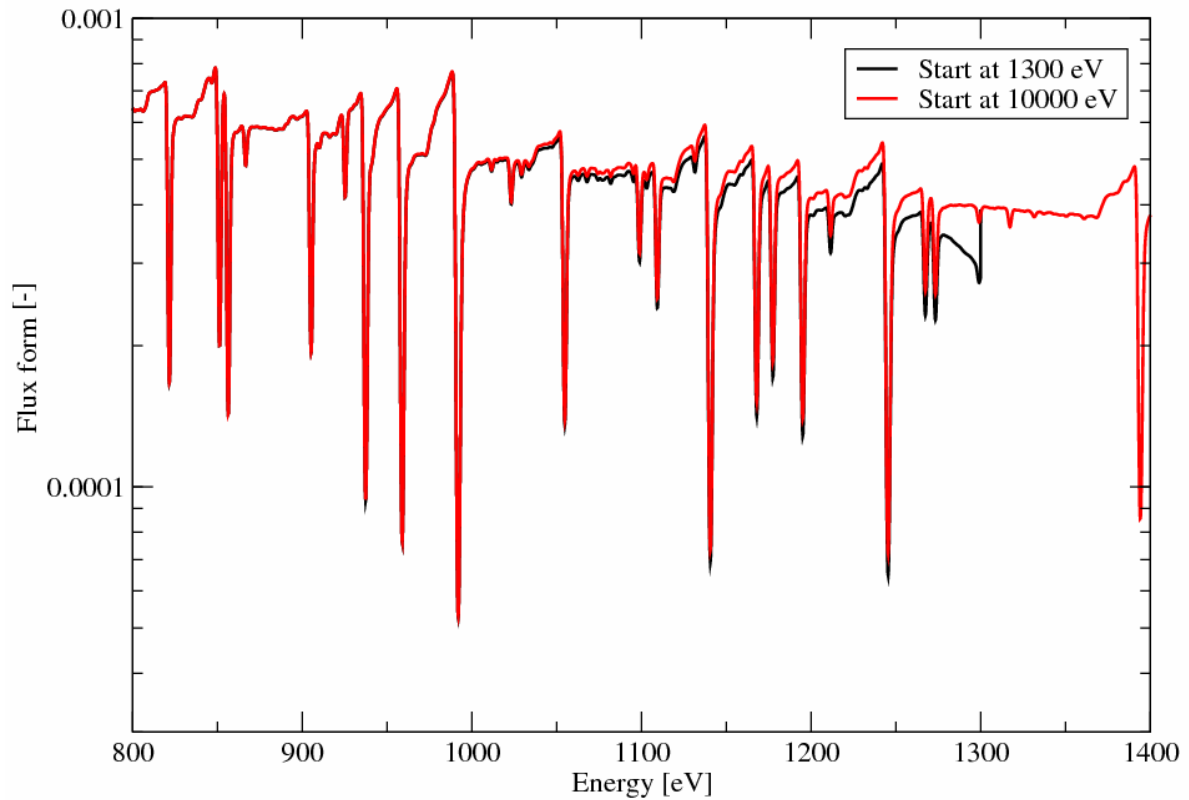


Figure 2.3: The flux “swing into” effect in the standard approach for a  $\text{UO}_2$  pin cell (fresh fuel, 4 wt. % U-235)

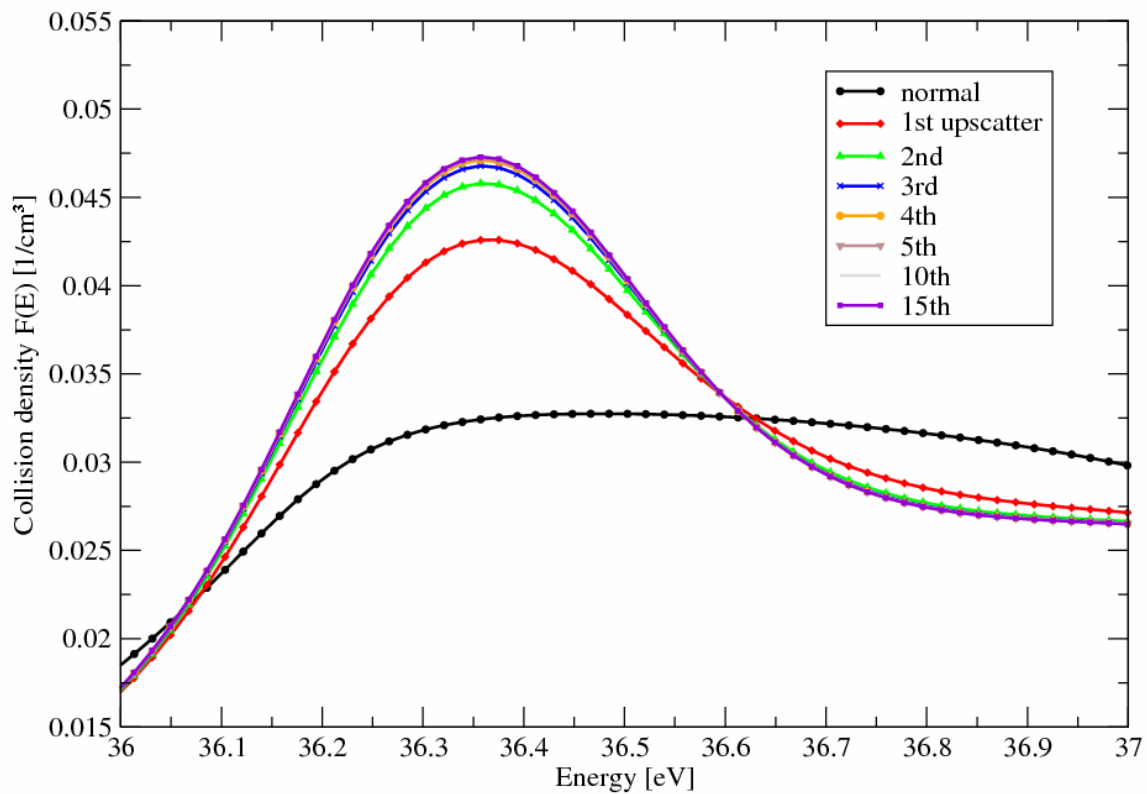


Figure 2.4: The collision density vs. energy as a function of iterations

In its standard version ULFISP creates a problem specific irregular energy grid which depends on the input cross sections and the chosen maximum change of cross section value over energy:

$$\Delta\sigma \cdot \Delta E = \text{constant} \quad (2.49)$$

Due to the scattering transfer probabilities calculated by DOUBLE3 (see chapter 2.2.2) the new scattering approach requires a constant lethargy grid in the applied energy region. The constant lethargy grid chosen for the pin cell calculations in chapter 3.1 and 3.2 is  $\Delta u = 0.9997$ . For the pin cell burnup and the assembly calculations presented later,  $\Delta u = 0.9990$  has been chosen because of calculation time and required larger memory space.  $\Delta u$  is defined as:

$$\Delta u = \frac{E_{x+1}}{E_x} = \text{const.} \quad (2.50)$$

Thereby  $E_{x+1}$  and  $E_x$  are successive energy points on the energy scale with  $E_x > E_{x+1}$ .

A sensitive point during the implementation of the new scattering model has been the energetic intersection between the two models. The choice of the highest and the lowest energy for which both of the two procedures are used is arbitrary in ULFISP. However there are some restrictions which need to be considered. The asymptotic approach always has to cover the energy region of the new approach plus an overlap at the energy intersection at the highest and at the lowest energy applied in the new approach.

The energy overlap at the upper energy border has to use the constant lethargy grid of the new approach and scattering kernels have to be provided for this energy region as well. The reason of this overlap is that like all other collision density points the energetically highest one is calculated partly from the down scattering from energetically higher collision densities for which transfer probabilities have to be provided. The required overlap depends on:

1. the energetically strongest neutron slowing down isotope in the fuel (in this study always oxygen)
2. temperature T
3. scattering limit  $P_{m,\min}$
4. the maximum energy for which the new scattering model is used

For the results presented in chapter 3, the strongest neutron slowing down isotope (in the fuel) considering energy loss in case of a scattering incident, is oxygen at a temperature of  $T=1200\text{K}$ . The scattering limit is  $P_{m,\min}=10^{-5}$  and the maximum energy is  $E=149\text{ eV}$ . The overlap was determined to  $\Delta E=50\text{ eV}$  by DOUBLE3. That means that the highest energy for which scattering kernels have to be provided is  $E=199\text{ eV}$ . The energetic overlap at the lower energy border is needed for up scattering correspondingly. The restrictions of the overlap at the lower energy border are consistent as well.

The two scattering models are two different approaches. Therefore, it is likely that the intersection from one to the other model is not smooth. Especially in the region of strong cross section resonances discontinuous collision density intersections are possible. For best calculation performance the intersections should always be placed at group cross section borders. Figure 2.5 shows a smooth intersection at energy  $E=149\text{ eV}$ .

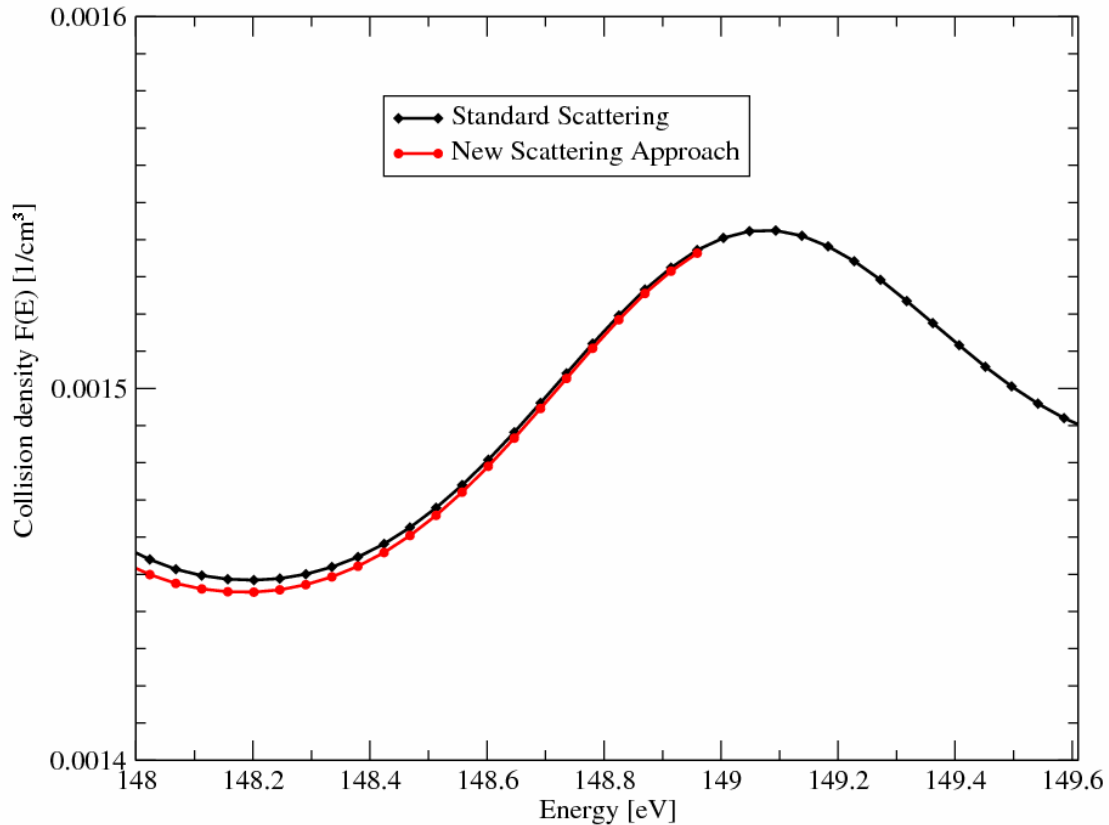


Figure 2.5: An intersection between the two ULFISP scattering approaches

### 2.3.3 The hybrid method

Calculating the collision density with the new scattering treatment follows always the same procedure. First the collision density is calculated according to the standard procedure developed by Broeders [16]. Then this collision density is considered as a first (quite close) approximation and taken as input for the new scattering method. The procedure demands that every isotope that contributes a noticeable part to the collision density is treated in the standard as well as in the new scattering working step. Due to the different methods it is not possible to treat a single (or a bunch of) isotopes only by the asymptotic scattering treatment. In other words, no mixing of these two working steps is possible.

However, for reduction of computing time and analyses of the importance of isotopes due to the new scattering method, it is preferable to use a hybrid method which allows a selection of isotopes which are treated by the asymptotic scattering method or which are treated by the energy and temperature dependent scattering method. This was realized in the so called hybrid method in this study.

This hybrid method has been realized by introducing asymptotic scattering transfer probabilities  $P_m(E' \rightarrow E)$  into the improved method algorithm which allow the calculation of the collision density in the same way as the standard method. The scattering probabilities of the asymptotic scattering inside the improved method algorithm feature the following attributes:

1. only the potential cross section is respected  $\rightarrow P_m(E' \rightarrow E) = \text{constant}$
2. the sum of all scattering probabilities has to be equal to one, like in the new method: 
$$\sum_i P_m^i \equiv 1$$
3. no up scattering is respected  $\rightarrow E' \geq E$

The calculation of  $P_{m, \text{const.}}(E' \rightarrow E)$  is performed by the following ansatz: since  $P_m$  is constant it can be determined by:

$$P_{m, \text{const.}}(E' \rightarrow E) = \frac{1}{x} \quad (2.51)$$

where  $x$  is the number of grid points in the scattering region. The scattering region  $\Delta E$  can be calculated by:

$$\Delta E = E - E \cdot \alpha, \quad \left[ \alpha = \left( \frac{A-1}{A+1} \right)^2 \right] \quad (2.52)$$

and by:

$$\Delta E = E - E \cdot [\Delta u]^x \quad (2.53)$$

Equalizing equation (2.52) and (2.53) leads to:

$$\Delta u^x = \alpha \quad (2.54)$$

Equation (2.54) logarithmized leads with equation (2.51) to:

$$P_{m, \text{const.}}(E' \rightarrow E) = \frac{\log \Delta u}{\log \alpha} \quad (2.55)$$

$\Delta u$  and  $\alpha$  do not depend on energy or temperature. Therefore,  $P_m$  depends only on the chosen constant lethargy grid and on each specific isotope.  $P_m$  is valid for all energies and has to be calculated for each isotope once. Figure 2.6 clarifies the differences between the improved scattering probability (same as in figure 2.2) and a constant scattering probability.

The hybrid method allows a detailed analysis of the importance of the new scattering method on single isotopes like it is presented in chapter 3.4. The character of constant lethargy grids combined with a constant scattering distribution allows the usage of one scattering distribution per isotope for all energies. This added to the facts that the algorithm itself is much easier and as visible in figure 2.6, for asymptotic scattering fewer distribution points are necessary. This significantly reduces the computation time.

Summarizing, the hybrid method allows the usage of the standard method inside the new method without changing the general procedure of calculating weighting spectra with the energy- and temperature respecting scattering treatment. Therefore, it enables the possibility to perform calculations in which the scattering method can be chosen separately for every isotope.

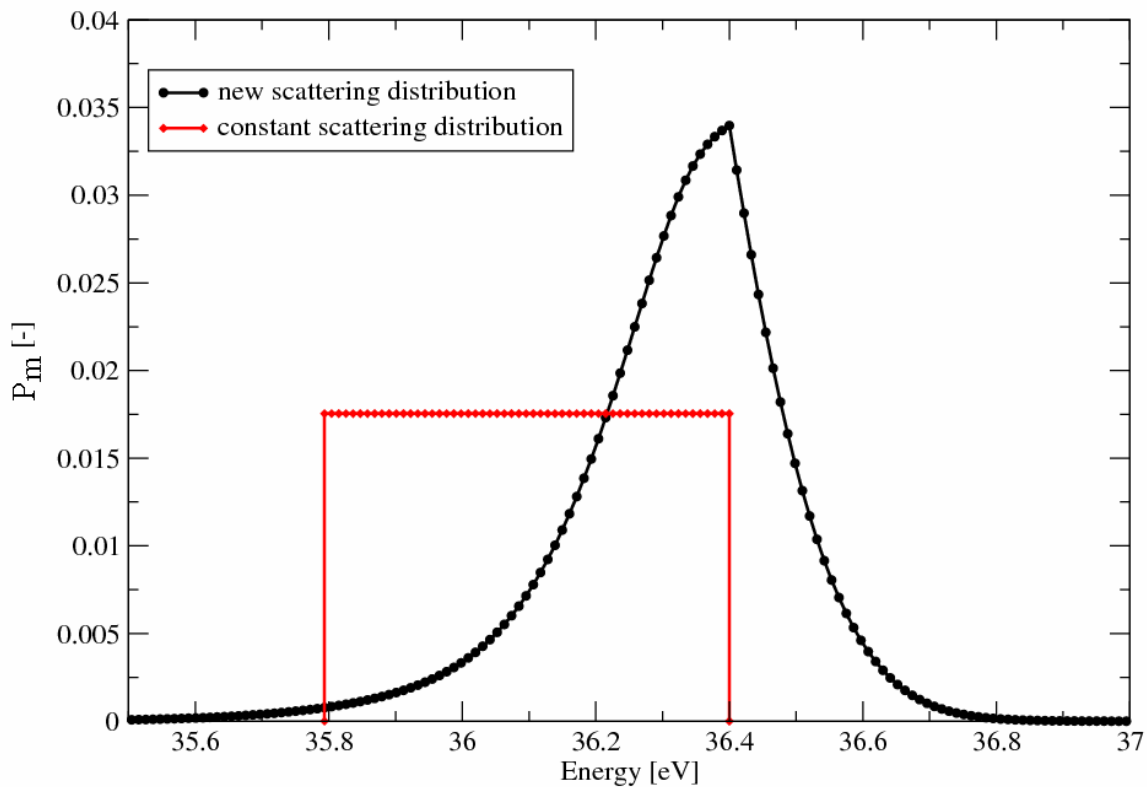


Figure 2.6: energetic resolutions and distributions  $P_m$  of the two scattering methods for a neutron of 36.4 eV having an elastic scattering interaction with U-238 at  $T=800$  K

## 2.4 Code descriptions

Light water reactor analyses and simulations in the past were characterized by efficient and accurate fuel management, based on nodal core physics methodologies [45]. These methodologies have utilized very detailed three-dimensional core neutronics models supplemented by simplified feedback thermal-hydraulics models - usually one-dimensional models for boiling water reactors and a “point” thermal hydraulic model for pressurized water reactors. Limited by the available computer power, earlier safety methods used point kinetics core response in conjunction with a conservative approach for physics input, in order to ensure safe reactor operation.

Commonly used code systems perform the safety analysis by coupled neutronics and thermal hydraulic systems. The standard proceeding for a reactor core safety analysis is illustrated in figure 2.7.

The basis of state of the art reactor analysis is a coupled thermal-hydraulic and neutron physic model. On the thermal hydraulic side a system code like RELAP5 [73] or TRACE [86] calculates fluid dynamics (code specific) in one dimension or multidimensional. Simplified models include only the reactor vessel while a detailed model of the whole primary system is possible in recent code applications [86].

The thermo-hydraulic codes describe the transfer of mass, energy and momentum of fluids. Also two phase flows can be modeled in some codes, e.g. TRACE. The coupling to the neutronic side is performed through the heat transfer. The thermo-hydraulic codes calculate fluid, structure and fuel temperatures as well as the fluid densities through the respective heat

transfers. These parameters are passed over to the neutronic side where the new neutron physics system conditions are calculated. The neutronic side recalculates the thermal power of the fuel and passes it again to the thermo-hydraulic side. In current coupled three dimensional neutronics – thermo-hydraulics simulations few group two dimensional cross-section sets are used as input data [45]. The amount of few group cross-section data is significant especially for transient analyses. The generation of these cross-section sets is performed by lattice codes. Usually, burnup calculations for single assemblies are performed at reference conditions.

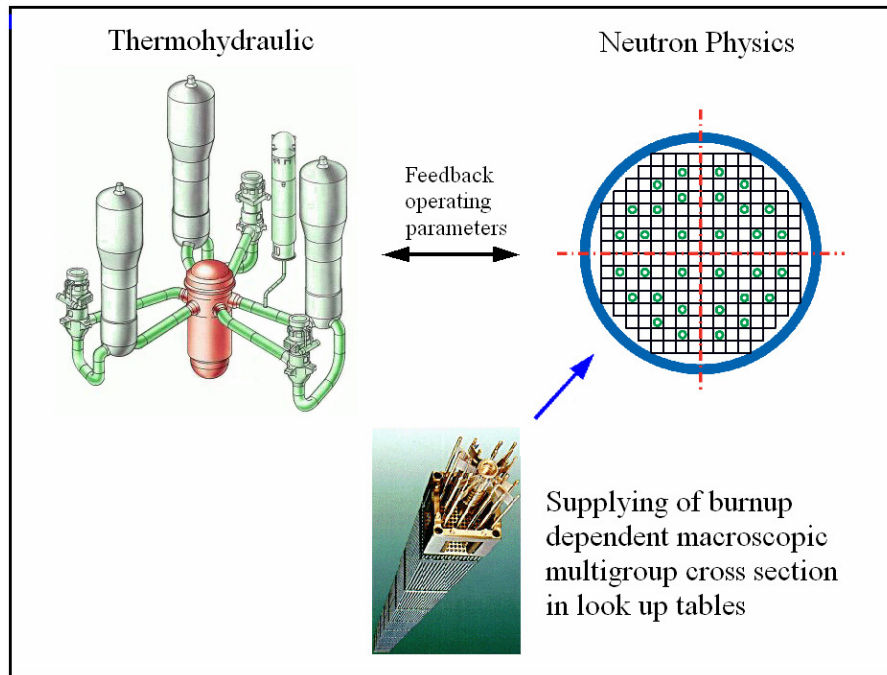


Figure 2.7: Standard procedure for LWR reactor core simulations

For transient analysis in codes like PARCS [36] or CORETRAN [39], for every burnup step and all different local feedback parameters like fuel temperature, moderator temperature and density, void (BWR) or boron concentration (PWR) cross section have to be provided. These cross-section data are produced burnup dependent by lattice codes like KAPROS/KARBUS [16] or SCALE/TRITON [87] in so called branch calculations. The cross sections are stored in look up tables for the reactor reactor core analysis codes.

The three dimensional neutronic core solver takes the required cross-section data from the look up tables and interpolates these if necessary. The energy and temperature dependent scattering treatment is performed only in the lattice code calculations during generation of the cross section look up tables. The new scattering treatment is therefore introduced into reactor core simulation only via the precalculated cross-section sets. For steady state analysis branch calculations or interpolation of cross-section data are not required. In this study only steady state analysis has been performed, which reduced the amount of required data immensely. For the determination of the impact of the new temperature- and energy dependent scattering treatment on reactor core calculations, it has been reasonable to maximize the number of energy groups of the cross section data. For the results presented in chapter 4, steady state reactor core calculations have been performed utilizing 28 energy groups. More detailed information of the calculation characteristics for reactor core calculations is recorded in chapter 4.3.

### 2.4.1 The lattice code KARBUS and its extended version KARBUSE

KARBUS and KARBUSE belong to the modular program system KAPROS [4], [16], [95]. Originally KAPROS came along with the development of the fast breeder reactor in the research centre of Karlsruhe in the 1970's. Later on, KAPROS has successively been extended for thermal light water reactors. A milestone in this development was the work of Broeders who developed the KARBUS procedure during his studies of Advanced Pressurized Water Reactors with hexagonal fuel assemblies [16]. KARBUS (KARlsruhe Reaktor BUrnup System) enables reactor burnup calculations for various systems. Therefore, it automatically operates several other KAPROS routines and modules as well as it controls the data flow between KAPROS modules and external codes like DANTSYS [33] or DOORS [35] which have been coupled to KAPROS. The most important codes for this work are shown in the flow chart of figure 2.8 and are explained in the following.

Next to the input description which contains problem dependent geometries, material specifications and calculation parameters KARBUS has to be provided with microscopic multigroup cross section libraries, burnup information libraries and in case of fine flux calculations with point cross section libraries. The microscopic multigroup cross section libraries are calculated by NJOY [54] and processed via KAPROS utility codes into the GRUMA [96] format. This cross section processing for the KAPROS system is documented e.g. in reference [67]. In dependence to the 69-groups in WIMS group structure ENDF/B 6.5 library which is used in all KARBUS and KARBUSE calculations in this work, this library is called "69-Multigroup XS-library" in figure 2.8.

For burnup calculations libraries containing isotope specific fission yields, half-lives, decay schemes, etc. have to be provided which are called KORFI [41] libraries in KAPROS. For fine flux calculations point wise cross section libraries are used in ULFISP. These are explained later in this chapter. The module NDCALC processes the user input information, calculates material densities, prepares input information for other modules and passes these over. In calculations which are not utilizing energy group discretization via fine flux, KARBUS calls directly the macroscopic cross section calculator GRUCAL [95]. GRUCAL determines effective macroscopic multigroup cross sections for homogenized zones. The resonance self shielding is treated via precalculated shielding factors which are included in the microscopic cross sections libraries.

A reactivated option in KAPROS is the calculation of effective (resonance shielded) multigroup cross sections in the epi-thermal energy range via the module ULFISP. These group cross sections can be transferred into GRUCAL by the secondary cross section input option. The module ULFISP which is the main program tool in this study is described in more detail later in this chapter.

The zone dependent macroscopic cross sections from GRUCAL are inserted into WEKCPM for one dimensional transport calculation or to the loosely coupled DANTSYS 3.0 [33] program for two or three dimensional transport calculations. WEKCPM has been adapted from WIMS/E [3] to the KAPROS system. WEKCPM is usually chosen for single pin cell calculations. It characterizes the geometric problem through a Wigner-Seitz cell and solves the transport equation utilizing the first collision probability method [13].

For two- or three dimensional geometric solutions the DANTSYS option can be applied. In this study TWODANT [33], the two dimensional discrete ordinate transport code of DANTSYS 3.0 has been applied for all assembly calculations. It uses the diamond difference scheme for phase space discretization. All TWODANT calculations have been performed with an angular discretization of  $S=8$  and conversion criteria for reactivity of  $10^{-6}$ . TWODANT is provided with rod wise homogenized cross section by GRUCAL. For burnup calculation the zone wise calculated neutron fluxes are transferred from WEKCPM or

TWODANT to ONEHOM which applies (one dimensional) pin cell wise problem cross section homogenization.

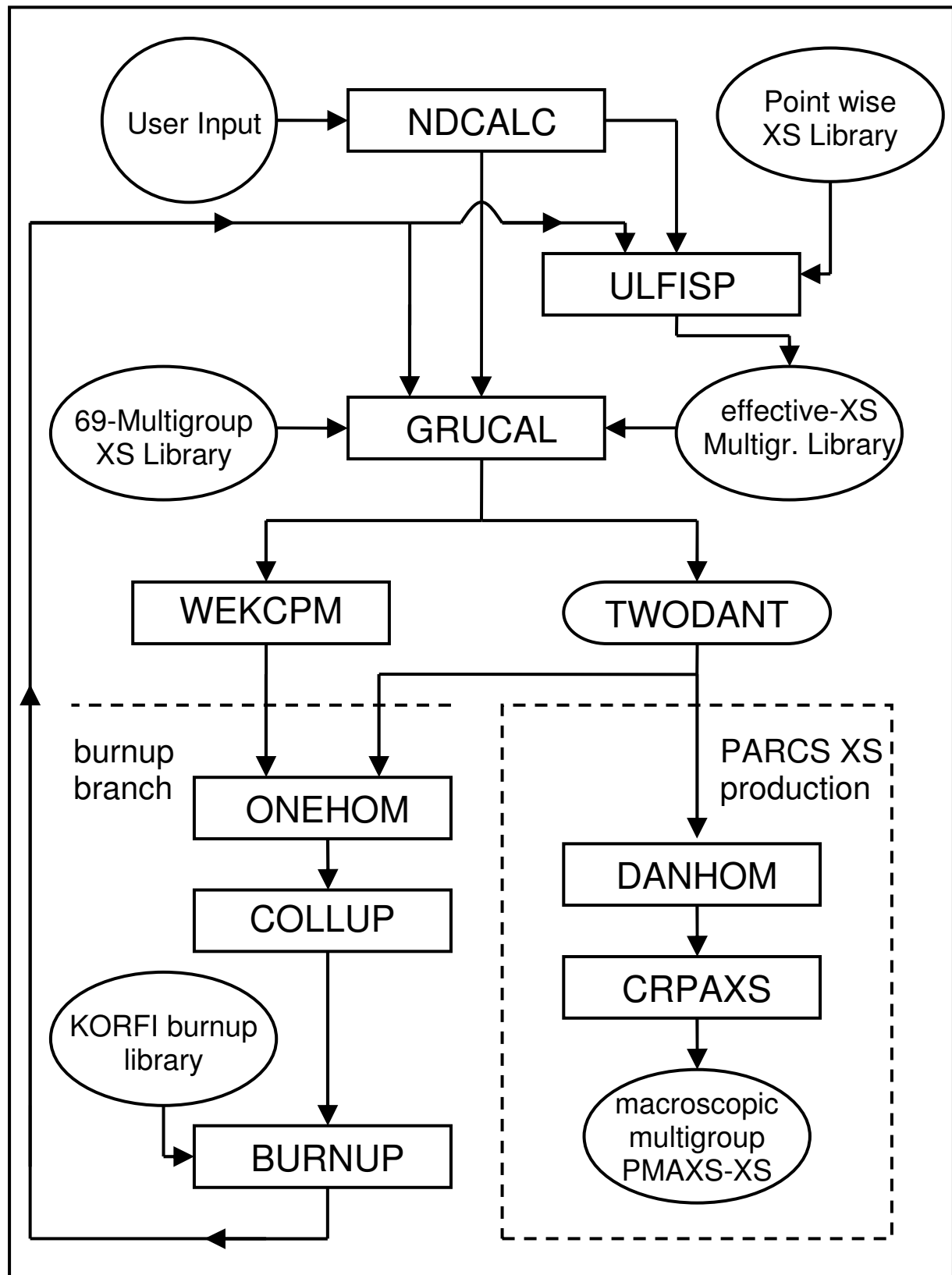


Figure 2.8: Flow chart of KARBUS and KARBUSE

Afterwards the zone dependent cross sections are passed over to COLLUP which performs one group condensation. These one group cross sections and one group neutron fluxes are then passed to the module BURNUP, a successor from KORIGEN [41] which itself was a further development from ORIGEN [11]. Together with the burnup informations from the KORFI libraries BURNUP calculates new material densities and passes them back to GRUCAL and in case of fine flux treatment to ULFISP.

For this study a new cross section processing option in KAPROS has been developed. It generates multi group cross sections in the PMAXS [97] format for the three dimensional core solver PARCS [36]. The burnup dependent macroscopic pin cell wise homogenized cross sections from GRUCAL are volume weighted by the neutron fluxes from TWODANT. This is performed by DANHOM, a two dimensional homogenization module recently developed by Broeders [15]. DANHOM weights macroscopic cross section in accordance to equation (2.56) which can be found in numerous literatures, e.g. reference [84].

$$\Sigma_{x,i} = \frac{\sum_{i=1}^I \Sigma_{x,i} \Phi_i V_i}{\sum_{i=1}^I \Phi_i V_i}, \quad \text{with } i \in I \quad (2.56)$$

Here,  $\Sigma_i$  is the zone dependent macroscopic cross section,  $\Phi_i$  is the zone dependent neutron flux and  $V_i$  is the volume of zone  $i$ . Afterwards, the assembly homogenized cross sections are passed to the KAPROS module CRPAXS. CRPAXS is a modified version of CRGIP [8]. It has been changed for this study to convert cross sections from the GRUMA format of KAPROS to the PMAXS format of PARCS. Current capabilities of CRPAXS are limited to the conversion of scalar cross sections and scattering matrixes for simplified steady state reactor analysis.

### 2.4.2 The fine flux module ULFISP

ULFISP calculates effective neutron cross sections in the energy region of neutron resonances. Therefore it solves the slowing down equation as explained in detail in chapter 2.1. The original version [16] of Broeders has been reactivated for this work. It has been adapted to the point cross section format of CENTRM [21] and uses the point cross section data from the SCALE [81] system since this adaptation. In figure 2.9 the most important routines of ULFISP are shown and explained in the following. The user input specifications are passed into the ULFISP module from the KARBUS procedure. RNUDAT (Read NUClear DATA) reads for every fuel isotope of the considered problem the elastic, capture, fission (if available) and total cross section. Square root temperature interpolation is performed for all cross sections as applied in CENTRM [21] automatically. The energy grid of every isotope and reaction is passed to GENFIN (GENerate FINE energy mesh) which generates a problem dependent energy grid. The accuracy of this energy grid is controlled by input specifications. If the new scattering option is applied in ULFISP, a predefined energy grid with constant lethargy is inserted in the concerning energy region in GENFIN.

After GENFIN, LINTBR (Linear INTerpolation BRoeders) interpolates all cross section data to the energy mesh generated by GENFIN. The interpolated cross section data is still microscopic. For burnup or assembly calculations this data can be stored and reused for every pin cell calculation. This can save a huge amount of calculation time especially if burnup

calculations are performed with a high number of fuel isotopes. The limitation for this option is that all isotopes which are used at any time or region step have to be included in the very first ULFISP calculation which generates the interpolated cross section data.

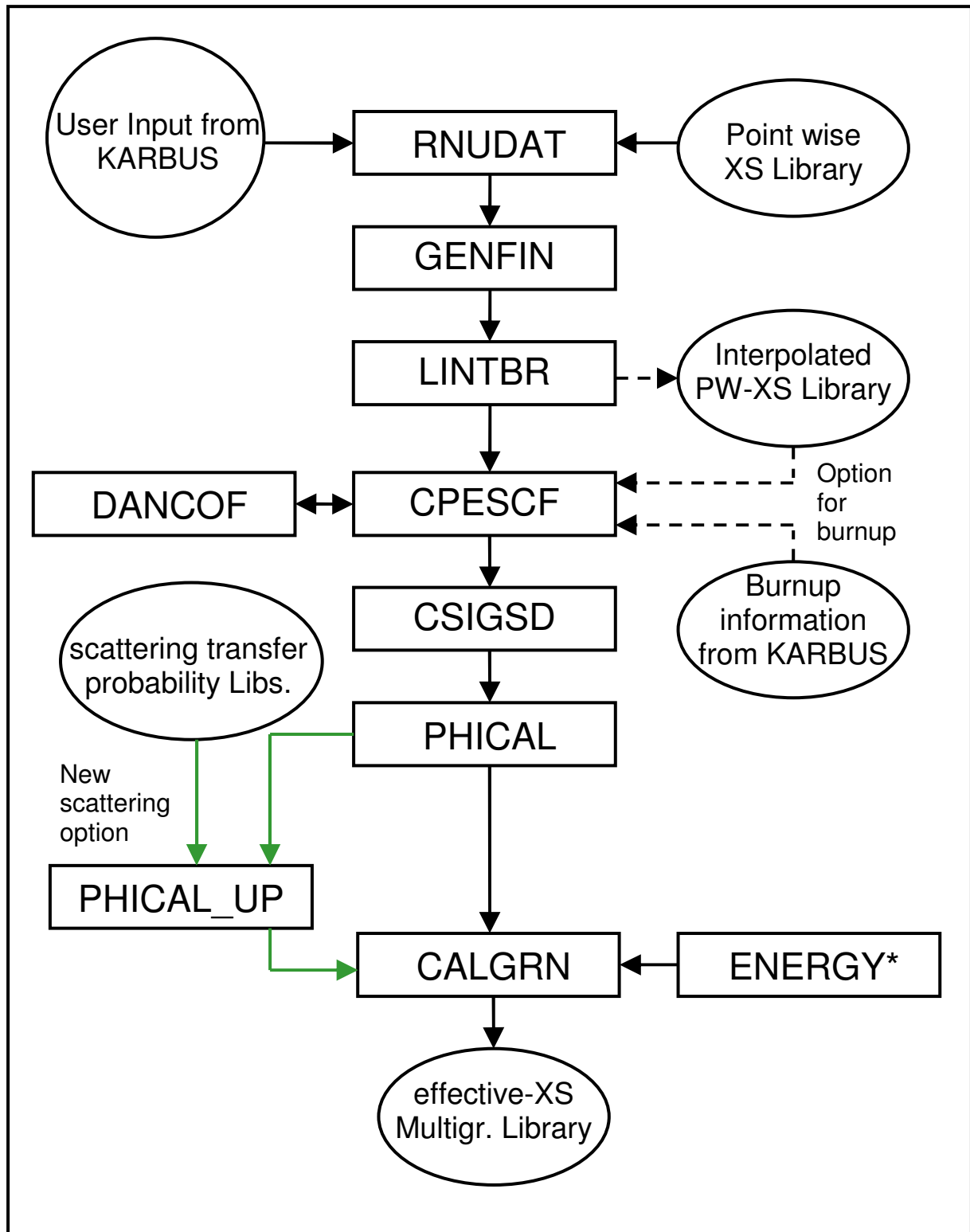


Figure 2.9: Flow chart of the fine flux module ULFISP

The determination of neutron form in ULFISP requires the calculation of transfer probabilities (probability  $P^{FM}$  in equation (2.35)) between different zones which is performed by the module CPESCF. The calculation of these probabilities is documented in the works of e.g. Dancoff and Ginsburg [31], Wigner, Creutz, Jupnik and Snyder [89], Bell [10] or Levine [53]. The exact escape probability for an infinite cylinder has been derived by Case, de Hoffmann and Placzek [20]:

$$P_e = \frac{1}{\Sigma_t \bar{l}} \left[ 1 - \frac{4}{\pi} \int_0^1 \frac{x^4}{\sqrt{1-x}} dx \int_x^\infty \frac{e^{-\Sigma_t \bar{l} y}}{y^3 \sqrt{y^2 - x^2}} dy \right] \quad (2.57)$$

where

$P_e$  is the escape probability

$\Sigma_t$  is the total cross section

$\bar{l}$  is the average chord length of a zone

A numerical solution of equation (2.57) is possible but time consuming. In ULFISP the escape probability is calculated after the method of Raghav [72] which uses a polynomial adaptation for equation (2.57):

$$P_e = (1 - X) + X(1 - X)^2 \cdot \sum_{n=0}^{11} Q_n X^n \quad (2.58)$$

with

$$X = \frac{\Sigma_t \bar{l}}{(1 + \Sigma_t \bar{l})} \quad (2.59)$$

In table 2.1 the  $Q_n$  values for an infinite cylinder are listed. Equation (2.58) and (2.59) are valid for infinite systems. Therefore it must be considered that a neutron which escapes the fuel zone does have its next collision in another fuel zone. This probability is considered by the Dancoff factor  $C$ . Different approximation calculation methods of the Dancoff factor are available in ULFISP but have to be chosen directly in the code. Implemented are the Dancoff factor calculation methods of Chao et al. [22], Bonalumi [13] and Sauer [80] as well as the exact but computational time intensive method of Carlvik [19]. Due to its fast calculation and good results the standard Dancoff factor calculation in ULFISP employs the method of Sauer. Equation (2.60) and (2.61), taken from [80], describe the method:

$$C = 1 - \frac{e^{-\tau \Sigma_t^M \bar{l}_M}}{1 + (1 - \tau) \Sigma_t^M \bar{l}_M} \quad (2.60)$$

with

$\Sigma_t^M$  total cross section of the moderator

$\bar{l}_M = \frac{4V_M}{S_M}$  average chord length of the moderator

$V_M$  volume of the moderator

$S_M$  surface of the moderator

$v_m$  volume ratio between moderator and fuel  
 $v_c$  volume ratio between clad and fuel

The geometric index  $\tau$  is defined for quadratic grids as:

$$\tau = \sqrt{\frac{\pi * (1 + v_c + v_m)}{4 v_m^2}} - \sqrt{\frac{(1 + v_c)}{v_m^2} - 0.08} \left[ 1 + \frac{1}{2} \sqrt{\frac{v_c}{1 + v_c}} \right] \quad (2.61)$$

n	$Q_n$
0	0.225644
1	2.100901
2	-6.058395
3	7.848099
4	12.33828
5	-32.32889
6	18.26813
7	-23.88533
8	55.26502
9	5.709876
10	-88.28482
11	49.89500

Table 2.1: Adjustment parameter of the Raghav formula

Williams and Gilai [91] developed a cladding correction for the Dancoff method of Sauer. It is implemented in ULFISP as well. It is described by equation (2.62) and (2.63):

$$C_{withClad} = C \cdot \left( 1 - \bar{l}_c \Sigma_t^C \cdot P_e^{Clad} \right)^2 \quad (2.62)$$

with

$C_{withClad}$  the cladding corrected Dancoff-factor  
 $\bar{l}_c$  the average chord length of the cladding  
 $\Sigma_t^C$  the total cross section of the cladding  
 $P_e^{Clad}$  the escape probability from a hollow cylinder which is after Sauer:

$$P_e^{Clad} = \frac{1}{\bar{l}_C \Sigma_t^C} \cdot \left( 1 - \frac{1}{\left( 1 + \frac{\bar{l}_C \Sigma_t^C}{n_{Clad} + 1} \right)^{n_{Clad} + 1}} \right) \quad (2.63)$$

with

$n_{Clad}$  geometric factor for the cladding:

$$n_{Clad} = 3.58 + 0.4X + 3.5X^2 \quad \text{for } X \leq 0.4$$

$$n_{Clad} = 0.474 + 15.057X + 13.73X^2 \quad \text{for } X > 0.4$$

$$X = \frac{\Sigma_t^C \bar{l}_C}{(1 + \Sigma_t^C \bar{l}_C)}$$

The combination of escape probability  $P_e$  and the Dancoff correction represents the total escape probability of a fuel neutron to have its next collision in the moderator. In ULFISP equation (2.64) taken from reference [44] is used for this:

$$P^{FM} = \frac{P_e \cdot (1 - C_{withClad})}{1 + C_{withClad} \cdot (1 - \tau \cdot P_e)} \quad (2.64)$$

with

$P^{FM}$  the neutron transition probability from fuel to moderator (see as well equation (2.35))

After the calculation of the energy dependent escape probability, the module CSIGSD calculates the moderator collision density by solving the second line of equation (2.35). This moderator collision density is used as starting value for the calculation of the fuel collision density in the module PHICAL. PHICAL solves the first line of equation (2.35). This collision density is then used as a first approximation in PHICAL\_UP if the new scattering option is chosen. Using the precalculated scattering transfer probabilities of DOUBLE3, PHICAL\_UP performs the energy- and temperature dependent scattering treatment. The improved neutron spectrum is then prepared for the use in CALGRN as weighting spectrum for multi group cross section calculation utilizing equation (2.3). Doing so CALGRN needs the considered group structure information which is provided by the KAPROS module ENERGY which is not a part of ULFISP. At the end of every ULFISP calculation a binary multigroup library in GRUMA format is written into the working directory and can then be used through the secondary input option of GRUCAL.

## 2.5 The Monte Carlo method

In contrast to deterministic methods which solve the transport equation, Monte Carlo methods do not solve an explicit equation [57]. They rather obtain answers by simulating individual particles and recording some aspects of their average behavior. An often mentioned way to characterize Monte Carlo simulations is: “Think as a particle” [17] which means that every single event during the “life” of a neutron is simulated. An example of “the life of a particle” in a Monte Carlo simulation is described in the following. In this work the Monte Carlo code MCNPX [58] is used for comparison with deterministic approaches. Therefore the different elastic scattering treatments which are performed in chapter 3.2 are introduced here.

### 2.5.1 Some principal aspects of the Monte Carlo method

The following describes the Monte Carlo method in general. Most of it has been taken from the MCNP 4C manual [57]. Monte Carlo can be used to theoretically describe a statistical process. An advantage in respect to deterministic methods is that it is very powerful in describing complex geometric models. The individual probabilistic events that comprise a process are simulated sequentially. The probability distributions governing these events are statistically sampled to describe the total phenomenon. The statistical sampling process is based on the selection of random numbers – analogous to throwing dice in a gambling casino – hence the name “Monte Carlo.” In particle transport the Monte Carlo technique is following each of many particles from its birth to its death. Death in a “neutron” sense means disappearance. Probability distributions are randomly sampled using transport data to determine the outcome of each step of a particles life. The probabilistic data can have a continuous energy structure or multigroup structure like deterministic application. In this work only continuous energy cross section data has been used. Figure 2.10, taken from the MCNP Manual, illustrates the random history of a neutron incident on a slab of material that can undergo fission.

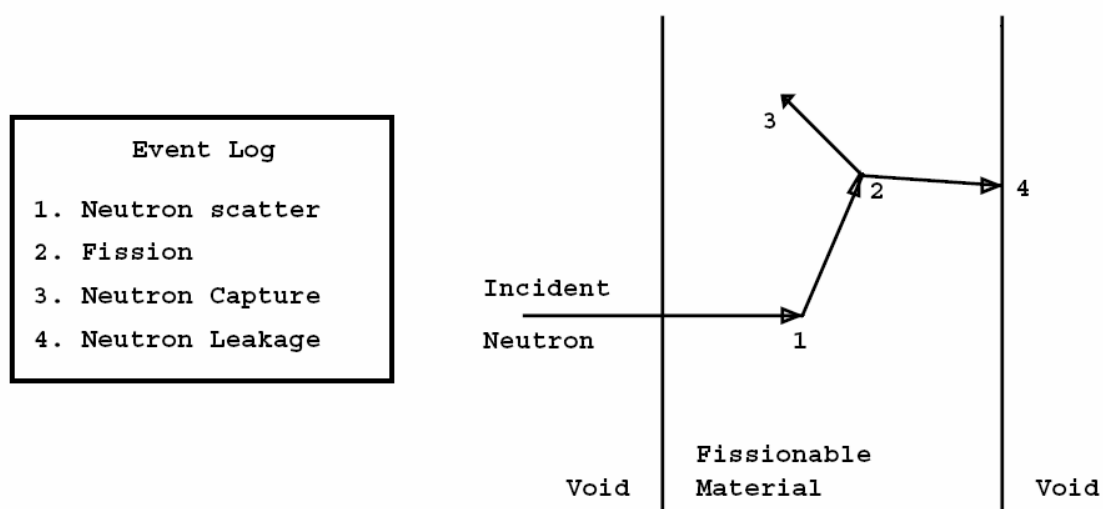


Figure 2.10: Random history of an incident neutron taken from [57]

By selecting randomly numbers between 0 and 1, by respecting laws of physics and probabilities (transport data), it is selected if, where and what kind of an interaction takes

place. In the example in figure 2.10 a neutron collision occurs at event 1. The neutron is scattered in a different direction which is determined randomly from the physical scattering distribution. At event 2 fission takes place, resulting in the termination of the incoming neutron and the birth of two outgoing neutrons. One neutron is banked for later analysis. The first fission neutron is captured in event 3 and terminated. The banked neutron is now retrieved and, by random sampling, leaks out at event 4. Now this neutron history is complete. The more histories are followed the more precise are the neutron distributions.

In this work the Monte Carlo application was used for comparison with the deterministic code KAPROS/ULFISP [16]. The comparison includes reaction rates in a part of the epi-thermal energy region between 4 and 150 eV. This comparison was performed for a thermal PWR-pin cell configuration. That's why the neutron density in this epi-thermal energy region was relatively low. For receiving good precise results, also called "results with a low standard deviation", a much higher number of histories had to be computed to receive low standard deviations for these reaction rates in the epi-thermal energy region. The computation time for this problem would have been in the range of days to over a week. Due to the fact that parallel computing is a standard feature of MCNPX the computation time could be reduced to hours by utilizing 40 CPU's. Following a high number of single particles allows the parallelization of Monte Carlo computations. Each history is independent from all other histories because neutron to neutron interactions can be neglected in nuclear reactor calculations.

## 2.5.2 Different scattering treatments used in this work with MCNPX

A collision between a neutron and an atom is affected by the thermal motion of the atom. The **free gas thermal scattering treatment** in MCNPX is based on the free gas approximation to account for the thermal motion of the target nucleus. It assumes that the medium is a free gas which implies that no effects of chemical bindings or crystal structures are taken into account. The elastic scattering cross section is considered as energy independent which means that no possible resonances are respected. The temperature dependence of the reaction cross sections can be adjusted by an energy, temperature and isotope dependent factor if the available cross sections do not coincide with the problem temperature. In this work a complete cross section set has been calculated for the exact problem temperatures (see chapter 3.1). Therefore this temperature adjustment was not used in any calculation.

The second aspect of the free gas thermal scattering treatment is respecting the velocity of the target nucleus when the kinematics of a collision are calculated. The target velocity is sampled and subtracted from the neutron speed to get the relative velocity. The effective scattering cross section depends then on the scattering cross section of the relative velocity and the probability density function for the Maxwellian distribution of target velocities. These assumptions allow a thermal scattering treatment which is adequate for light isotopes which have nearly constant cross sections in the thermal- and lower epi-thermal energy region. The computation time for this treatment is almost as fast as a completely non-thermal scattering treatment. In MCNPX standard versions the free gas scattering treatment is applied up to energies of  $E=400$  kT. Above this value the velocity of the target is set to zero. For the calculations in this work the  $E=400$  kT border has been set to  $E=200$  eV for all temperatures for consistent comparisons of calculations at different temperatures.

**The  $S(\alpha,\beta)$  treatment** as implemented originally in MCNPX is a complete representation of thermal neutron scattering by molecules and crystalline solids. Two different approaches are allowed [57]. The free gas model, which does not take into account any interactions between nuclides, and the molecular treatment [28], which depends also upon the chemical binding of the particular analyzed atom within its molecule or crystal lattice. In the region of thermal neutron energies, the binding of the scattering nucleus in a solid, liquid or gas

material affects the neutron cross section and the energy and angular distribution of secondary neutrons. These effects are described in thermal sub-libraries where the thermal scattering law  $S(\alpha, \beta)$  is parameterized in terms of momentum transfer parameter  $\alpha$  and energy transfer parameter  $\beta$  [88]. For bound moderators like hydrogen in water LEAPR [54], [56], a module of the NJOY [54] code, is used to prepare the scattering law  $S(\alpha, \beta)$ . The input  $\alpha, \beta$  data for bindings in solids and liquids is provided by ENDF File 7 format [25] in nuclear data libraries like ENDF/B 6 [24] or JEF3.1 [47], [48]. With these  $S(\alpha, \beta)$  scattering laws THERMR, another NJOY module, is able to calculate thermal incoherent scattering cross sections following equation (2.65) taken from reference [54]:

$$\sigma(E, E', \mu) = \frac{\sigma_b}{2kT} \sqrt{\frac{E'}{E}} e^{-\beta/2} S(\alpha, \beta) \quad (2.65)$$

where  $E$  is the initial neutron energy,  $E'$  is the energy of the scattered neutron,  $\mu$  is the scattering cosine in the laboratory system and  $T$  is the temperature in Kelvin. The dimensionless energy transfer  $\beta$  is defined as:

$$\beta = \frac{E' - E}{kT} \quad (2.66)$$

and  $\alpha$ , the dimensionless momentum transfer, is calculated via equation (2.67):

$$\alpha = \frac{E' + E - 2\mu\sqrt{EE'}}{AkT} \quad (2.67)$$

$k$  is the Boltzmann constant and  $A$  is the ratio of the scatter mass to the neutron mass. The bound scattering cross section  $\sigma_b$  can be obtained from the free scattering cross section  $\sigma_f$ :

$$\sigma_b = \sigma_f \frac{(A+1)^2}{A^2} \quad (2.68)$$

The scattering law  $S(\alpha, \beta)$  describes the binding of the scattering atom in a material. For a free gas of scattering nuclei with no internal structure it is given in equation (2.69):

$$S(\alpha, \beta) = \frac{1}{\sqrt{4\pi\alpha}} \exp\left\{-\frac{\alpha^2 + \beta^2}{4\alpha}\right\} \quad (2.69)$$

The values of the  $S(\alpha, \beta)$  scattering law tables are provided for certain  $\alpha$  and  $\beta$  values. Between these values interpolation must be performed.

The presented  $S(\alpha, \beta)$  treatment does only treat energy independent cross sections [28]. For light isotopes, this is a justified assumption since their cross sections are nearly constant in the thermal and epi-thermal energy region. For heavy isotopes this assumption is rather bad. An improved  $S(\alpha, \beta)$  treatment for heavy isotopes which accounts for the energy dependence of cross sections, has been implemented into the NJOY code by Rothenstein [78]. This new scattering treatment is presented in more detail in chapter 2.2. In this study the MCNPX calculations performed in chapter 3.2 have been performed with the standard  $S(\alpha, \beta)$  scattering treatment of MCNPX for water and with the energy- and temperature dependent scattering approach of Rothenstein for uranium-238.

# 3 Pin Cell Application

Chapter 3 presents results for  $\text{UO}_2$  - pin cell calculations utilizing temperature and cross section dependent scattering kernel in ULFISP. In the first part the pin cell problem is specified and phenomena resulting from the new scattering treatment are presented and explained. In the second part a first validation of the new scattering approach in ULFISP is performed via a comparison with the Monte Carlo solution of Dagan and Rothenstein [26] of the new energy- and temperature dependent scattering treatment. The third part is dealing with the influence of the new scattering treatment on burnup and isotope vectors. Again the  $\text{UO}_2$  pin cell is analyzed. Furthermore, the analysis is extended for MOX fuel. In the last part results utilizing the hybrid scattering method are presented. Analyses with the hybrid method are performed for the determination of isotopes which cause significant changes, e.g. in reactivity, by utilizing different scattering treatments.

## 3.1 Pin cell results

### 3.1.1 Problem specifications

The new scattering treatment in ULFISP leads to changes in the group cross section weighting spectra. These changes in the weighting spectra or neutron flux form are analyzed in the following chapter on the basis of a typical PWR pin cell. Basic specifications have been taken from a PWR assembly benchmark [71] from “Gesellschaft für Anlagen- und Reaktorsicherheit” but slightly changed for simplicity. E.g. instead of Zircalloy-4 with several different isotopes only natural Zirconium was considered and therefore the atomic density was adjusted slightly. The presented geometric pin cell model corresponds to a cylindrized Wigner-Seitz cell. The fuel contains three isotopes uranium-238, uranium-235 and oxygen-16. The moderator is water with a boron concentration of 500 ppm. The fuel rod power is 170,5 W/cm. The problem specifications are summarized in table 3.1. Additionally, the exact isotopic concentrations are listed in table 3.2.

Zone	Content	dimensions	Temperature & pressure
fuel	$\text{UO}_2$ (4% U-235)	Outer radius = 0.411 cm	T=800 K
cladding	Zircalloy-4	Outer radius = 0.475 cm	T= 605 K
moderator	$\text{H}_2\text{O}$ , 500ppm $\text{Bor}_{\text{nat}}$	Pitch=1.272 cm (equivalent outer radius= 0.71765 cm)	T=583 K, p=15,8 MPa

Table 3.1: Problem specification of the  $\text{UO}_2$  pin cell

Material	Fuel pin	Cladding	Moderator
U-238	2.095999E-02	---	---
U-235	8.844818E-04	---	---
O-16	4.368894E-02	---	2.500190E-02
Zr-nat	---	5.10376E-02	---
H-1	---	---	5.000381E-02
B-10	---	---	4.1419E-06
B-11	---	---	1.6672E-05

Table 3.2: Isotopic concentrations ( $10^{24}$  atoms/cm<sup>3</sup>)

The effective group cross section constants are calculated for all fuel isotopes by ULFISP and have been taken as input for pin cell calculations with KAPROS/KARBUS [16]. The group structure used is the 69-group structure from the WIMS system [3]. Effective group cross section have been calculated for the 20-27 WIMS-groups according to 907 – 4 eV. The groups which are effected by the new method are group 22-27 according 149-4 eV. Group 20 and 21 have been added to the procedure because of their high influence on integral results. The new scattering treatment has not been applied at higher energies because the importance of up scattering decreases strongly at higher energies (>100 eV) which will be shown later in this chapter.

For the weighting of the group cross sections the neutron flux form is used. For analysis of the new scattering approach it can be advantageous to have a look at the collision density. The collision density is defined as the neutron flux density multiplied with the total cross section as presented in equation (3.1). A high cross section represents a high probability for reactions. Therefore this multiplication denotes energy regions with high cross sections (resonances) more precisely.

$$F(E) = \Phi(E) \cdot \Sigma_t(E) \quad (3.1)$$

with:

- F collision density
- $\Phi$  neutron flux density
- $\Sigma_t$  total cross section

### 3.1.2 Fine flux calculation results

Figure 3.1 shows the collision densities of the asymptotic and the energy- and temperature dependent scattering treatments between 4 and 160 eV. The large peaks result from uranium-238 s-wave resonances while the small ones mainly follow from uranium-235 p-wave resonances. The two curves look very similar except at the large uranium-238 resonance peaks where a slightly enhanced collision density is visible at the second (~20 eV), third (~37 eV), fourth (~66 eV) and fifth (~102 eV) resonance. At the first uranium-238 resonance a slightly decreased collision density is visible.

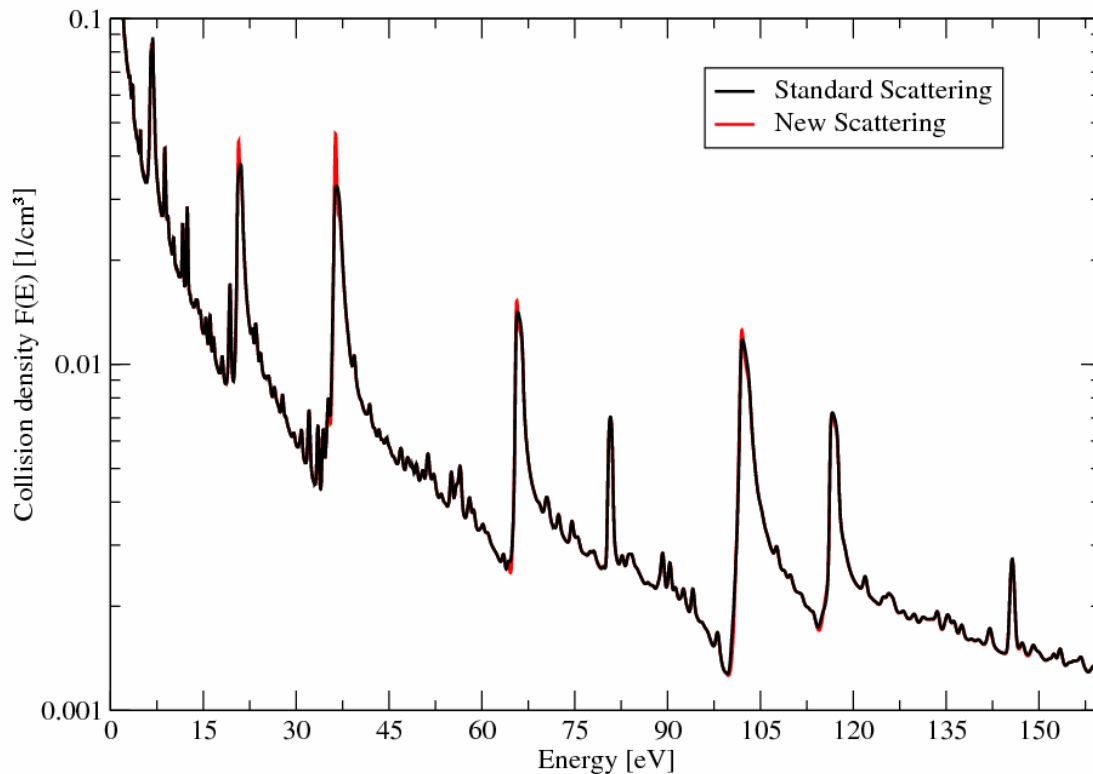


Figure 3.1: Collision Densities of a PWR-UO<sub>2</sub> fuel over energy in the lower epithermal energy region at T=800K

A closer look at the shapes of the collision densities in the energy region of the first uranium-238 resonance in figure 3.2 shows that the total differences are relatively small but the different physical description is clearly visible as well.

The black curve representing the collision density of the standard approach has a single peak at the right side of the resonance showing the increased absorption of down scattered neutrons. The red curve shows the collision density of the new scattering method. It points out two peaks on each side of the resonance, one resulting from down scattering and one from up scattering. Furthermore the collision density calculated by the new method shows a small dent between the two peaks resulting from resonance self shielding.

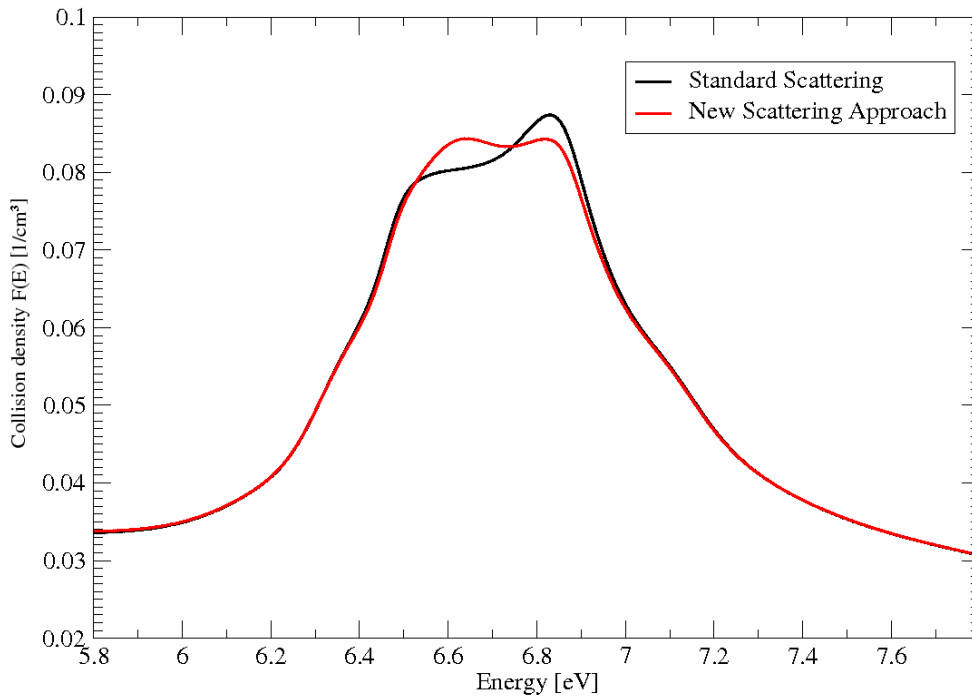


Figure 3.2: Collision densities of PWR-UO<sub>2</sub> fuel in the energy range of the first U-238 resonance at T=800 K

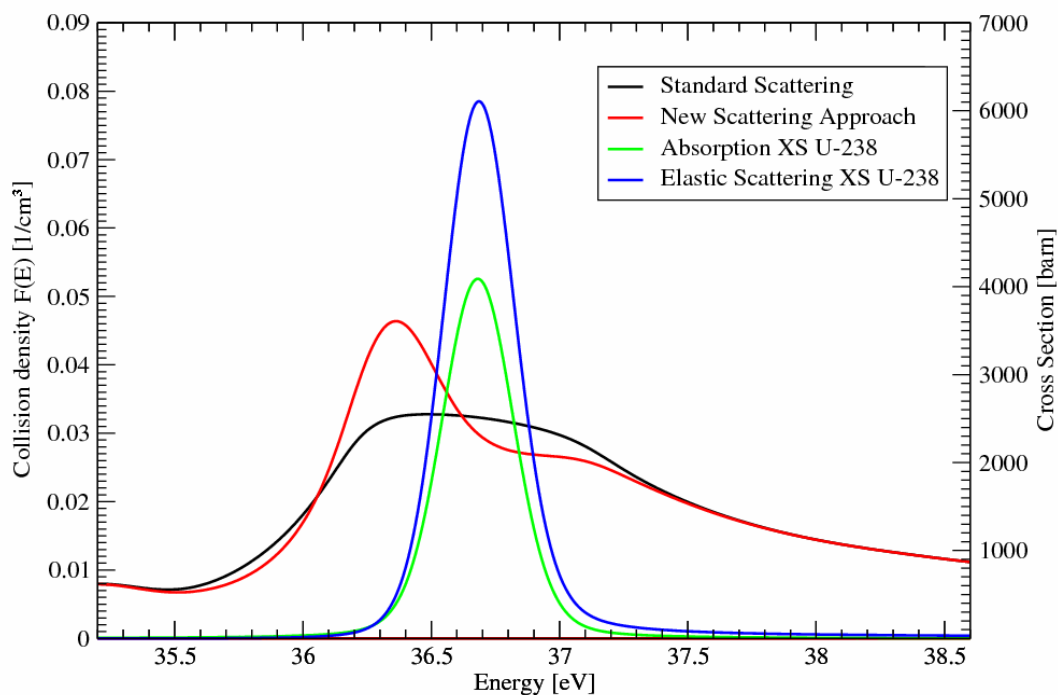


Figure 3.3: Collision densities of PWR-UO<sub>2</sub> fuel in the energy range of the third U-238 resonance and U-238 elastic scattering and absorption cross sections at T=800 K

Figure 3.3 shows the collision densities (black and red curves, left, linear scale) of the two different scattering treatments at the energy range of the third uranium-238 resonance and the absorption and the elastic scattering cross section of uranium-238 (green and blue curves, right, logarithmic scale). The collision density provided by the new scattering method (red

curve) reflects the strongly increased collision density at the energetic lower shoulder of the resonance while it shows a decreased collision density at the energetic higher shoulder. The differences in the collision densities result from up scattering. At the left resonance shoulder more neutrons are scattered into the resonance region due to up scattering while on the right shoulder less neutrons are scattered into the resonance due to reduced down scattering. The large values of the elastic scattering cross section in the resonance energy region increase the effect.

The corresponding flux forms of the third large uranium-238 resonance are presented in figure 3.4. The flattened flux shape left to the flux depression is resulting from the increased up scattering into the resonance. Taking the new flux form as weighting function for group cross section calculation leads to a lower importance of the energy region close to the left resonance shoulder. This leads to a relatively higher importance of all other energy regions in the energy group of the third uranium-238 resonance. Of course, the resonance region with its extremely high absorption cross section gains importance too and therefore leads to a higher absorption group cross-section constant.

For the chosen pin cell, effective group cross-sections with both scattering methods have been calculated. With these group cross-sections sets two pin cell calculations have been performed. Intermediate and integral results are discussed in chapter 3.2.

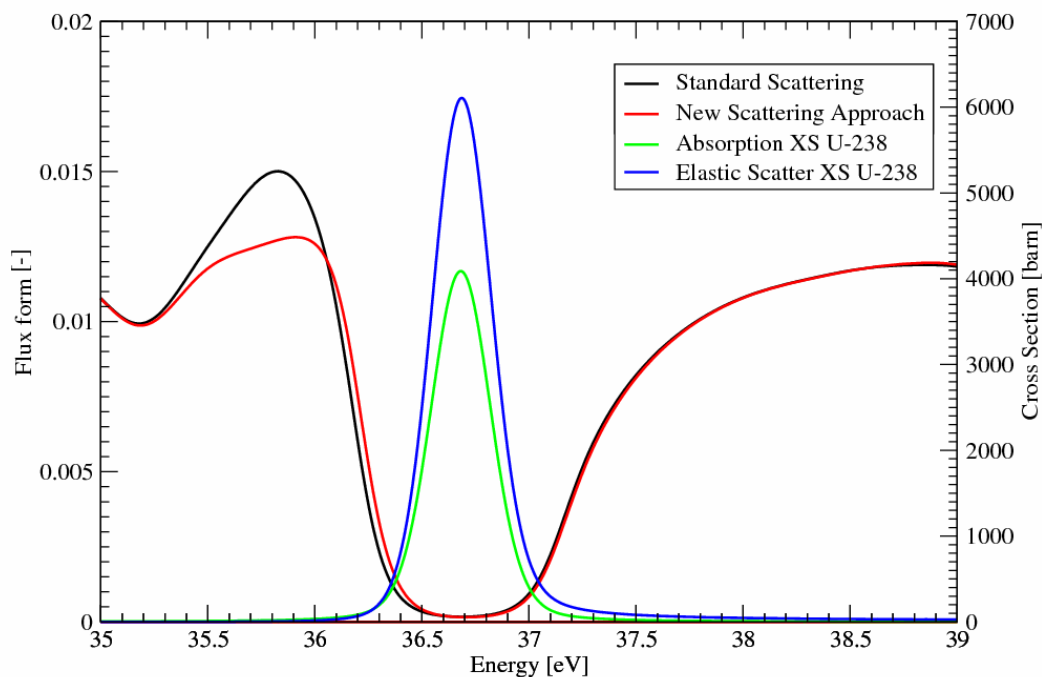


Figure 3.4: Neutron flux forms of PWR- $\text{UO}_2$  fuel in the energy range of the third U-238 resonance and U-238 elastic scattering and absorption cross sections at  $T=800$  K

Having a look over the whole energy region treated by the new scattering method in figure 3.5 presents hardly visible differences of the two flux form except in the energy range of the third uranium-238 resonance. The reason why the method has its strongest influence at the third uranium-238 resonance lies in the ratio between elastic scattering and the total cross section.

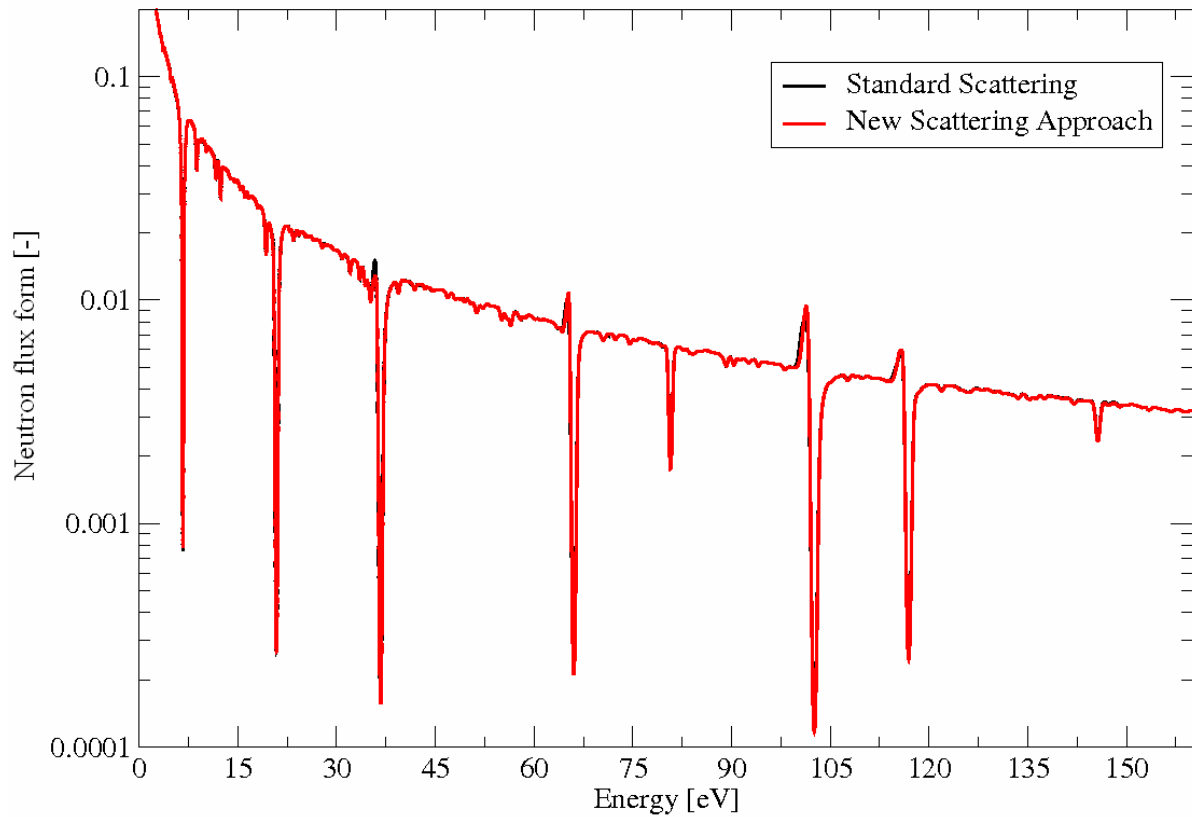


Figure 3.5: Neutron flux form of a PWR-UO<sub>2</sub> fuel over energy in the lower epithermal energy region at T=800K

Figure 3.6 indicates the elastic scattering cross section and the difference between the total and the elastic scattering cross section of uranium-238. The shape of the difference between total and elastic cross section is very close to the absorption cross section because absorption and elastic scattering are the dominating cross sections of uranium-238 in the considered energy range. The elastic scattering cross section gets ahead all other cross sections at the peak of the third large resonance at E=36,7 eV. At this energy the ratio of elastic scattering to

the sum of all other reactions is approximately  $\frac{\sigma_e}{\sigma_t - \sigma_e} \approx 1.5$

Clearly visible in figure 3.6 is the dominance of the elastic scattering at the fifth large uranium-238 resonance at E=102,5 eV, too. The ratio of elastic scattering to the sum of all

other cross sections in the resonance peak is there even  $\frac{\sigma_e}{\sigma_t - \sigma_e} \approx 3$ .

Nevertheless, the double value, the changes in the flux form shown in figure 3.5 are much smaller. Responsible for this is the higher energetic difference between neutron and target nucleus. The probability for up scattering at energy E=102,5 eV is relatively small compared to the probability at energy E=36,7 eV. The importance of the ratio of elastic scattering cross

section to sum of all other cross sections  $\frac{\sigma_e}{\sigma_t - \sigma_e}$  is investigated further in the following

chapter.

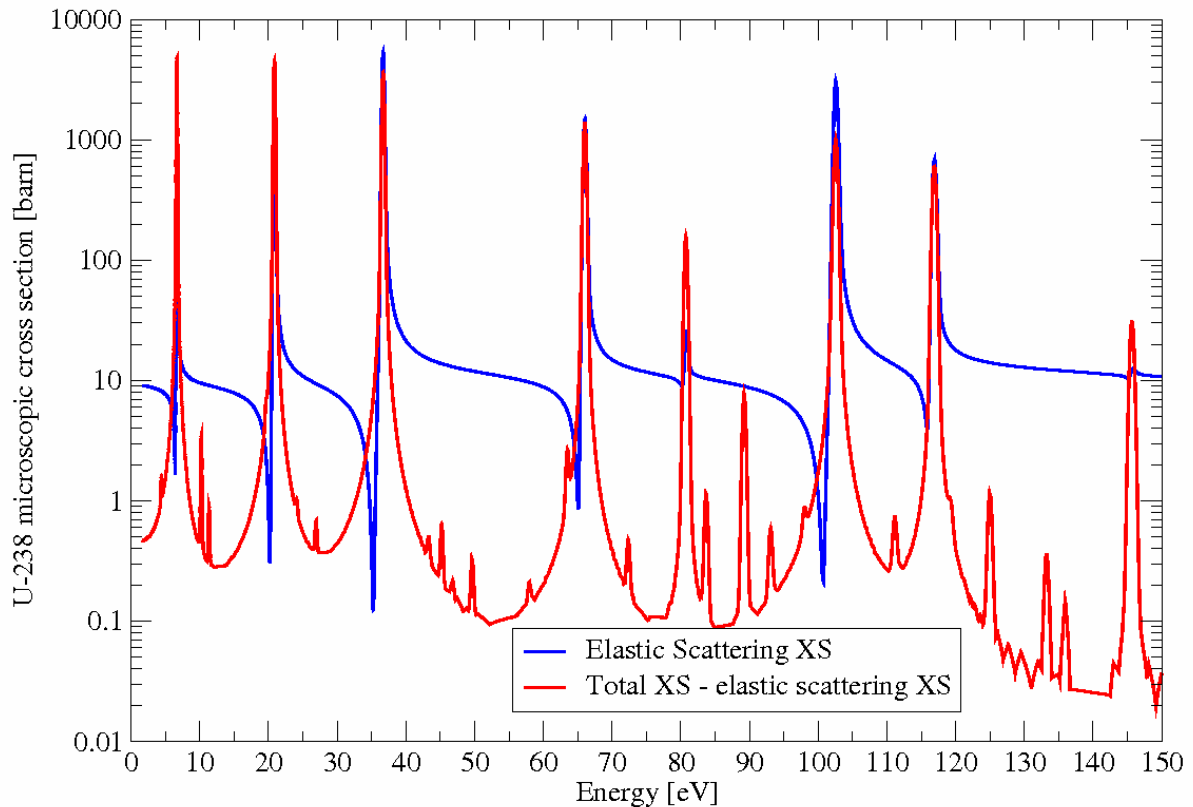


Figure 3.6: Elastic scattering cross section and difference between total and elastic scattering cross section of U-238

## 3.2 First validation of ULFISP using MCNPX

The new deterministic scattering approach in ULFISP will be validated by the existing energy and temperature dependent scattering treatment available in MCNPX. In chapter 3.2.1 the different scattering approaches of ULFISP and MCNPX are shortly introduced. Then differences between the two ULFISP scattering approaches are presented for the pin cell problem introduced in chapter 3.1.1. In chapter 3.2.3 a comparison between ULFISP and MCNPX is presented along changes in absorption rates and changes in reactivity values occurring through the different scattering approaches.

### 3.2.1 Scattering treatments in ULFISP and MCNPX

In the deterministic fine flux module ULFISP two different scattering treatments are analyzed. The asymptotic scattering treatment implemented by Broeders [16] is introduced first. This approach calculates the neutron flux form in the epithermal energy region ( $>$  thermal Maxwell spectra). Therefore it assumes constant scattering cross sections (it does not take into account cross section resonances) which lead to a constant slowing down value. Beyond, it adopts that the target nucleus is at rest, which means its temperature is  $T = 0$  K. All

calculations with the asymptotic scattering approach have been performed by weighting the group constants in the energy interval from 911,8 to 4 eV (energy group 20 to 27) with the flux spectrum calculated by ULFISP. Further simplifications and functions of ULFISP are summarized in chapter 2.4. More detailed information about the scattering treatments is presented in chapter 2.2 and chapter 2.3.

The new scattering treatment implemented into ULFISP in this work enables the usage of energy dependent cross sections (cross section resonances are respected), as well as taking into account the movement of the target nucleus. This means that the real temperature of the target nucleus is considered which can lead to up scattering of the neutron. All calculations with the new scattering approach presented in chapter 3 have been performed in the energy interval from 4 to 149 eV (WIMS [3] energy group 22 to 27). As explained in chapter 2.3, for the new scattering approach a precalculation is necessary with the asymptotic treatment in ULFISP. The precalculation was performed exactly like mentioned above leading to fine flux weighted multi group cross sections with the asymptotic method for group 20 and 21 and with the new scattering method from group 22 to 27. Chapter 2.3 explains the ULFISP scattering treatments in detail.

For validation of the new scattering approach in ULFISP comparisons with the Monte Carlo code MCNPX are presented in this chapter. Therefore three different scattering options in MCNPX have been utilized and compared with the two ULFISP fine flux methods. The first scattering option is the standard MCNPX scattering approach for the epithermal energy region. It facilitates up scattering up to energies of  $E=200$  eV taking into account the movement of the target nucleus via the Maxwell-Boltzmann spectra but is not taking care of the energy dependence of cross sections and uses therefore only the potential scattering cross section. Above the energy of  $E=200$  eV neither target nucleus movement nor up scattering is performed. In the following, this scattering treatment will be called “Standard MCNPX” treatment.

The second option is the use of  $S(\alpha,\beta)$ - probability tables [28] for heavy nuclei in the epithermal energy resonance region. Based on the thermal neutron scattering for light isotopes this “ $S(\alpha,\beta)$  method” has been expanded by Rothenstein and Dagan for heavy isotopes in the lower epithermal energy ( $E < 200$  eV) region, respecting the thermal motion of heavy isotopes as well as taking the energy dependence of their cross sections into account. It will be named “ $s(\alpha,\beta)$  MCNPX” later on.

The third option was established for better comparison with the deterministic asymptotic method used in ULFISP. The  $E = 200$  eV border mentioned before is lowered to  $E = 4$  eV which means that no target nucleus movement (and therefore no up scattering) is respected for energies higher than  $E = 4$  eV and no energy dependence of cross sections is accounted for, but only the potential scattering cross section. This scattering method will be called “0 K MCNPX” (zero Kelvin) method according to the target nucleus being at rest for energies  $E > 4$  eV. A more detailed description of the scattering treatments in the Monte Carlo code MCNPX and of the Monte Carlo method itself is provided in chapter 2.5.

Rothenstein and Dagan implemented the cross section and temperature dependent scattering kernel for heavy isotopes into the NJOY module THERMR [54] which generates  $S(\alpha,\beta)$  tables for MCNPX [58]. Hence, NJOY enables the usage of the cross section and temperature dependent scattering kernel in Monte Carlo calculations. In addition to the normal differences between deterministic and stochastic neutronic codes the energy- and temperature dependent scattering approaches differ in following aspects:

1. For an energy range between 4 eV and 200 eV about 1260 scattering kernels energy points are used in MCNPX, which makes interpolation between these points necessary. In ULFISP for every energy point in the fine flux calculation scattering kernels are used (~13100 energy points (1.6-200 eV))
2. The absolute energetic resolution in the examined energy range has been ~13100 points in ULFISP compared to the continuous energy resolution in MCNPX
3. The  $S(\alpha,\beta)$  tables contain anisotropic scattering information (eight angular directions have been applied), in ULFISP only isotropic scattering is applied. For the simple geometry of the examined pin cell the difference between anisotropic and isotropic scattering is insignificant
4. In the MCNPX calculations the scattering kernels are only applied for uranium-238 while in ULFISP it is used for every fuel isotope, uranium-238, uranium-235 and oxygen-16. The importance of isotopes to the single differential scattering kernel is investigated in chapter 3.4

For first validation a comparison on the basis of a typical PWR pin cell has been applied between MCNP and KARBUS/ULFISP. The problem specifications are summarized in chapter 3.1. For comparison, MCNPX-26f [58] and KAPROS [16] have been used. A detailed program flow chart of KARBUS and ULFISP which are modules inside the KAPROS system is presented in chapter 2.4.

### 3.2.2 PWR pin cell calculations with ULFISP

The code comparison presented in this chapter is related to the pin cell problem presented in chapter 3.1. Differences in absorption rates per energy group, criticality and Doppler coefficient are shown. Therefore, in each case of the two scattering methods in ULFISP and the three scattering methods in MCNPX, two calculations have been performed one with fuel temperature of  $T=800$  K and one with  $T=1200$  K.

The group wise absorption rates in ULFISP have been calculated by multiplying the effective absorption group constants with the corresponding neutron fluxes from WEKCPM [16] the one dimensional diffusion solver used in KARBUS [16] for solving the complete pin cell problem. Table 3.3 shows the absorption rates of the two different ULFISP calculations and their differences of important energy groups for temperature  $T=800$  K.

Table 3.3 presents absorption changes occurring between the two different scattering options in ULFISP. The effect leads in total to increased neutron absorption of 0.754 %. The biggest difference between the two models appears in energy group 24 with an increase of over 3% absorption resulting from the third large uranium-238 resonance. The second large resonance provides as well an important addition of ca. 1.1% increased absorption. Also group 23 with the fourth large uranium-238 resonance contributes ca. 0.6 % increased absorption. The higher the energy, the lower the probability for up scattering and the lower the importance of the new scattering treatment. Despite the fact of three large resonances inside one group, the increase of absorption in group 22 is of the same amount as the increase in group 26 where no large uranium-238 resonances exist. The increased absorption in group 26 results only because of up scattering from the potential cross section. The new scattering treatment does not necessarily lead to more absorption. Group 27 shows a decreased absorption rate although it includes a huge resonance.

WIMS group number, energy range, important U-238 resonance	<b>I</b> Asymptotic scattering method (only down scattering) Absorption Rate	<b>II</b> XS- and temperature dependent scattering kernel Absorption Rate	<b>II - I</b> $\Delta$ Absorption rate [%]
27 (4 – 9,877 eV) 1 <sup>st</sup> U-238 resonance	$1.64022 \cdot 10^{-1}$	$1.63582 \cdot 10^{-1}$	- 0.268
26 (9,877-16 eV)	$6.03162 \cdot 10^{-3}$	$6.02074 \cdot 10^{-3}$	+ 0.180
25 (16 – 27,7 eV) 2 <sup>nd</sup> U-238 resonance	$9.17083 \cdot 10^{-2}$	$9.27006 \cdot 10^{-2}$	+ 1.082
24 (27,7 – 48 eV) 3 <sup>rd</sup> U-238 resonance	$7.27511 \cdot 10^{-2}$	$7.5059 \cdot 10^{-2}$	+ 3.172
23 (48 – 75,5 eV) 4 <sup>th</sup> U-238 resonance	$3.26878 \cdot 10^{-2}$	$3.2896 \cdot 10^{-2}$	+ 0.637
22 (75,5 – 149 eV) 5 <sup>th</sup> , 6 <sup>th</sup> , 7 <sup>th</sup> U-238 resonance	$5.86023 \cdot 10^{-2}$	$5.8716 \cdot 10^{-2}$	+ 0.194
<b>Total</b> 27-22 (4 – 149 eV)	$4.25803 \cdot 10^{-1}$	$4.28975 \cdot 10^{-1}$	+ 0.754

Table 3.3: Capture group cross section of U-238 and their relative deviations for the two ULFISP scattering models for the first seven U-238 resonances at T=800 K

The change in absorption rates depends on two values: Energy and  $\lambda$  which is the ratio of elastic scattering to total cross section (equation (3.2)). In general it can be stated that the lower the energy E of the incident neutron and the higher the ratio  $\lambda$ , the higher the change will be of the absorption rate.

$$\lambda = \frac{\sigma_s}{\sigma_t} \quad (3.2)$$

To be more specific, the presented results depend on the ratio  $\Lambda$  of the macroscopic elastic scattering cross section of uranium-238  $\Sigma_s^{U-238}$  to the total macroscopic cross section of the fuel  $\Sigma_t^{fuel}$ :

$$\Lambda = \frac{\Sigma_s^{U-238}}{\Sigma_t^{fuel}} \quad (3.3)$$

Table 3.4 lists the ratios of elastic scattering to total cross section in the peak of the first seven large uranium-238 resonances. All these macroscopic cross sections have been taken directly from the calculations and are problem dependent, of course. Nevertheless, ratios  $\lambda$  calculated with problem independent microscopic cross sections would show very similar values.

The cross section ratios fit very well to the absorption gain through the new scattering model. Looking at the 22<sup>nd</sup> group with resonance number five, six and seven shows the impact of energy to the change in the absorption rate. Although the sixth resonance is the “strongest scattering” resonance with a ratio  $\Lambda=0.753$  and a high absolute scattering cross section value as well, the absorption rate change is significantly lower in comparison to the second, third or fourth resonance (table 3.3).

WIMS group number, number resonance, resonance peak energy	Macroscopic elastic scattering XS U-238 [barn/cm <sup>3</sup> ]	Macroscopic total XS Fuel [barn/cm <sup>3</sup> ]	Ratio $\Lambda$
27 1 <sup>st</sup> U-238 resonance 6.67 eV	6.69	107.42	0.062
25 2 <sup>nd</sup> U-238 resonance 20.87 eV	42.71	138.08	0.309
24 3 <sup>rd</sup> U-238 resonance 36.7 eV	114.03	190.48	0.599
23 4 <sup>th</sup> U-238 resonance 66.06 eV	30.85	60.22	0.512
22 5 <sup>th</sup> U-238 resonance 80.74 eV	0.49	3.94	0.125
22 6 <sup>th</sup> U-238 resonance 102.55 eV	64.56	85.74	0.753
22 7 <sup>th</sup> U-238 resonance 116.95 eV	14.32	27.27	0.525

Table 3.4: Macroscopic elastic scattering cross sections of U-238 and macroscopic total fuel cross sections and their ratios  $\Lambda$  in the peak of the first seven large U-238 resonances at T=800 K taken from a KARBUS/ULFISP calculations

### 3.2.3 Comparison calculations between ULFISP and MCNPX

For first validation of the new scattering approach in ULFISP a comparison with the existing Monte Carlo approach in MCNPX will be performed along the pin cell problem introduced in chapter 3.1. Figure 3.7 compares neutron flux from ULFISP (left ordinate) and MCNPX (right ordinate) for temperature T= 800K in the energy range of the third large uranium-238

resonance ( $\sim 36.6$  eV). The absolute values of the flux form are arbitrary. Visible differences at the left ordinate of figure 3.7 result from a more thermal neutron flux in the deterministic calculation. This may have numerous reasons. The most probable one seems to be the different treatment of the escape probability in the two codes. However this effect is not of high importance for this study because only the differences between methods of one code are compared to differences between methods of the other code. Direct comparisons of absolute values between ULFISP and MCNPX are not part of this study.

Clearly visible in figure 3.7 is the similar trend of the four curves. Also visible is that the difference between the black and the red curve which represent ULFISP neutron spectra is larger than the difference between the green and the blue curve which represent the MCNPX neutron spectra. This is consistent with the values presented in table 3.3 and table 3.5 in energy group 24 where the difference in absorption is higher in the ULFISP calculations. The MCNPX curves in figure 3.7 show a serrated trend which is especially visible between 35.5 and 36 eV. This results from the relatively high standard deviation of the energy flux resolution in the Monte Carlo approach. Although an extreme high number of histories ( $4 \cdot 10^9$ ) has been applied, the fine energy group structure of 3000 groups between 4 and 50 eV is still too high for the calculation performance of the Monte Carlo calculation.

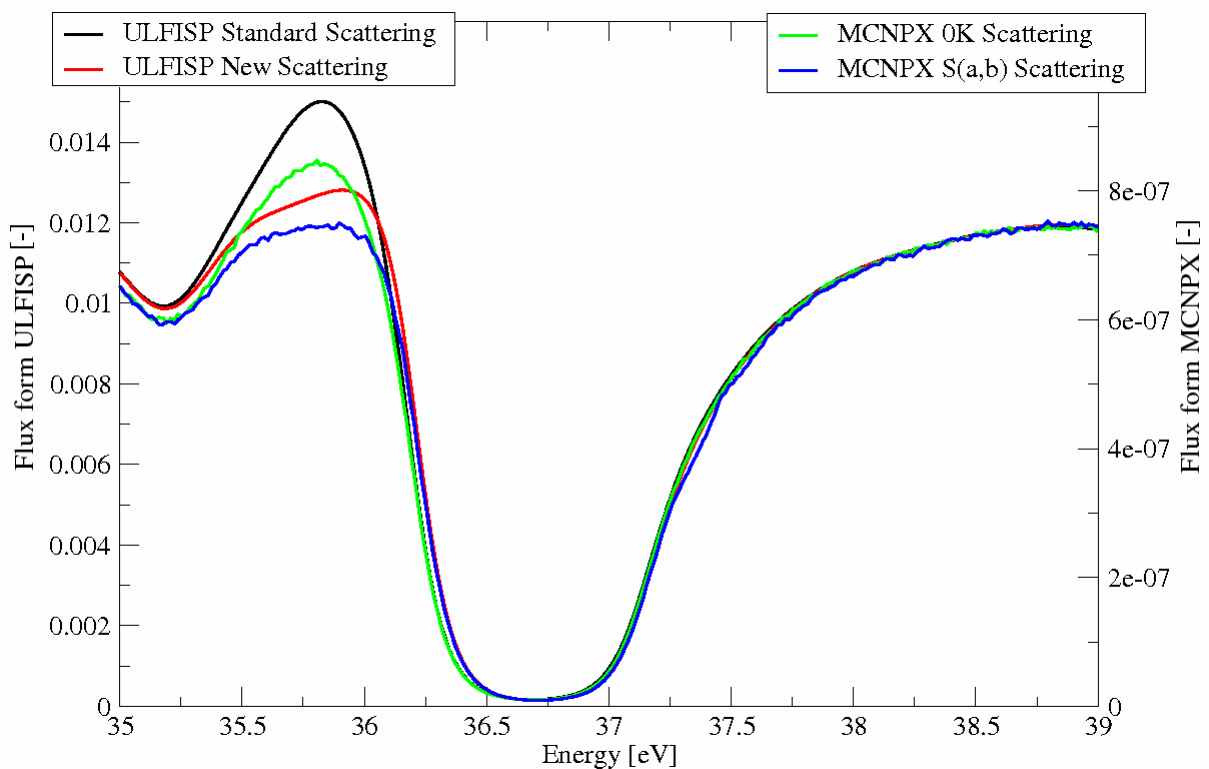


Figure 3.7: Neutron flux forms of ULFISP and MCNPX for a PWR-UO<sub>2</sub> fuel in the energy range of the third U-238 resonance at T=800 K

Table 3.5 shows absorption rates, standard deviations, relative differences and corresponding relative deviations. Table 3.5 presents these for the “standard” MCNPX scattering model, for the “0 K” scattering model and for the advanced “s( $\alpha,\beta$ )” scattering model.

The energy- and cross section dependent scattering treatment leads in total to increased neutron absorption of 0.91 % between the standard MCNPX and the “s( $\alpha,\beta$ )” approach and to 0.60 % between the “0 K” and the “s( $\alpha,\beta$ )” model. Although the calculations have been

performed with a very high number of histories ( $1.2 \cdot 10^8$ ) for a single pin cell, the standard deviations of the absorption sum of all considered energy groups is still relatively high. The reason for this is the “thermal” character of the analyzed PWR pin cell problem, which means that the neutron flux is relatively low in the analyzed epi-thermal energy region.

WIMS group number, energy range, important U-238 resonance	Absorption Rates (Reaction standard deviation)			$\Delta$ Absorption Rates [%] (+/-)	
	MCNPX standard	MCNPX 0 K	MCNPX $s(\alpha,\beta)$	$\Delta$ MCNPX $s(\alpha,\beta)$ - standard	$\Delta$ MCNPX $s(\alpha,\beta)$ - 0 K
27 (4 – 9,877 eV) 1 <sup>st</sup> U-238 res.	1.094E-02 (4.0E-04)	1.096E-02 (4.0E-04)	1.096E-02 (4.0E-04)	0.18% (0.06%)	-0.06% (0.06%)
26 (9,877-16 eV)	4.168E-04 (4.0E-04)	4.168E-04 (4.0E-04)	4.160E-04 (4.0E-04)	-0.18% (0.06%)	-0.19% (0.06%)
25 (16 – 27,7 eV) 2 <sup>nd</sup> U-238 res.	6.027E-03 (5.0E-04)	6.079E-03 (5.0E-04)	6.124E-03 (5.0E-04)	1.60% (0.07%)	0.74% (0.07%)
24 (27,7 – 48 eV) 3 <sup>rd</sup> U-238 res.	4.778E-03 (5.0E-04)	4.784E-03 (5.0E-04)	4.903E-03 (5.0E-04)	2.61% (0.07%)	2.49% (0.07%)
23 (48 – 75,5 eV) 4 <sup>th</sup> U-238 res.	2.178E-03 (8.0E-04)	2.177E-03 (8.0E-04)	2.188E-03 (8.0E-04)	0.48% (0.11%)	0.53% (0.11%)
22 (75,5 – 149 eV) 5 <sup>th</sup> , 6 <sup>th</sup> , 7 <sup>th</sup> U-238 res.	3.943E-03 (6.0E-04)	3.949E-03 (6.0E-04)	3.950E-03 (6.0E-04)	0.17% (0.08%)	0.04% (0.08%)
Total 27-22 (4 – 149 eV)	2.828E-02 (1.3E-03)	2.837E-02 (1.3E-03)	2.863E-02 (1.3E-03)	0.91% (0.19%)	0.60% (0.19%)

Table 3.5: Absorption rates of U-238 and their relative deviations for three scattering models in MCNPX for the first seven large U-238 resonances at T=800 K

The differences ( $\Delta$ Absorption Rates in table 3.5) are similar in all energy groups except group 25 which shows an almost doubled absorption rate increase. The general trend of all single energy groups present a bigger absorption increase between the “normal” and the new scattering model than between the “0 K” and the advanced “ $s(\alpha,\beta)$ ” scattering model. Surprisingly, this means that the simpler “0 K” method, which does not respect any target nucleus movement and therefore no up scattering, provides more accurate solutions than the “standard” method which does respect the target nucleus movement. Becker explains in comparable Monte Carlo studies [6] that the temperature- and energy dependent scattering

treatment leads to increased up scattering at the energetically lower resonance shoulder but to increased down scattering at the energetically higher resonance shoulder as well. The dominating effect is problem dependent. If the increase in down scattering is higher than the increase in upscattering the “0 K” scattering method will be closer to the new than to the standard scattering method. For the presented pin cell problem a dominating down scattering effect could be a possible explanation, especially for the absorption rates of the 25<sup>th</sup> group but this could not be investigated further in this study.

Summarizing the comparisons between the ULFISP and the MCNPX enhancement in absorption rates, show first of all, that all three comparisons in absorption rate changes (table 3.3 and table 3.5) show similar trends in general. The biggest changes occur in group 24 in all three cases but with slightly higher values for the ULFISP differences. Group 25 reveals the biggest differences between the Monte Carlo comparisons but with the ULFISP results in between. Group 23 shows small increases for the Monte Carlo approaches and slightly higher changes in the ULFISP comparison. The changes in the 27<sup>th</sup>, 26<sup>th</sup> and the 22<sup>nd</sup> energy groups are negligible for all three cases. The accuracy of the MCNPX calculations despite the standard deviations can be estimated in group number 26. Group 26 does not contain any uranium-238 resonances. Therefore the differences between the  $s(\alpha,\beta)$  and the standard approach should be inside the standard deviations which is not the case.

The better agreement between the ULFISP comparison with the “0 K” and the  $s(\alpha,\beta)$  MCNPX comparison is consistent to the more similar asymptotic (T=0 K) scattering treatment in the “standard” ULFISP approach.

The same calculations as for temperature T= 800 K have been applied for T=1200 K. The changes in the absorption rates are similar but increased compared to the analysis at T= 800 K because of Doppler broadening. The two advanced methods (new ULFISP method,  $s(\alpha,\beta)$  MCNPX method) are compared with their corresponding “0 K” treatment. The reactivity  $k_{inf}$  for the different calculations for temperature T=800 K and T=1200 are shown in table 3.6. The standard deviation for the Monte Carlo reactivity values is  $6 \cdot 10^{-5}$  for all calculations.

	ULFISP standard	ULFISP new	MCNPX 0 K	MCNPX $s(\alpha,\beta)$
$k_{inf}$ T=800K	1.30836	1.30694	1.32204	1.32081
$\Delta k$ [pcm]	142		123	
$k_{inf}$ T=1200K	1.29620	1.29356	1.30936	1.30611
$\Delta k$ [pcm]	264		242	

Table 3.6: Reactivity values and corresponding differences for the pin cell calculations for T=800 K and T= 1200 K

The energy- and temperature dependent scattering treatments in ULFISP and MCNPX are compared with their corresponding “0 K” treatments again. The enlarged reactivity differences  $\Delta k$  show the temperature dependence of the energy- and temperature dependent scattering treatment. The higher temperature leads to higher absorption and a bigger reactivity decline. Secondly, the reactivity change shows very good agreement between ULFISP and MCNPX.

For safety analysis fuel Doppler coefficients  $\alpha_T$  are important indicators. The Doppler coefficient of reactivity is defined by [83]:

$$\alpha_T \equiv \frac{\partial \rho}{\partial T} = \frac{\partial}{\partial T} \left( \frac{k-1}{k} \right) = \frac{1}{k^2} \frac{\partial k}{\partial T} \quad (3.4)$$

Table 3.7 shows the reactivity values, reactivity differences for the temperatures  $T= 800$  K and  $T= 1200$  K and corresponding Doppler coefficients for the different scattering calculation methods in ULFISP and MCNPX.

The temperature dependence of the new scattering treatment leads to a more negative Doppler coefficient as well. In ULFISP the Doppler coefficient is more negative by 10.2 % compared to its 0 K treatment. For MCNPX (using  $s(\alpha,\beta)$  method) the Doppler coefficient is more negative by 9.6 % compared to its 0 K treatment. Nevertheless, the absolute Doppler coefficient values are slightly higher for these two MCNPX calculations. Again worth mentioning is the fact that the “0 K” comparisons are closer to the energy- and temperature dependent methods than the standard MCNPX method which provides the smallest absolute value of the Doppler reactivity coefficient.

compared methods	$k_{\text{inf}}$ , T=800K (st. deviation)	$k_{\text{inf}}$ , T=1200K (st. deviation)	$\Delta k_{\text{inf}}$ [pcm]	$\alpha_T$ [pcm/K] (st. deviation)
ULFISP standard	1.30836	1.29620	1216	-1.776
ULFISP new	1.30694	1.29356	1338	-1.958
MCNPX 0 K	1.32204 ( $6 \cdot 10^{-5}$ )	1.30936 ( $6 \cdot 10^{-5}$ )	1268	-1.814 ( $1.61 \cdot 10^{-3}$ )
MCNPX standard	1.32267 ( $6 \cdot 10^{-5}$ )	1.31066 ( $6 \cdot 10^{-5}$ )	1201	-1.716 ( $1.61 \cdot 10^{-3}$ )
MCNPX $s(\alpha,\beta)$	1.32081 ( $6 \cdot 10^{-5}$ )	1.30694 ( $6 \cdot 10^{-5}$ )	1387	-1.988 ( $1.62 \cdot 10^{-3}$ )

Table 3.7: Reactivity values, differences and Doppler coefficients for the different presented scattering methods for  $T= 800$ K and  $T= 1200$ K

The first validation of ULFISP shows good agreement between the new deterministic and the existing Monte Carlo approach. The absorption rates and corresponding reactivity values show the same trends. The results of the Doppler coefficients are very good, too. The belonging scattering treatments of the deterministic and the Monte Carlo approach show better agreement than the different scattering treatments of single calculation approaches.

### 3.3 Pin cell burnup results

In chapter 3.3 burnup results of the  $\text{UO}_2$  pin cell problem introduced in chapter 3.1 are presented. As the whole problem the burnup steps have been taken from a benchmark [71] proposed by GRS.  $\text{UO}_2$  and MOX fuel burnup calculations have been applied by KARBUS using the two different scattering options in ULFISP for providing problem and burnup dependent cross sections. For determination of the impact of the new scattering treatment on isotopic vectors in the fuel a comparison is presented between the asymptotic scattering approach and the energy- and temperature dependent scattering treatment in ULFISP which is performed for 80 isotopes in the burnup calculations.

In the burnup problem 41 burnup steps are applied, reaching a total burnup of 80 MWd/kg HM after 2157 days. All fuel isotopes which occur in significant amounts are respected in the fine flux calculations in ULFISP. Due to the huge memory requirement for up scattering kernels for 80 isotopes the energy grid resolution has to be reduced to the constant lethargy grid point difference of  $\Delta u=0.9990$  (equation 3.5 for explanation) instead of  $\Delta u=0.9997$  used in previous chapters.

#### $\text{UO}_2$ pin cell burnup results

In the following two burnup calculations are presented for the “GRS-Benchmark” utilizing the two fine flux approaches of ULFISP. Figure 3.8 shows the time dependent reactivity loss of the standard calculation over burnup for the  $\text{UO}_2$  - PWR pin cell with 4 wt. % uranium-235. The differences in reactivity between the two scattering approaches are very small and are not visible in figure 3.8. For this reason the reactivity differences of the two fine flux calculations are presented in figure 3.9.

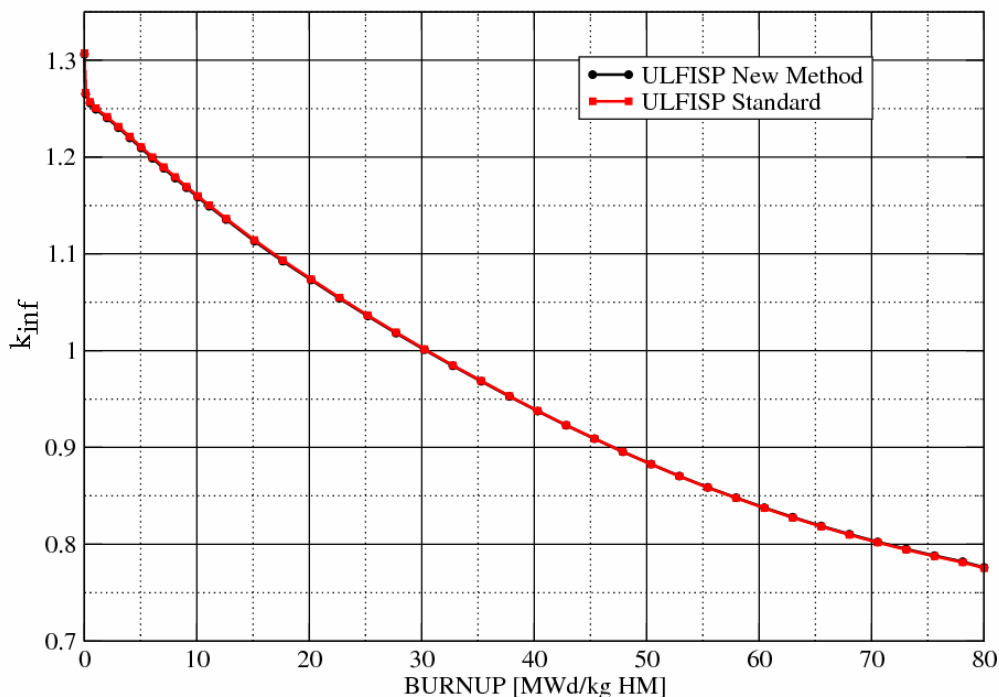


Figure 3.8:  $K_{\text{inf}}$  versus burnup for the two ULFISP approaches for the  $\text{UO}_2$  PWR pin cell with 4 wt. % U-235

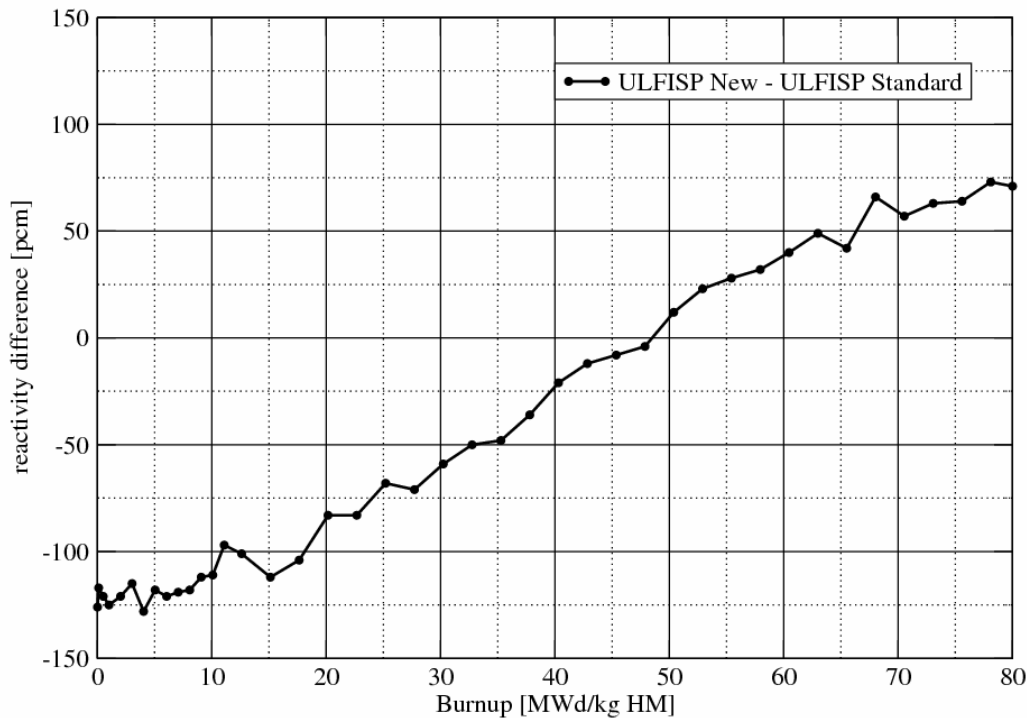


Figure 3.9:  $\Delta k_{\text{inf}}$  versus burnup for the two ULFISP approaches

The characteristic of the differences of the ULFISP fine flux methods indicates that the reactivity decline during burnup of the standard method in ULFISP is slightly higher than the reactivity decrease of the new method.

As shown in previous chapters the new scattering treatment leads to increased neutron absorption in uranium-238 compared to the standard fine flux method. At begin of life (BOL) this manifests itself in a decreased reactivity. During burnup the decreased reactivity is neutralized by the reactivity “insertion” of higher content of produced plutonium-239. After approximately 1300 days (~48 MWd/kg HM) burnup the increased conversion of plutonium-239 causes a higher reactivity in the ULFISP calculation with the new scattering treatment. Figure 3.10 shows the fuel content differences of uranium-235 and plutonium-239 for the two burnup calculations utilizing the two scattering approaches in ULFISP.

The enhanced neutron absorption in uranium-238 leads to a steadily increasing difference of the plutonium-239 content. Since the power is kept constant and more fission is originated from plutonium-239, the difference of the uranium-235 content is increasing, too. The differences of plutonium-239 at BOL and of uranium-235 at EOL appear to be misleading because the shown differences are percentaged. The correct description of increased fissile material is provided by the green curve which presents the combined differences of uranium-235 and plutonium-239. The total increase of fissile material (without plutonium-241) is about 1 % after approximately 2100 days (80 MWd/kg HM). This matches very well to the results of 1 % increased neutron absorption in uranium-238 in thermal reactors investigated by Bouland et al. [14]. Becker et al. [5] determined an increased plutonium-239 content for a PWR-assembly (T=800 K) at 80 MWd/kg HM via Monte Carlo approach to 1.4 %.

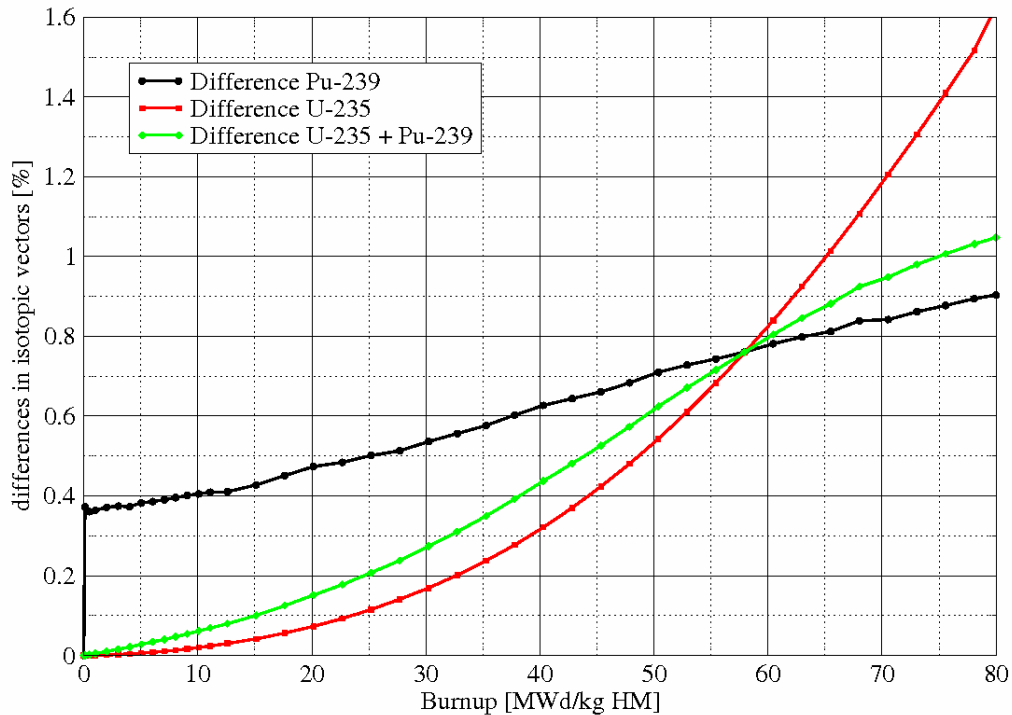


Figure 3.10: Percentaged differences of U-235 and Pu-239 fuel inventory versus burnup for the two ULFISP burnup calculations

The maximum burnup which can be achieved today in pressurized water reactors is approximately 60 MWd/kg HM. At this burnup the investigated fuel pin content with the new method shows an increased fissile material inventory of ca. 0.8 %. This increased fissile material leads to a reactivity difference of  $\Delta k_{\text{inf}} = +40$  pcm compared with the asymptotic scattering approach. By calculating the reactivity decrease per burnup-day ( $dk_{\text{inf}}/\text{one day}$ ) at 60 MWd/kg HM an extended burnup time through the higher reactivity for the fuel pin can be extrapolated to approximately 2.6 days. However this extended burnup time is only valid for the investigated single fuel pin cell. In a complete real operating nuclear power reactor with several different batches this extended burnup time would be smaller because of a lower average burnup (30-40 MWd/kg HM) at end of cycle.

### MOX pin cell burnup results

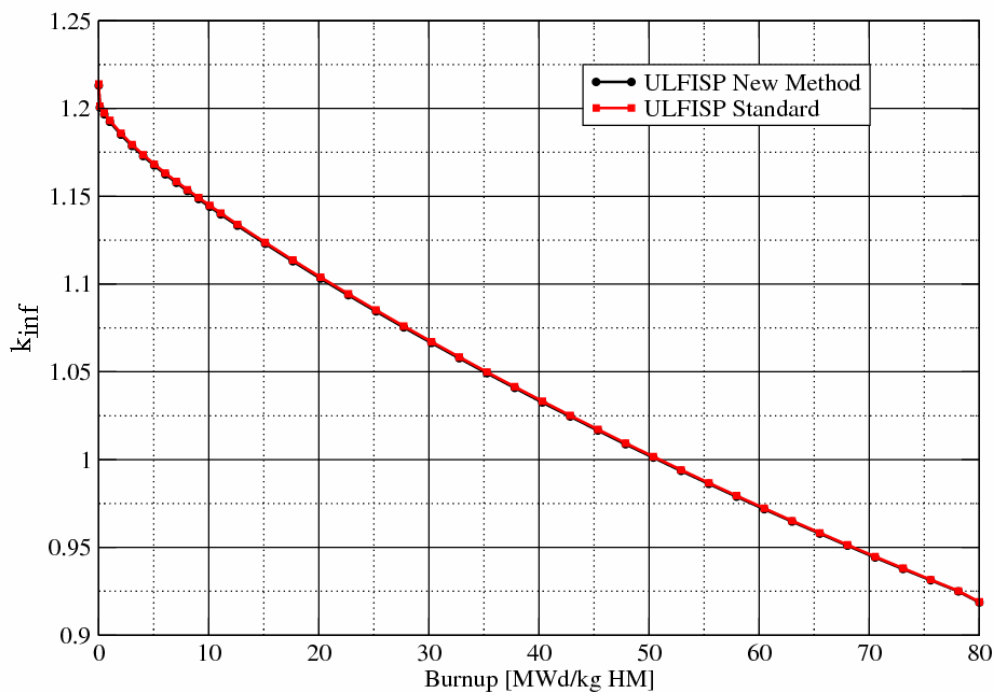
Along the lines of the burnup calculations with  $\text{UO}_2$  fuel, a MOX pin cell burnup analysis has been performed. The  $\text{UO}_2$  burnup pin cell problem has been taken and the  $\text{UO}_2$  was replaced by MOX with 8 % plutonium. This very high plutonium fuel content has been chosen to achieve a neutron spectrum which is explicitly very hard but in principle possible for a PWR application. This hard spectrum stands in contrary to the just presented the  $\text{UO}_2$  spectrum and represents the opposite extreme. Table 3.9 contains the plutonium and uranium vectors and the corresponding atomic densities for fresh fuel.

Figure 3.11 shows the time dependent reactivity loss for the two ULFISP fine flux approaches versus burnup. As in the previous  $\text{UO}_2$  case the reactivity differences are very small and are only visible in figure 3.12. There, the absolute reactivity differences are pictured between the two fine flux approaches versus burnup. The lower reactivity of about 80 pcm at BOL of the new scattering treatment results from the increased neutron absorption mainly in uranium-238. Due to the increased conversion from uranium-238 to plutonium-239 the reactivity difference shrinks during burnup to a difference of ca. 30 pcm at EOL.

Fuel Isotope	PU / U vector [%]	Atom density [ $10^{24}$ atoms/cm <sup>3</sup> ]
Pu-239	53 %	1.33280E-03
Pu-240	25 %	6.26080E-04
Pu-241	15 %	3.74090E-04
Pu-242	7 %	1.73850E-04
U-235	0.2 %	3.9348E-05
U-238	99.8 %	1.9386E-02
O-16		4.3867E-02

Table 3.9: Isotope concentrations for the MOX-fuel (BOL)

The reactivity in the simulation utilizing the new scattering treatment is still lower at EOL than in the standard fine flux approach. In contrary to the  $\text{UO}_2$  pin cell burnup calculation the more built up of plutonium-239 (demonstrated in figure 3.13) could not compensate the increased neutron absorption during burnup. By calculating the reactivity decrease per burnup-day ( $dk_{\text{inf}}/\text{one day}$ ) at 60 MWd/kg HM a decreased burnup time through the lower reactivity ( $\sim -30$  pcm) for the fuel pin can be extrapolated to approximately 3 days.

Figure 3.11: Reactivity  $k_{\text{inf}}$  over burnup for the two ULFISP approaches for the MOX pin cell at  $T=800$  K

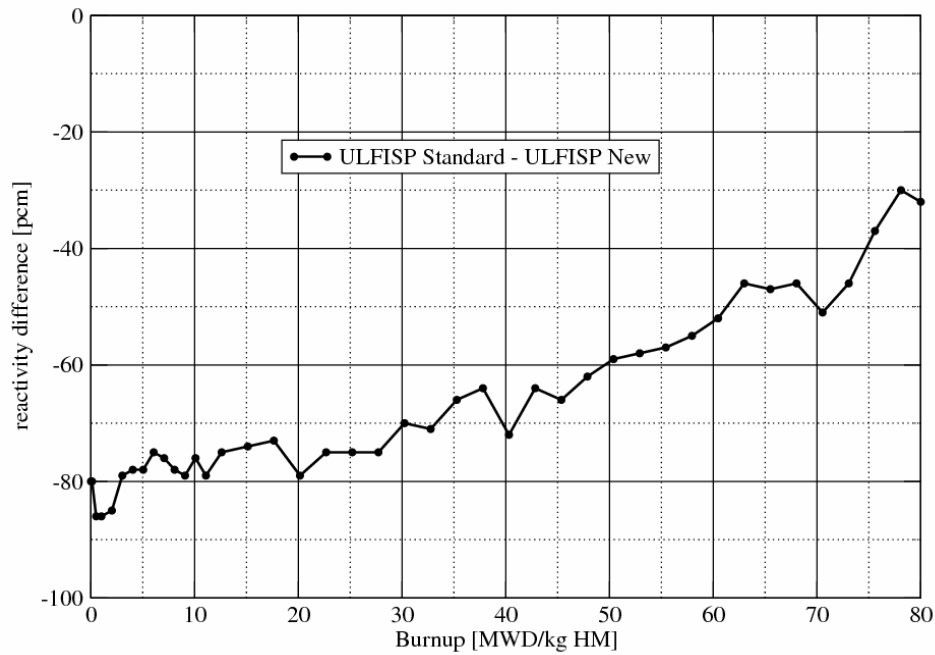


Figure 3.12:  $\Delta k_{\text{inf}}$  versus burnup for the two ULFISP approaches for MOX fuel at  $T=800\text{ K}$

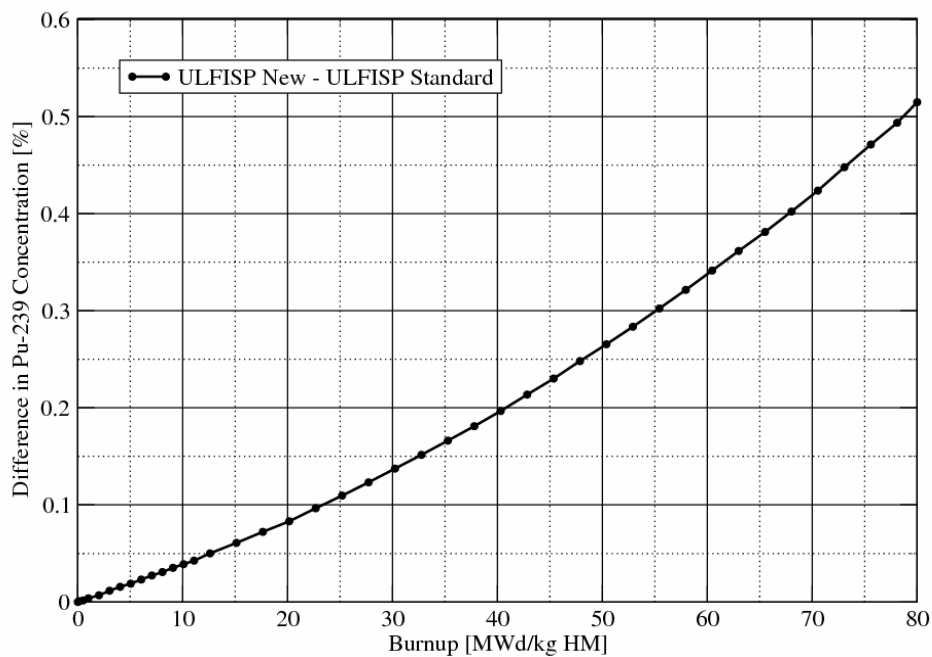


Figure 3.13: Percentage differences of the Pu-239 inventory for the two MOX burnup calculations

The presented pin cell burnup calculations show different results for  $\text{UO}_2$  fuel and for MOX fuel. In both cases the new scattering approach leads to a lower reactivity at BOL and to a higher fissile fuel content at EOL. In the MOX case the increased built up of plutonium-239 does not countervail against the higher neutron absorption. Therefore the positive effect of a longer fuel “lifetime” of  $\sim 2.6$  days of the  $\text{UO}_2$  fuel, is negative by a shorter fuel “lifetime” of  $\sim 3$  days in the MOX case.

### 3.4 Sensitivity of specific isotopes to the new scattering formalism

The hybrid method combines the standard and the new scattering formalism of ULFISP. It allows the user to choose for every single isotope the scattering treatment. The hybrid method theory is introduced in detail in chapter 2.3.3. In this chapter at first the hybrid method will be validated by a comparison between the standard asymptotic scattering approach of ULFISP and the new hybrid scattering approach in which only asymptotic scattering is performed. Secondly, the hybrid method will be used to determine the influence of all fuel isotopes on reactivity and isotopic vectors over burnup. The important isotopes are pointed out which produce significant changes when applying the new scattering treatment.

#### 3.4.1 Validation of the hybrid method

The pin cell calculation of the GRS-Benchmark will again be used for the validation. Since the hybrid method is included in the algorithm of the new scattering treatment in ULFISP it will be solved by iteration too. For this special comparison the transfer probabilities of all isotopes will be temperature- and cross section independent and therefore no up scattering will be performed of course. Because of this, iteration at the computing of the collision density should not be necessary. In fact the algorithm proves itself if the collision density and the reactivity respectively do not show significant changes with iteration. Table 3.10 presents reactivity  $k_{inf}$  for the pin cell of the GRS-Benchmark at BOL for the asymptotic scattering treatment and the hybrid scattering treatment (utilizing only asymptotic down scattering (energy- and temperature independent)) after different number of iterations.

	$k_{inf}$	$\Delta k_{inf}$ (standard-hybrid) [pcm]
Standard	1.308329	0
Hybrid 3 iterations	1.308262	6.7
Hybrid 6 iterations	1.308209	12
Hybrid 10 iterations	1.308184	14.5
Hybrid 15 iterations	1.308184	14.5

Table 3.10: Reactivity comparison between the asymptotic scattering treatment and the hybrid method utilizing only asymptotic scattering transfer probabilities

For the usual iteration number of three the difference in  $k_{inf}$  is about 6.7 pcm. For higher number of iterations the deviation raises up to 14.5 pcm. After 10 recurrences the results stays constant. Therefore the hybrid method shows very similar convergence behavior than the new scattering treatment presented in chapter 3.2. The fact that the hybrid method provides slightly different results in respect to the standard ULFISP method is due to the different algorithms used. In the following the number of iterations is chosen to three according to the new scattering treatment. The deviations which occur because of the hybrid method, will definitely be submerged into the general uncertainties of the calculations.

### 3.4.2 Sensitivity of specific isotopes for UO<sub>2</sub> fuel

The following presents reactivity differences between the new scattering method used for all fuel isotopes and different hybrid calculations utilizing the new scattering method only for chosen fuel isotopes. Figure 3.14 presents reactivity differences over burnup. EOL is again at 2157 days equivalent with 80 MWd/kg HM burnup. The calculation computing the new scattering treatment for all isotopes is used as reference solution. The jagged progressions of the curves give an impression about the accuracy of the reactivity values. Nevertheless, general trends are clearly visible.

The black curve shows the reactivity differences between the new and the standard method over burnup. As analyzed in chapter 3.4 the higher neutron absorption in uranium-238 leads to a decreased reactivity in the new approach at BOL up to approximately 1100 days burnup (~41 MWd/kg HM). Afterwards the increased built up of plutonium-239 induces higher reactivity. The blue line shows the differences between the reference solution and a hybrid calculation utilizing the new scattering treatment only for oxygen-16. The light and therefore strong scattering isotope (in the meaning of maximum energy loss for a neutron through collision) provides an even higher reactivity discrepancy. The red line indicates the deviation of a hybrid calculation utilizing the new scattering method only for uranium-238 to the reference solution. It shows a totally different trend. The reactivity at BOL is decreased while the reactivity at EOL is increased. The green curve shows despite some deviation the same trend as the “hybrid uranium-238” curve. It stands for the differences of a hybrid calculation utilizing the new scattering for all fuel isotopes except oxygen-16. This means that all other isotopes (all actinides and all fission products) which were taken into account additionally do not have a significant influence on reactivity because of the new scattering treatment. The green and the red curve show that only uranium-238 and oxygen-16 do play a significant role in the new scattering treatment. Also the orange curve which demonstrates the differences for a “hybrid uranium-238 and oxygen-16” calculation, shows nearly no deviations and confirms the exclusive importance of uranium-238 and oxygen-16 for the new scattering approach.

At first sight the importance of oxygen for reactivity calculation utilizing the new scattering kernel seems surprising due to the fact that oxygen does not have any resonances below 100 keV. The explanation lies in the problem definition. The comparisons done in this chapter always compare the asymptotic scattering approach with the new scattering approach in ULFISP. While the asymptotic approach does not provide any up scattering the observed importance of oxygen has its origin only in the up scattering of the potential elastic cross section ( $\sigma_{\text{O-16,elastic}}(E=4-150 \text{ eV}) \approx 4 \text{ barn}$ ). In presented problems oxygen is the lightest and therefore strongest scattering isotope considering energy loss and energy gain through collision. Combined with the fact that it is the most numerous isotope in the considered fuel, the importance of oxygen through the new scattering treatment can be seen similar to that of uranium-238 for the presented problem. The difference between the importance of the energy- and temperature dependent scattering treatment of uranium-238 and oxygen-16 depends to the energy region. While for uranium-238 the important energy regions are in the energetic “neighborhood” of resonances, the important energy regions of oxygen-16 are everywhere where no large resonances of any other isotope appear. Of course, like for all other isotopes, for oxygen-16 the more thermal the energy region is, the importance rises because of the higher probability of up scattering.

It must be added that this “oxygen-16 importance” is only valid for the deterministic approach in ULFISP. Monte Carlo solutions like the presented MCNPX results in previous chapters do not include this “oxygen-16 importance” because the potential elastic up scattering is already taken into account in the standard solutions.

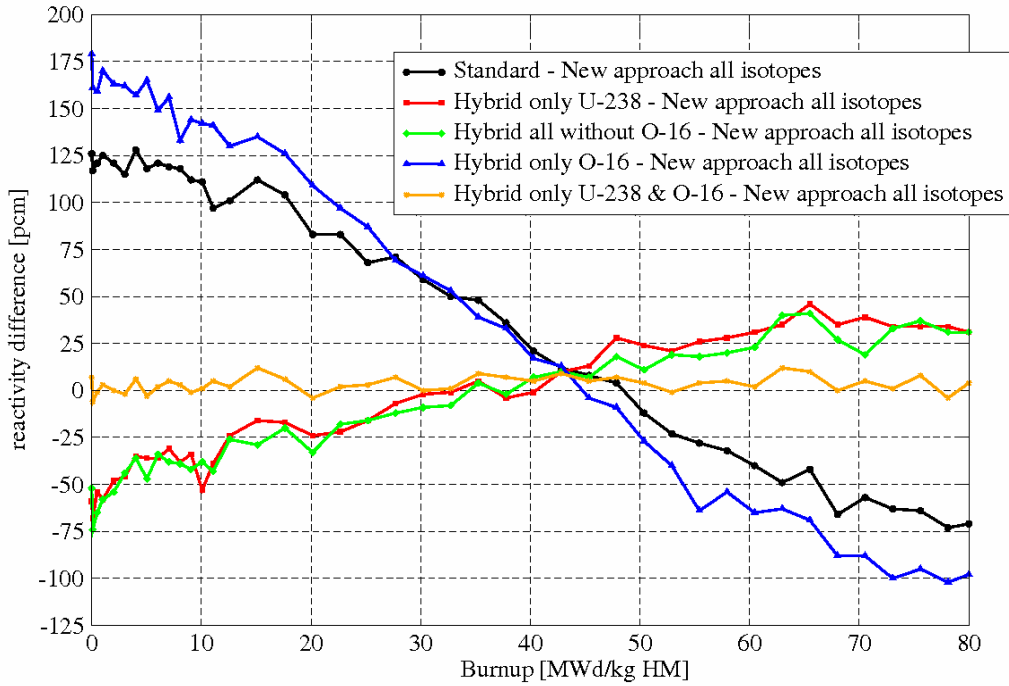


Figure 3.14: Reactivity differences between four specific hybrid calculations and the new scattering treatment for all isotopes at  $T= 800$  K

Exactly the same burnup calculations have been performed for a fuel temperature of  $T=1200$  K. The reactivity differences between the standard, the new and selected hybrid calculations are shown in figure 3.15.

The trends of the results are very similar but the amplitudes of the differences are larger which is caused by the enlarged impact of the energy- and temperature dependent scattering treatment at higher temperatures. Again the importance of uranium-238 and oxygen-16 is demonstrated.

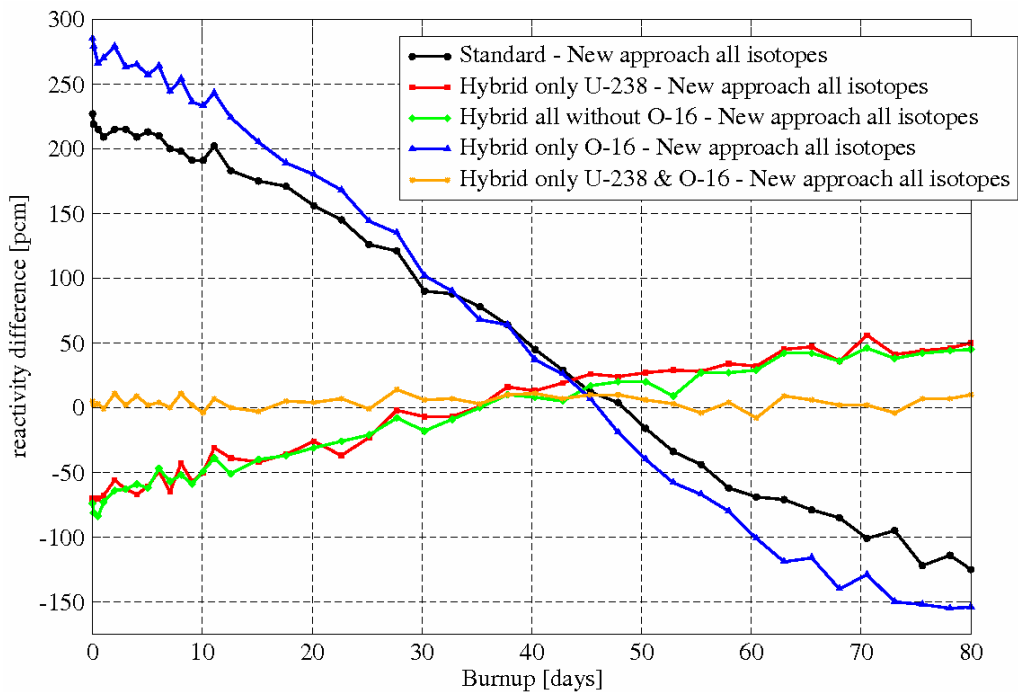


Figure 3.15: Reactivity differences between four specific hybrid calculations and the new scattering treatment for all isotopes at  $T= 1200$  K

### 3.4.3 Sensitivity of specific isotopes for MOX fuel

Further sensitivity studies of the hybrid method is performed by calculating the MOX fuel burnup problem of chapter 3.3 for fuel temperatures of  $T= 800$  K and  $T= 1200$  K. For simplicity for one temperature only the differences between the standard ULFISP, the new ULFISP and the hybrid method applying the new method for uranium-238 and oxygen-16 are presented. Figure 3.16 shows the differences of the standard and the new ULFISP method to give an impression of method deviations for the MOX problem at temperature  $T= 800$  K and  $T= 1200$  K. The blue and the red curve show the differences of the hybrid method (applying the new scattering treatment for uranium-238 and oxygen-16 and the standard treatment for all other isotopes) and the new method (applying the new scattering treatment for all isotopes). Again the differences are very small over burnup for both temperatures. The biggest differences are  $\Delta k=12$  pcm for  $T= 800$  K and  $\Delta k=13$  pcm for  $T=1200$  K.

The MOX results in figure 3.16 point out that plutonium isotopes do not contribute to any noticeable change in reactivity. Similar to uranium-235, plutonium-239 and plutonium-241 do not have such pronounced elastic scattering resonances as uranium-238. Moreover, all three isotopes are thermal fissile isotopes with huge thermal and epi-thermal fission cross sections.

This reduces the importance ratio  $\lambda = \frac{\sigma_s}{\sigma_f}$  (see chapter 3.2, equation 3.3) decisively and diminishes the impact of the new scattering approach to a level of insignificance.

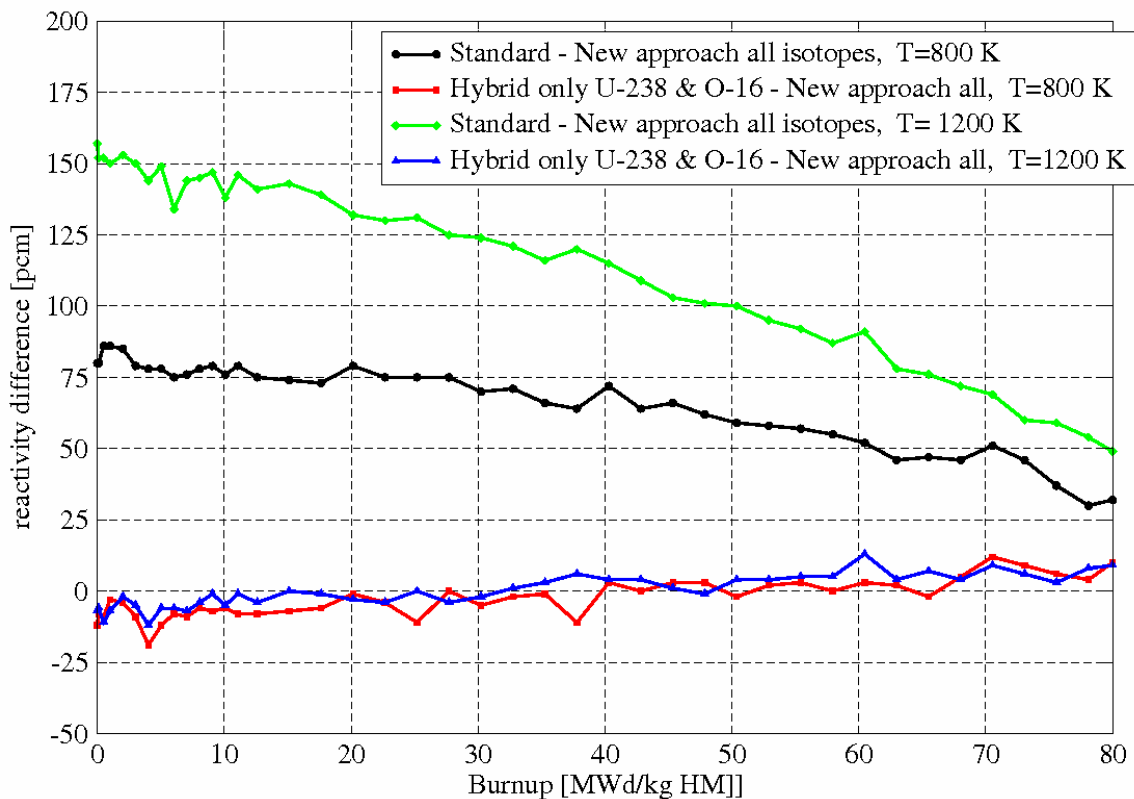


Figure 3.16: Reactivity differences for MOX fuel burnup calculations at  $T= 800$  K and  $T= 1200$  K

Plutonium-240 and plutonium-242 have well pronounced elastic scattering resonances (e.g. the fifth large resonance of plutonium-240 at  $E \approx 66.6$  eV or the 2<sup>nd</sup> large resonance of plutonium-242 at  $E \approx 53.5$  eV). The fifth large resonance of plutonium-240 has a ratio

$$\lambda = \frac{\sigma_s}{\sigma_t} \approx 0.65 \quad (\text{at } T = 800\text{K})$$

which is even higher than the corresponding uranium-238 ratio  $\lambda \approx 0.6$  (at  $T = 800$  K) for the third large resonance. A look at the problem specific importance

$$\text{ratio } \Lambda = \frac{\sum_s}{\sum_t^{fuel}} \quad (\text{see chapter 3.2, equation 3.4})$$

reveals for plutonium-240 a ratio of  $\Lambda_{\text{Pu-240}} \approx 0.2$  while the corresponding uranium-238 ratio still amounts to  $\Lambda_{\text{U-238}} \approx 0.59$ . Furthermore the 2<sup>nd</sup> large resonance of plutonium-240 is at a significantly higher energy ( $E \approx 66.6$  eV) than the third large resonance of uranium-238 ( $E \approx 36.6$  eV) which reduces the probability of up scattering.

Summarizing the validation of the hybrid method reveals similar iteration behavior of the standard approach like the iteration of the new scattering method. The deviations through iterations are very small. The convergence of the hybrid method was shown. The importance of uranium-238 and oxygen-16 has been shown for oxide fuel for different temperatures. By reducing the number of isotopes in the new scattering treatment the calculation time can be reduced significantly. All calculations in chapter 4 which deals with a reactor core MOX/UO<sub>2</sub> benchmark will be provided by the hybrid method utilizing the energy- and temperature dependent scattering treatment only for uranium-238 and oxygen-16.

# 4 Fuel Assembly and Reactor Core Application

In chapter 4 the effect of the temperature- and energy dependent scattering treatment on real reactor core simulations is analyzed. The chosen application is the “OECD/NEA and U.S. NRC PWR MOX/ $UO_2$  Core Transient Benchmark” [49]. The benchmark includes two different  $UO_2$  and two different MOX fuel assemblies. For these four assembly types burnup calculations have been performed with KAPROS utilizing different resonance treatments. The KAPROS produced cross sections are inserted into the PARCS code via a new developed cross section transformation tool and some specific simulations of the stationary part of the benchmark have been accomplished. Comparisons with results of other benchmark participants will be shown. The influence of the new scattering treatment on reactor core simulations will be analyzed.

## 4.1 MOX/ $UO_2$ core benchmark specifications

The MOX/ $UO_2$  core can be simulated by one quarter of the whole core because of symmetry. The quarter core consists of 42  $UO_2$  and 14 MOX fuel assemblies with different burnup states as shown in figure 4.1. All assemblies contain control and shutdown rods which are out of core for all calculations presented in this work. In the neutron transport calculation the inner quarter core interfaces (top and left boundary in figure 4.1) have reflective boundary conditions while the outer core interfaces (down- and right boundary in figure 4.1) are surrounded by a steel reflector and vacuum boundary conditions. The core was designed as a three batch equilibrium cycle with fresh fuel, once burned fuel with an average burnup of 20 MWd/kg HM and twice burned fuel with an average burnup of 35 MWd/kg HM.

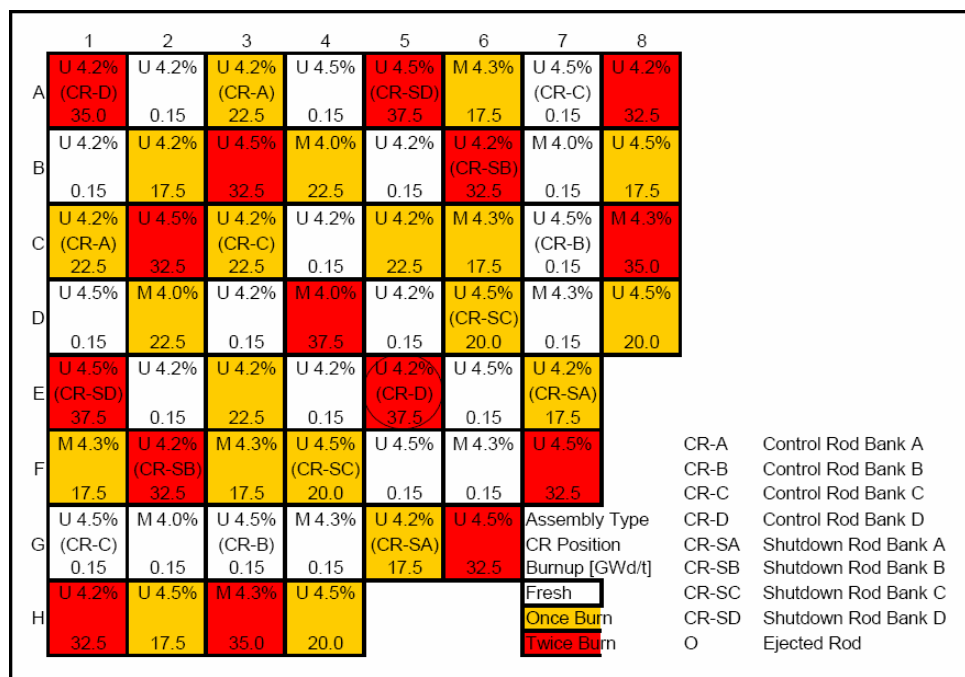
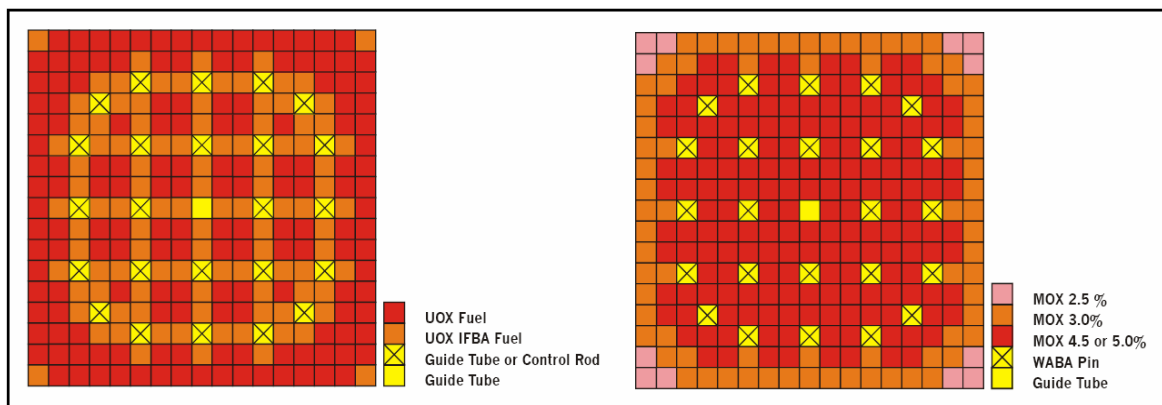


Figure 4.1: MOX/ $UO_2$  quarter core configuration taken from [49]

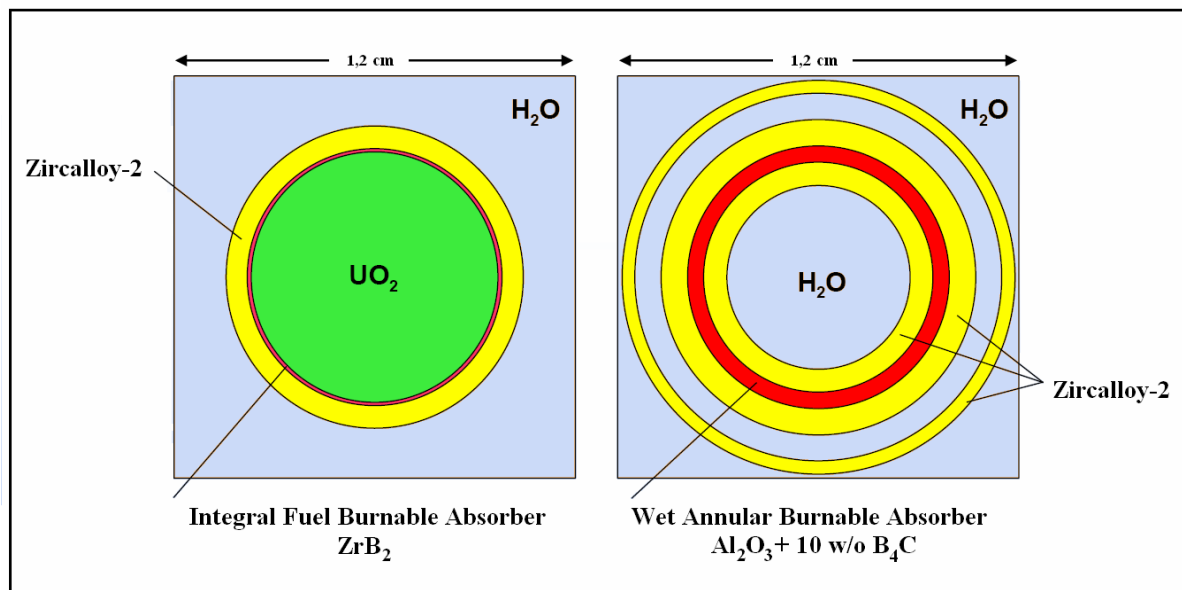
Assembly Type	Density [g/cm <sup>3</sup> ]	HM Material		
UO <sub>2</sub> 4.2%	10.24	U-235: 4.2 wt%, U-238: 95.8 wt%		
UO <sub>2</sub> 4.5%	10.24	U-235: 4.5 wt%, U-238: 95.5 wt%		
MOX 4.0%	10.41	Corner zone: 2.5 wt% Pu-fissile	Uranium vector: 234/235/236/238 = 0.002/0.2/0.001/99.797 wt%	
		Peripheral zone: 3.0 wt% Pu-fissile		
		Central zone: 4.5 wt% Pu-fissile		
MOX 4.3%	10.41	Corner zone: 2.5 wt% Pu-fissile		Plutonium vector: 239/240/241/242 = 93.6/5.9/0.4/0.1 wt%
		Peripheral zone: 3.0 wt% Pu-fissile		
		Central zone: 5.0 wt% Pu-fissile		

Table 4.1: Fuel composition of the MOX/UO<sub>2</sub> core Benchmark

The fuel assemblies consist of 289 pin cells each. The UO<sub>2</sub> assemblies have 36 guide tubes for control rod positions included. In this study the control rods are not taken into account which means that the guide tubes are always filled with water. Both assembly types have a guide tube in the center of the assemblies which is always filled with water as well. The UO<sub>2</sub> assemblies contain the same fuel in their 100 IFBA cells (Integral Fuel Burnable Absorber, see next paragraph for description) and 152 fuel pin cells. The MOX assemblies consist of three differently enriched fuel pin cells. The corner positions contain 12 fuel pins in total of 2.5 wt% fissile plutonium. The borders are filled with 76 fuel pins of 3 wt% fissile plutonium while the inner assembly region contains 4.5 wt% or 5.0 wt% fissile plutonium pin cells (176 pins in total). Figure 4.2 shows the assembly design in detail.

Figure 4.2: UO<sub>2</sub> (left) and MOX (right) fuel assembly taken from [49]

Both MOX and UO<sub>2</sub> assembly types contain burnable poisons. In the UO<sub>2</sub> assembly 100 of 252 fuel pins contain IFBA (Integral Fuel Burnable Absorber) as a thin zirconiumdiborid (ZrB<sub>2</sub>) layer around the fuel. In the MOX assemblies 36 of 289 pin cells are WABA cells (Wet Annular Burnable Absorber). The WABA cells do not contain any fuel. Both burnable poison cell types are presented in figure 4.3. The burnable absorber and control rod material is listed in table 4.2.


 Figure 4.3: Burnable absorber for the  $\text{UO}_2$  assembly (IFBA) and the MOX assembly (WABA)

Absorber material	Density [ $\text{g}/\text{cm}^3$ ]	Material
Control Rod	1.84	$\text{B}_4\text{C}$
IFBA	1.69	$\text{ZrB}_2$
WABA	3.5635	$\text{Al}_2\text{O}_3\text{-B}_4\text{C}$ , 10.0 wt% $\text{B}_4\text{C}$

 Table 4.2: Absorber materials of the MOX/ $\text{UO}_2$  benchmark

## 4.2 Fuel assembly burnup calculations

### 4.2.1 Burnup step sensitivity study

The energy- and temperature dependent scattering treatment is included in the core simulation via the generated macroscopic cross sections. The MOX/ $\text{UO}_2$  benchmark was originally accomplished by taking cross sections from the organizers. Therefore no burnup steps are defined in the benchmark specifications which made a burnup step sensitivity analysis necessary. The complete burnup calculations of KAPROS using the new ULFISP scattering option took approximately 10 days on a 1 GHz Linux computer. Because of this long calculation time the burnup sensitivity analysis has been performed by KAPROS standard calculations which take approximately 30% of the calculation time of ULFISP utilized neutron fine flux computations. Of course this calculation time difference depends very strong on the investigated problem. Figure 4.4 shows the reactivity loss over burnup for the  $\text{UO}_2$  fuel assembly with 4.5 % uranium-235 enrichment for various number of burnup steps. For all calculations the first two burnup steps are identical in order to respect the important xenon build up correctly. Afterwards four burnup calculations have been performed up to 35

MWd/kg HM, 810 days of full power, respectively. The blue curve (48 burnup steps) can be taken as reference calculation with no burnup step longer than 19 days which constitutes a very detailed time discretization. During the first two burnup steps the reactivity drops due to xenon build up. Afterwards, an increase in reactivity can be observed up to 5 MWd/kg HM burnup. This results from the burnout of the boron-10 in the integral burnable absorber (IFBA). Then the reactivity values show a smooth decline over burnup to EOL at 35 MWd/kg HM.

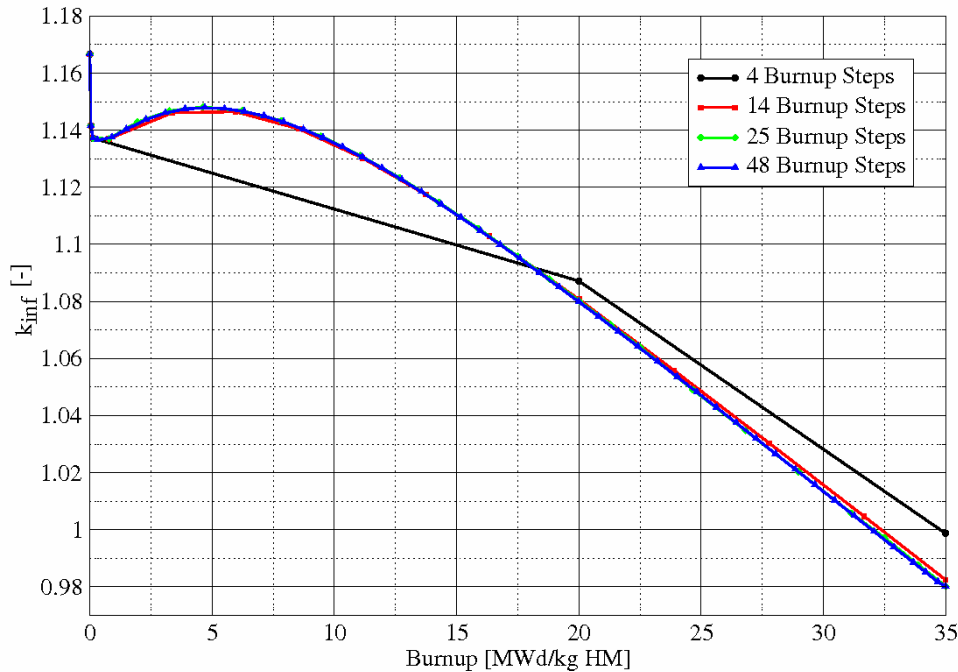


Figure 4.4: Reactivity over burnup for four different numbers of burnup steps for the  $\text{UO}_2$  assembly with 4.5 wt% U-235

The black curve in figure 4.4 shows the burnup calculation with four burnup steps. The unfavorable representation of the loss of reactivity over burnup is obvious. The red curve describes the reactivity loss for 14 burnup steps and shows already a quiet good agreement with the blue curve. The 25 burnup steps line (green) cannot be recognized because it lies under the blue reference curve and is therefore a very good approximation. The reactivity values and differences to the reference solution are summarized in table 4.3.

Figure 4.5 shows the same burnup calculations for the MOX assembly with 4.3 wt% fissile plutonium. Again the blue curve (48 burnup steps) can be considered as reference calculation. The characteristics of the reactivity decline over burnup differ to those of the  $\text{UO}_2$  assembly. Again the reactivity depression because of the xenon build up can be observed at the first two burnup steps. In contrary to the  $\text{UO}_2$  assembly reactivity decline, no reactivity increase due to the burnout of the burnable poison can be observed. The reason is that the burnable poison (WABA) content in the MOX assemblies is much smaller and spatially located in neighboring pin cells but not directly on the fuel as it is the case in the  $\text{UO}_2$ -assemblies.

The black curve (4 burnup steps) shows again a very bad reactivity loss approximation. The red (14 burnup steps) approximates the reference solution very good lower burnup but presents slight differences at EOL. The green curve (25 burnup steps) is again hardly visible except near EOL where a small deviation to the reference solution is visible. The absolute reactivity values and differences to the reference solution at EOL are summarized in table 4.3.

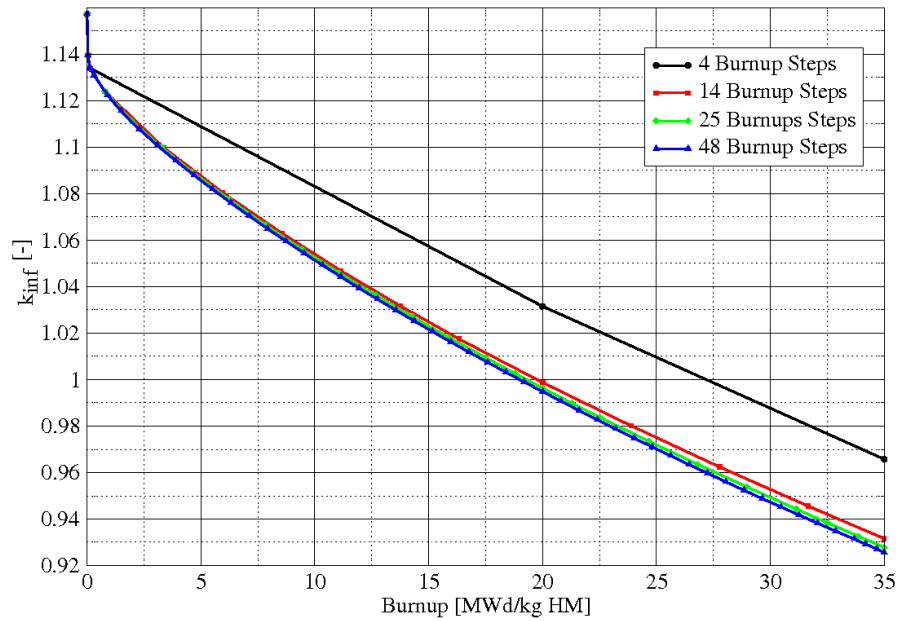


Figure 4.5: Reactivity over burnup for four different numbers of burnup steps for the MOX assembly with 4.3 wt% fissile plutonium

	4 burnup steps	14 burnup steps	25 burnup steps	48 burnup steps
UO <sub>2</sub> 4.5 wt% $k_{inf}$ (EOL)	0.99874	0.98249	0.98020	0.97963
$\Delta k_{inf}$ at EOL to 48 burnup steps	1911 pcm	286 pcm	57 pcm	-
MOX 4.3 wt% $k_{inf}$ (EOL)	0.96577	0.93163	0.92786	0.92586
$\Delta k_{inf}$ at EOL to 48 burnup steps	3991 pcm	577 pcm	200 pcm	-

Table 4.3: Reactivity and reactivity differences at EOL for the UO<sub>2</sub> and the MOX assembly for different number of burnup steps

The cross section calculations for the four assembly types have all been performed with 25 burnup steps. The reactivity difference of the MOX assembly between 25 and 48 burnup steps at EOL could not be avoided because the long calculation time the new scattering treatment requires. Therefore this deviation has to be taken into account in later chapters when the results from this study are compared to benchmark results from official participants. The comparisons of core simulations using only “self created” cross sections are not affected, of course.

### 4.2.2 Reactivity comparison between different fine flux options in ULFISP

For the two UO<sub>2</sub> assemblies and the two MOX assemblies presented in chapter 4.1, burnup calculations with KAPROS have been performed. For every assembly type three calculations utilizing three different resonance scattering treatments have been applied. First is the KAPROS standard treatment which uses precalculated resonance self shielding factors (SSF) which have been generated by NJOY utilizing the narrow resonance approach. Second is the ULFISP standard fine flux method performing constant energy and temperature (T= 0K) down scattering. Third, is the new ULFISP fine flux method utilizing energy- and temperature dependent up- and down scattering. In this chapter ULFISP does only calculate group cross section from 4 to 149 eV which are the WIMS energy groups 27 to 22 respectively, because of the high computational cost of assembly burnup calculations. The fine flux calculations start at 250 eV in these ULFISP calculations. Hence, the total computation time for one assembly could be reduced by half to approximately one week when utilizing the energy- and temperature dependent scattering treatment.

The impact of the neglected two groups in comparison to the calculations in chapter 3 is analyzed through assembly calculations without burnup (at BOL) utilizing ULFISP in the same way as in chapter 3 (cross section calculation from WIMS energy group 20 to 27, energy E=906 to E=4 eV, respectively). Table 4.4 summarizes the reactivity values for all calculations for fresh fuel. Also the differences  $\Delta k_{\text{inf}}$  between the same ULFISP calculation

Assembly type	KAPROS SSF	KAPROS ULFISP Standard 149 eV	KAPROS ULFISP Standard 904 eV	KAPROS ULFISP New 149 eV	KAPROS ULFISP New 904 eV
UO <sub>2</sub> 4.2 % $k_{\text{inf}}$	1.14262	1.14320	1.14285	1.14218	1.14180
UO <sub>2</sub> 4.2 % $\Delta k_{\text{inf}}$		35 pcm		38 pcm	
UO <sub>2</sub> 4.5 % $k_{\text{inf}}$	1.16641	1.16617	1.16582	1.16509	1.16474
UO <sub>2</sub> 4.5 % $\Delta k_{\text{inf}}$		35 pcm		35 pcm	
MOX 4.0 % $k_{\text{inf}}$	1.14279	1.14300	1.14317	1.14221	1.14223
MOX 4.0 % $\Delta k_{\text{inf}}$		17 pcm		2 pcm	
MOX 4.3 % $k_{\text{inf}}$	1.15448	1.15488	1.15500	1.15406	1.15412
MOX 4.3 % $\Delta k_{\text{inf}}$		12 pcm		6 pcm	

Table 4.4: Reactivity and reactivity differences for the analyzed KAPROS methods for the four different benchmark fuel assemblies for fresh fuel (BOL)

types for different fine flux energy ranges are listed. These differences represent the introduced error due to the fact that for the energy groups 21 and 20 no cross section calculation via ULFISP are included in the assembly burnup calculations.

For the  $UO_2$  assemblies the reactivity deviation  $\Delta k_{inf}$  represent between 30 and 40 pcm. For the MOX assemblies the deviations are nearly insignificant with differences of  $\Delta k_{inf} < 20$  pcm. These deviations are relatively small compared to other uncertainties in deterministic reactivity calculations. Nevertheless they should be kept in mind when looking at the reactor core calculation results of chapter 4.3.

### 4.2.3 $UO_2$ fuel assembly burnup results

The reactivity differences for the  $UO_2$ -assembly burnup calculations with 4.2 wt.% uranium-235 for the different KAPROS resonance treatments over burnup are shown in figure 4.6. The reactivity differences for the  $UO_2$ -assembly with 4.5 wt.% uranium-235 are very similar so these are omitted here. In these calculations, effective cross sections from 149 to 4 eV (WIMS energy groups 22 – 27) have been provided by ULFISP.

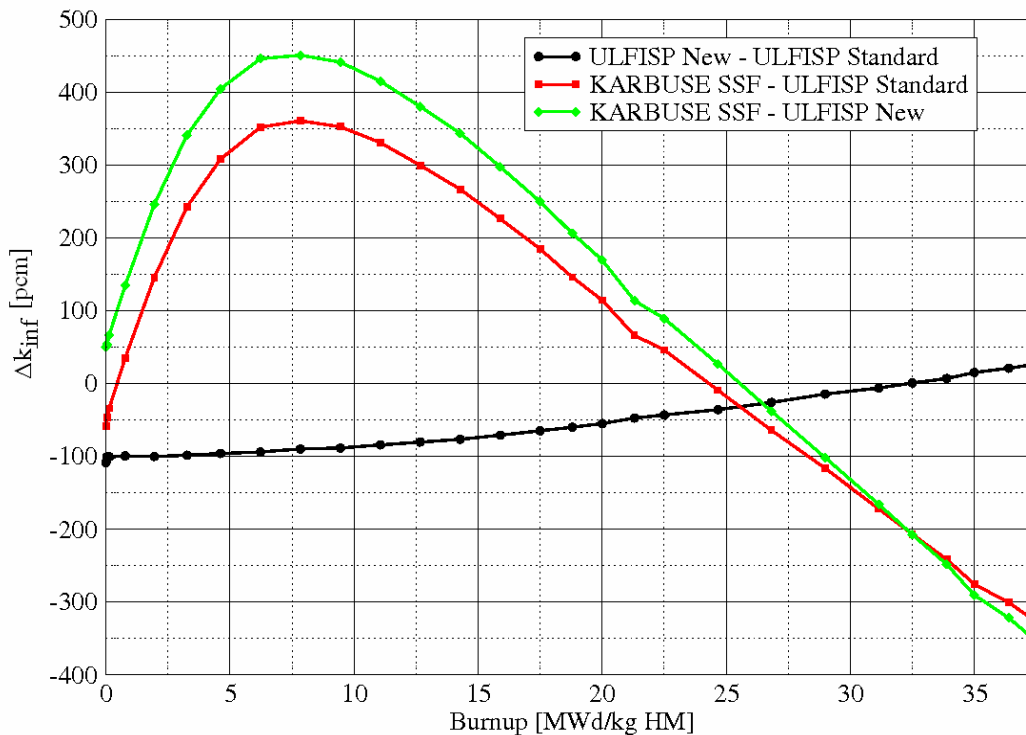


Figure 4.6: Reactivity differences  $\Delta k_{inf}$  over burnup for the  $UO_2$  (4.2 wt.% U-235) assembly

The reactivity differences between the calculations, which utilized the KARBUSE narrow resonance (SSF) method and the fine flux methods at begin of life, are smaller than  $\Delta k = 60$  pcm (see table 4.4 as well). During the burn out of the burnable absorber the differences raise to maxima of 450 and 550 pcm at  $\sim 7.5$  MWd/kg HM burnup. At this burnup the importance of the burnable absorber decreases compared to the importance of the build up of plutonium-239 through the higher conversion of uranium-238 in the fine flux calculations. Figure 4.7 presents the reactivity of the  $UO_2$  4.2 wt.% assembly over burnup on the left ordinate and the boron-10 concentration at the right ordinate. After  $\sim 10$  MWd/kg HM the differences in figure 4.6 decrease again, driven from the higher build up of plutonium-239 in

the fine flux methods. At approximately 25 MWd/kg HM the reactivity values of the fine flux methods exceed the reactivity of the KARBUSE standard approach (narrow resonance method, SSF).

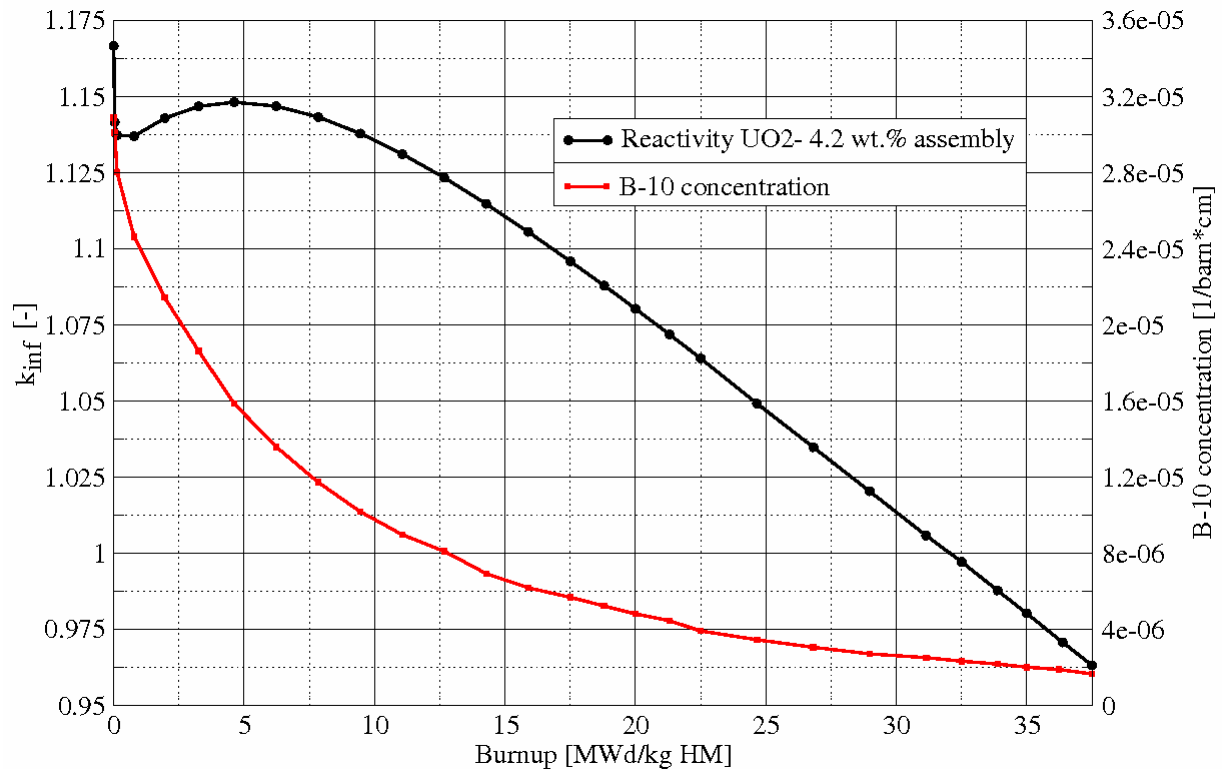


Figure 4.7: Reactivity and B-10 (in IFBA pins) concentration over burnup for the UO<sub>2</sub> (4.2 wt.% U-235) assembly

The reactivity differences presented in figure 4.6 between the two fine flux methods are very similar to the differences shown in chapter 3.3.1 (pin cell burnup analyses). The energy- and temperature dependent scattering treatment leads to more neutron absorption in uranium-238 which causes a lower reactivity value at BOL. Because of more absorption during burnup, more uranium-238 is converted to plutonium-239 which causes the reactivity differences to shrink. At EOL (37.5 MWd/kg HM) the reactivity difference of the two fine flux calculations is close to zero.

Figure 4.8 shows the absolute differences of plutonium-239 fuel inventories between the three methods for the UO<sub>2</sub> 4.2 wt% assembly. The absence of plutonium at BOL and the illustrated relative differences lead to high values at the first burnup step. The results are very similar to the pin cell burnup results in chapter 3.3.1 (figure 3.13). The relative inventory difference at EOL is about 2.5 % and 3 % between the KARBUS standard method and the fine flux approaches. The relative difference between the two fine flux methods is about 0.5 % at 37.5 MWd/kg HM. Including the other fissile isotopes, uranium-235 and plutonium-241 as well, this leads to 0.35 % more fissile material at end of life which approximately complies with additional 3 days of reactor operation.

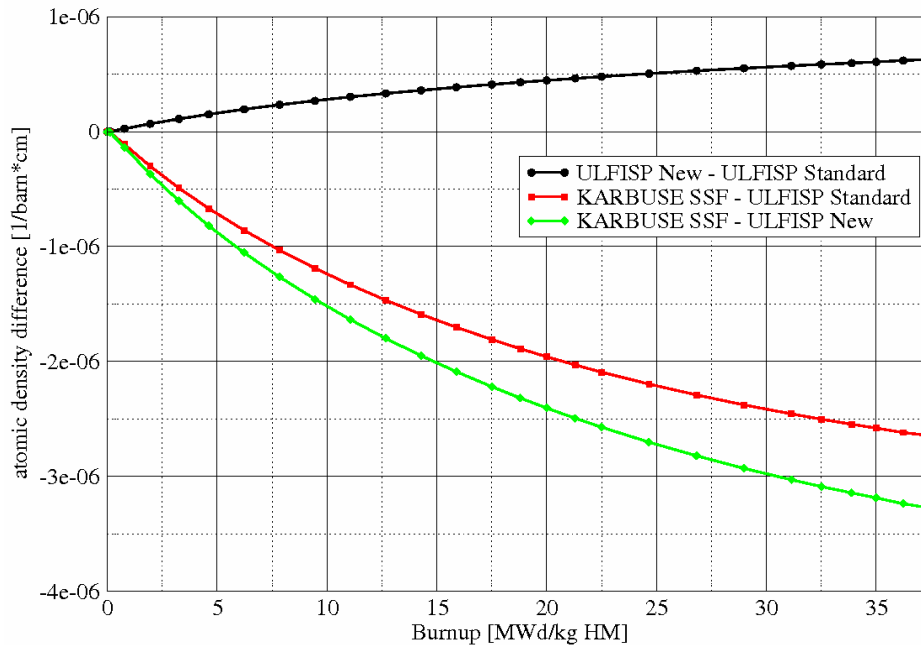


Figure 4.8: Differences of the Pu-239 vectors over burnup through different resonance treatment for the  $\text{UO}_2$  (4.2 wt.% U-235) assembly

#### 4.2.4 MOX fuel assembly burnup results

The reactivity differences for the different KAPROS resonance treatments over burnup are shown in figure 4.9 for the MOX assembly with 4.3 wt.% fissile plutonium. Again, ULFISP calculated effective cross sections from 149 to 4 eV (WIMS energy groups 22 – 27), have been used. The different enrichments (4.0, 4.3 wt.%) of the MOX assemblies do not lead to significant reactivity differences. Therefore the analysis of the MOX assembly with 4.3 wt.% fissile plutonium is neglected.

The reactivity differences of the two fine flux calculations show a very similar progression as the corresponding reactivity differences in the  $\text{UO}_2$  assembly calculation and the pin cell burnup analyses in chapter 3.3. At BOL the energy- and temperature dependent scattering treatment leads to higher neutron resonance absorption and therefore to a decreased reactivity value. The time dependent reactivity versus burn-up decreases more slowly if the conversion of uranium-238 to plutonium-239 is enhanced by an increased resonance absorption. As presented in figure 4.10 an increased plutonium-239 content of approximately 0.375 % at EOL (37.5 MWd/kg HM) can be observed.

The reactivity differences between the fine flux methods and the standard KARBUSE method (SSF method) are relatively small to the observed differences of the MOX pin cell burnup calculations of chapter 3.3.2. They result from the interaction of the lower plutonium-239 content in the SSF method as shown in figure 4.10 and the changing differences of plutonium-240 contents. Surprisingly the plutonium-240 content of the SSF approach is higher than in the fine flux calculations up to 25 MWd/kg HM as illustrated in figure 4.11. The conversion of plutonium-240 to plutonium-241 is higher in the SSF method until the higher plutonium-239 fuel content in the fine flux calculations reduces and later reverses this conversion difference.

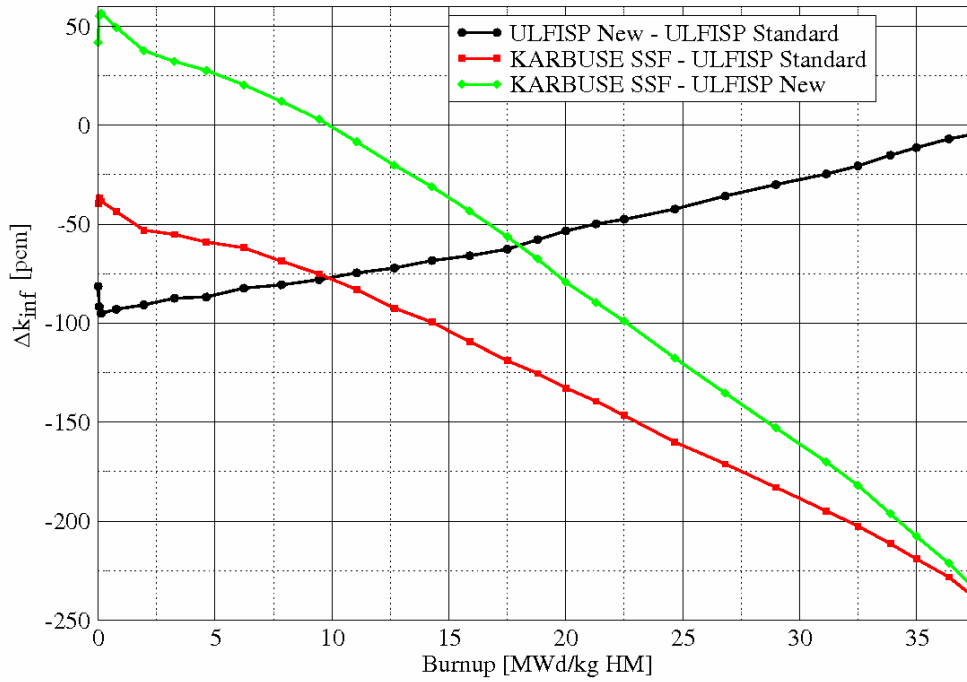


Figure 4.9: Reactivity differences over burnup for the MOX (4.3 wt.% Pu fissile) assembly resulting from different resonance treatments

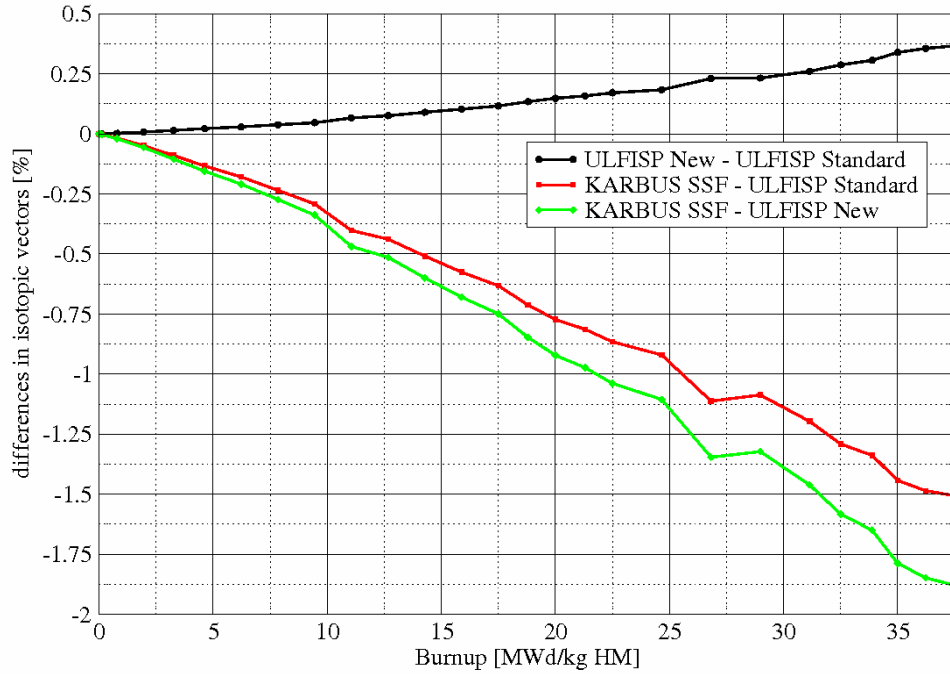


Figure 4.10: Relative differences of Pu-239 vectors over burnup for the MOX (4.3 wt.% Pu fissile) assembly for the three resonance approaches

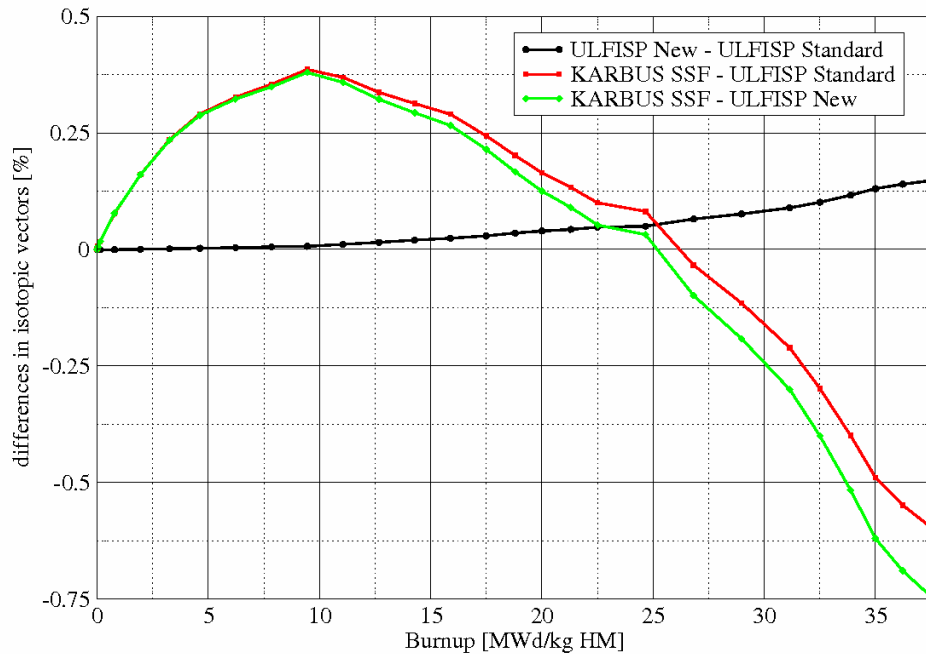


Figure 4.11: Relative differences of the Pu-240 vectors over burnup for the MOX (4.3 wt.% Pu fissile) assembly for the three resonance approaches

### 4.3 Reactor core calculations

The cross sections produced with KAPROS are assembly wise homogenized and collapsed to 28 and 8 groups. These effective macroscopic cross sections are converted by the new KAPROS module CRPAXS to the PMAXS cross section format of PARCS. The reactor core calculations are then performed with PARCS for the reactor conditions hot zero power (HZP) and hot full power (HFP). The hot zero power case is the same as part one of the OECD/NEA benchmark. Constant coolant and fuel temperatures of  $T = 560$  K are assumed in the core. Therefore, the thermo-hydraulic core calculation can be neglected. The results are compared with the results of the OECD/NEA benchmark participants.

The hot full power calculation had to be performed with fixed thermo-hydraulic conditions as well which is a strong simplification. This simplified hot full power simulation was added to show the impact of the energy- and temperature dependent scattering treatment on a reactor simulation at operating fuel temperature conditions.

The macroscopic cross sections for the reactor core calculations have been produced by KAPROS burnup calculations. Cross section sets of 8 and 28 energy groups have been computed by collapsing the 69 energy group cross sections. The 8 group results are provided for best comparison with the benchmark results of the Purdue University who calculated the benchmark with PARCS with 8 groups as well. The 28 energy group structure was chosen for best comparison of the asymptotic scattering fine flux approach with the energy- and temperature dependent scattering fine flux approach. This 28 group structure includes the energy groups 22-27 of the WIMS-69 group structure in their original form. Thereby it can be assured that no information introduced by the energy- and temperature dependent scattering treatment is erased by the collapsing from 69 to 28 groups. The number of 28 groups is close to the maximum number of groups PARCS is able to handle for the performed reactor core simulations. The 8, 28 and the 69 WIMS energy structures are presented in table 4.5.

WIMS-69 group	28 group	8 group	Upper Energy (eV)	WIMS-69 group	28 group	8 group	Upper Energy (eV)
1	1	1	1.0000E+07	36	20		1.0970E+00
2			6.0655E+06	37			1.0710E+00
3			3.6790E+06	38			1.0450E+00
4	2	2	2.2310E+06	39	21		1.0200E+00
5			1.3530E+06	40	22		9.9600E-01
6	3	3	8.2100E+05	41	23		9.7200E-01
7	4		5.0000E+05	42			9.5000E-01
8			3.0250E+05	43			9.1000E-01
9			1.8300E+05	44			8.5000E-01
10			1.1100E+05	45			7.8000E-01
11	5		6.7340E+04	46	24	7	0.6250E-01
12			4.0850E+04	47			5.0000E-01
13			2.4780E+04	48			4.0000E-01
14	6		1.5030E+04	49	25		3.5000E-01
15	7	4	9.1180E+03	50			3.2000E-01
16	8		5.5300E+03	51	26		3.0000E-01
17			3.5191E+03	52			2.8000E-01
18			2.2394E+03	53	27		2.5000E-01
19	9		1.4251E+03	54			2.2000E-01
20			9.0689E+02	55			1.8000E-01
21	10		3.6726E+02	56	28	8	1.4000E-01
22	11	5	1.4872E+02	57			1.0000E-01
23	12		7.5501E+01	58			8.0000E-02
24	13		4.8052E+01	59			6.7000E-02
25	14		2.7700E+01	60			5.8000E-02
26	15		1.5968E+01	61			5.0000E-02
27	16		9.8770E+00	62			4.2000E-02
28	17	6	4.0000E+00	63			3.5000E-02
29			3.3000E+00	64			3.0000E-02
30	18		2.6000E+00	65			2.5000E-02
31			2.1000E+00	66			2.0000E-02
32	19		1.5000E+00	67			1.5000E-02
33			1.3000E+00	68			1.0000E-02
34			1.1500E+00	69			5.0000E-03
35			1.1230E+00				1.0000E-03

Table 4.5: The WIMS-69 [3], the 28 and 8 neutron energy group structures

The Benchmark cross sections have been provided by the Purdue University. They used the lattice cell code HELIOS [43] utilizing a 47 energy group library to generate the macroscopic cross sections. The simulations with BARS [2], DeCart [46], DORT [75] and MCNP [57] provide heterogeneous solutions which means that the reactor core has been

discretized geometrically pin cell wise. All other solutions are nodal solutions, which means that the cross sections have been homogenized assembly wise. The nodal benchmark simulations performed with PARCS [36], NUREC [98], CORETRAN [39] and SKETCH-INS [60] used the provided benchmark cross sections. The “heterogeneous” simulations with BARS and MCNP utilized the burnup dependent material number densities of the benchmark. Only the DeCART and DORT cross sections have been prepared by the participants themselves. For this purpose they used the HELIOS code as well.

### 4.3.1 Comparison with benchmark participants at hot zero power

At hot zero power the fuel, the moderator and all other components temperatures of the core are fixed at  $T_{\text{all}} = 560$  K. Hence, thermo-hydraulic feedback is neglected. The reactivity results for the reactor core simulations at hot zero power utilizing cross sections which have been produced with different KAPROS resonance treatments are shown in table 4.6. These are listed under “KAPROS-PARCS Results”. Additionally the results of the participants of the OECD/NEA Benchmark [49] are listed in table 4.6 as well. These are presented under “Nodal Benchmark participants’ results” and “Heterogeneous Benchmark participants’ Results”. All results have been performed for all rods out (ARO) of core conditions.

The agreement of the nodal benchmark results is extremely good, with the only difference inserted by the spatial discretization used by each node. Even the different number of 8 groups in the PARCS simulation compared to the other nodal calculations which used 2 groups does not lead to significant differences. The heterogeneous benchmark results are still close to the nodal benchmark results but the differences are obviously of another magnitude. The reactivity difference of e.g. the BARS and the NUREC results is about  $\Delta k_{\text{eff}} = 550$  pcm. The BARS simulation uses the same material number densities which are included in the cross section used by the NUREC code. Therefore the reactivity difference probably results from the different core modeling.

The results of this study (KAPROS-PARCS results in table 4.6) fit very well with the heterogeneous benchmark results. Considering the totally different cross section generation and calculation methods, the reactivity difference between the 28 PARCS-KAPROS simulation and the benchmark Monte Carlo simulation with MCNP is excellent with only about  $\Delta k_{\text{eff}} = 15$  pcm. The biggest difference between the 28 PARCS-KAPROS result with a heterogeneous benchmark result, which is the DORT result, is only  $\Delta k_{\text{eff}} = 322$  pcm. The differences of approximately  $\Delta k_{\text{eff}} \approx 630\text{-}720$  pcm between the results of this study and the nodal benchmark results are much higher, although the core modeling is much more similar. Especially the PARCS 8 group calculation of benchmark participants has the identical reactor core simulation modeling as the KAPROS-PARCS calculations. Therefore the reactivity difference of  $\Delta k_{\text{eff}} = 609$  pcm between e.g. the “KAPROS-PARCS standard fine flux method 8 groups” calculation and the “nodal benchmark PARCS 8 groups” calculation, has its origin only in the input cross sections.

Summarizing, the KAPROS-PARCS solutions show very good agreement with the heterogeneous benchmark results. Surprisingly the agreement with the nodal benchmark solutions, where the modeling is more similar, is not as good as.

XS production code, XS library, resonance treatment	Neutron Physics Core Solver	$k_{\text{eff}}$
KAPROS-PARCS results (nodal):		
KAPROS, 69-ENDF/B-6.5, narrow resonance method (SSF-formalism)	PARCS 28 groups	1.056489
KAPROS, 69-ENDF/B-6.5, standard fine flux method	PARCS 8 groups	1.057453
KAPROS, 69-ENDF/B-6.5, standard fine flux method	PARCS 28 groups	1.057212
KAPROS, 69-ENDF/B-6.5, new fine flux method	PARCS 8 groups	1.057378
KAPROS, 69-ENDF/B-6.5, new fine flux method	PARCS 28 groups	1.057136
Nodal Benchmark participants' results:		
Benchmark cross sections	PARCS 8 groups	1.06354
Benchmark cross sections	NUREC 2 groups	1.06378
Benchmark cross sections	CORETRAN 2 groups	1.06379
Benchmark cross sections	SKETCH-INS 2 groups	1.06379
Heterogeneous Benchmark participants' results:		
ENDF/B 6 with Benchmark number densities	BARS	1.05826
HELIOS, 47group HELIOS-library	DeCART	1.05852
HELIOS, 190 group HELIOS-library	DORT	1.06036
ENDF/B 6 with Benchmark number densities	MCNP	1.05699

Table 4.6: Reactor core reactivity results for HZP from this study and from benchmark participants taken from [49]

### Differences between the KAPROS-PARCS results caused by different scattering models

The KAPROS-PARCS results do only differ in the resonance treatments in their cross section generation. The core modeling is identical in all five presented results in table 4.6. The differences between the simulations applying the fine flux methods for cross section generation, are of about  $\Delta k_{\text{eff}} = 7$  pcm for the 28 group solution. This very small difference results on one hand from the low fuel temperature at hot zero power of  $T_f = 560$  K where the impact of the energy- and temperature dependent scattering treatment is very small. On the other hand the presented reactor core is close to an equilibrium core ( $k \approx 1$ ) which leads to compensation of the differences resulting from the eigenvalue calculation (due to different scattering treatments) with the differences caused of the different fissile fuel inventory which occurs during burnup. In more detail, the decreased reactivity value because of higher neutron absorption rates is compensated during burnup by the higher conversion of uranium-238 to plutonium-239 which increases the fissile fuel inventory.

For the determination of the reactivity Doppler-coefficient  $\alpha_T$  (calculated with equation 3.4) modified hot zero power calculations with fuel temperature of  $T_f = 900$  K have been performed. These results and the results of table 4.6 ( $T_f = 560$  K) have been used for the calculation of the Doppler-coefficients presented in table 4.7. All results have been provided by using the 28 groups cross section sets in PARCS.

The Doppler-coefficient results emphasize the importance of the energy- and scattering dependent scattering treatment for PWR core simulations even at low temperatures. Compared to the standard fine flux treatment the negative Doppler coefficient is increased by  $\Delta\alpha_T = 7.2$  %. This is more than the increase of the negative Doppler coefficient from the self shielding factor method to the standard fine flux method which is about  $\Delta\alpha_T = 5$  %. The increase between the self shielding factor method and the new fine flux method is of about  $\Delta\alpha_T = 12,6$  %.

XS Production description	Fuel Temperature [K]	$k_{\text{eff}}$	Doppler Coefficient $\alpha_T$ [pcm/K]
KAPROS, narrow resonance method (SSF)	560	1.056489	-1.5942
	900	1.050439	
KAPROS, standard fine flux method	560	1.057212	-1.6744
	900	1.050849	
KAPROS, new fine flux method	560	1.057136	-1.7954
	900	1.050314	

Table 4.7: Doppler reactivity coefficients for hot zero power

### 4.3.2 Hot full power

Hot full power simulations need thermo-hydraulic feedbacks to represent the heterogeneous temperature distribution in the core correctly. At the moment it is not possible to transform KAPROS cross section with CRPAXS into the PARCS format PMAXS in the needed extend to perform coupled neutronic thermo-hydraulic calculations. Therefore several improvements in the KAPROS module CRPAXS would have to be developed but could not be accomplished in this work.

Giving an outlook on the importance of the energy- and temperature dependent scattering treatment for a PWR at normal operating conditions, a hot full power core simulation with fixed thermo-hydraulic conditions will be presented. Fixed thermo-hydraulic conditions for a hot full power calculation are a strong simplification of course. The averaged axially and radially constant moderator and fuel temperatures in the core were specified by the benchmark to temperatures  $T_m = 580$  K and  $T_f = 900$  K.

For estimating the error introduced when neglecting the thermo-hydraulic feedback and the correct temperature distributions, two PARCS hot full power simulations have been performed with the benchmark cross section set provided by Purdue University. The first simulation uses a thermo-hydraulic feedback solution which is based on one-dimensional mass-energy equations, one phase flow, constant mass flow rate and a constant pressure of 15.5 MPa. The second simulation neglects the thermo-hydraulic feedback as it has to be done with the KAPROS generated cross sections. Table 4.8 shows the reactivity rates for these two simulations at hot full power. The boron concentration is fixed at 1000 ppm.

XS Production description	Core Simulation description with PARCS	$k_{\text{eff}}$	Introduced Error
Benchmark XS 8 groups	Coupled Neutronic- Thermo-Hydraulic	1.04337	318 pcm
Benchmark XS 8 groups	Neutronics only	1.04655	

Table 4.8: Hot Full Power reactivity results respecting and neglecting the thermo-hydraulic feedback

For the hot full power simulations PARCS was used again. The introduced error by neglecting the thermo-hydraulic feedback at hot full power for the MOX/UO<sub>2</sub> benchmark core is 318 pcm. An error of this magnitude can be expected, for the absolute values of the hot full power core simulations with KAPROS generated cross sections, too. Nevertheless the error is included in all results of table 4.9 in the same way.

Table 4.9 presents the reactivity values and the corresponding fuel reactivity Doppler coefficients (calculated with equation 3.4) for the three different KAPROS resonance treatments. For all three KAPROS methods two calculations have been carried out. These vary only in the fuel temperature. One was performed at  $T_f = 900$  K, the other at  $T_f = 1000$  K.

The reactivity results differ only slightly. For fuel temperature  $T = 900$  K the reactivity difference between the two fine flux approaches account for  $\Delta k_{\text{eff}} = 56$  pcm. At temperature  $T = 1000$  K they represent  $\Delta k_{\text{eff}} = 75$  pcm which once more shows the temperature dependence of the new scattering treatment.

The Doppler coefficient shows again the importance of the energy- and temperature dependent scattering treatment for safety analyses for PWR's. Compared to the standard fine flux treatment the negative Doppler coefficient is increased by  $\Delta\alpha_T = 9\%$ . The increase of the negative Doppler coefficient from the self shielding factor method to the standard fine flux method is determined to  $\Delta\alpha_T = 3.2\%$ . The increase between the self shielding factor method and the new fine flux method is of about  $\Delta\alpha_T = 12\%$ .

XS production description	Fuel Temperature [K]	$k_{\text{eff}}$	Doppler Coefficient $\alpha_T$ [pcm/K]
KAPROS, narrow resonance method (SSF)	900	1.051080	-1.62296
	1000	1.049287	
KAPROS, standard fine flux method	900	1.051446	-1.67701
	1000	1.049592	
KAPROS, new fine flux method	900	1.050881	-1.842347
	1000	1.048847	

Table 4.9: Doppler reactivity coefficients for hot full power with fixed thermo-hydraulic feedback

## 5 Summary

The improvement of reactor simulations leads to more precise safety analyses and therefore to a reduction of uncertainties and conservative assumptions. A better prediction of nuclear reactor conditions will improve economics without affecting safety.

The presented thesis deals with the task of increasing the accuracy of neutron physics reactor simulations. A more precise model for the scattering of neutrons in the lower epithermal resonance energy region is implemented into a deterministic code system. This new scattering formalism leads to a more precise determination of the neutron flux form which is applied as weighting function for generation of effective multigroup cross-sections. For the determination of the neutron flux form special care has to be taken in the energy range of resonances. Several different methods like the narrow-, wide-, intermediate resonance approximations or the Nordheim integral method deal with this task. The most precise but computational very costly as well, is the fine flux method as applied in RESAB [74], ULFISP [16] and CENTRM [21] [74]. All of these established fine flux modules are based on the classical neutron slowing-down equation, simplifying the elastic scattering of neutrons with a target nucleus in the same way. First, it is assumed that the target nucleus scattering cross section is the constant potential cross section. That is a strong simplification for isotopes with pronounced resonances like uranium-238. Second, the target nucleus movement which occurs from thermal agitation is neglected. It is assumed that the target nucleus is at rest or in other words at temperature  $T=0$  K. This – in essence – means that by scattering a neutron can only lose energy while it can never gain energy.

These two simplifications have been replaced by the implementation of an energy- and temperature dependent scattering formalism into the existing KAPROS [16] module ULFISP. The new scattering treatment is based on earlier work [27] of Rothenstein and Dagan [Ref]. Pre-calculated data files with improved scattering kernel information, created by a modified version of their code DOUBLE, are applied. The new scattering formalism in ULFISP respects not only the energy dependence of the elastic scattering cross section, but accounts also for the thermal movement of the target nucleus, enabling both down-scattering and up-scattering.

In the original version of ULFISP only neutron down-scattering can be provided. This means that the neutron density at certain energy is fully determined by the neutrons at higher energies. For the handling of up-scatter probabilities an iterative solution method is applied. A fast convergence after about three iterations could be observed. The more precise form of the neutron flux can then be used as weighting function for the calculation of more accurate effective multigroup cross sections.

First results for a PWR-UO<sub>2</sub> pin cell (4 wt.% uranium-235) are discussed in chapter 3. The differences between the collision densities of the old asymptotic and the new energy- and temperature dependent scattering fine flux calculations identify the important energy region where the new scattering approach leads to a significant change. At energy regions close to the large resonances of uranium-238 and especially at the third large resonance at 36.6 eV, explicit differences in the collision density occur. The up-scattering which is introduced into the fine flux calculation via the new approach leads to an increased collision density at the energetically lower region of the resonances while a decreased collision density at the energetically higher part of the resonances results from reduced down scattering. The comparison of the corresponding neutron flux forms confirms this issue. The impact of the

new scattering approach has its strongest effect in the resonance regions because of the extremely high neutron cross sections there. Two effects determine the importance of a resonance to the energy- and temperature dependent scattering treatment:

1. The energy of the resonance. The lower the energy of the scattered neutron the higher is the neutron probability for up-scattering and the higher is the maximal possible energy benefit of the neutron. This is as well the reason for the increasing importance of the new approach for higher temperatures. Faster movement of the target nucleus, caused by thermal agitation, leads to possible higher energy transfers from the target nucleus to the neutron.
2. The ratio between the elastic and the total scattering cross section. Generally it can be stated that the higher the ratio of elastic to total cross section the larger will be the change in the calculated neutron fine flux form with the new scattering approach.

The main impact on integral results by the new approach is a modified neutron absorption rate in the range of resonances. This can be observed in the presented results especially at the third large uranium-238 resonance.

The new formalism in ULFISP was also applied to PWR-UO<sub>2</sub> pin cell comparison simulations with MCNPX [58]. Here the single differential new scattering treatment in ULFISP is compared with the double differential scattering treatment as introduced by Dagan in MCNPX [28] previously. The results show generally a good agreement. The comparison shows again that the third large uranium-238 resonance has the highest differences. The reactivity changes with the new approach at temperature T= 800 K show very similar decreased values of  $\Delta k_{inf} = 142$  pcm for ULFISP and  $\Delta k_{inf} = 123$  pcm for MCNPX for the examined PWR-UO<sub>2</sub> pin cell. At temperature T= 1200 K these reactivity decreases are  $\Delta k_{inf} = 264$  pcm in the ULFISP and  $\Delta k_{inf} = 242$  pcm in the MCNPX calculation. The corresponding fuel Doppler coefficients increased by 10.2 % in ULFISP and 9.6 % in MCNPX.

The long term impact of the energy- and temperature dependent scattering method on the fuel inventory has been analyzed in UO<sub>2</sub> (4 wt.% uranium-235) and MOX (5 wt.% fissile plutonium) pin cell burnup calculations for typical LWR lattices. For both fuel types an increased build up of plutonium is observed. This results from the increased neutron absorption mainly in uranium-238 because of the new method. More uranium-238 is converted to plutonium-239 and to higher plutonium isotopes. The reactivity decrease at begin of life with the new method is continuously reduced by the increase of fissile material inventory because of the higher conversion. For the UO<sub>2</sub> fuel the decreased reactivity at begin of life changed during burnup to increased reactivity at end of life. Balance was reached at approximately 45 MWd/kg HM burnup.

A "hybrid method" was developed to analyze the importance of individual isotopes for the energy- and temperature dependent scattering approach. For this purpose the asymptotic scattering kernel was introduced into the new scattering algorithm. This hybrid method allows the selection of isotope-wise scattering approach in one calculation. The burnup results utilizing the hybrid method again show the importance of uranium-238. The pronounced large resonances at low energies combined with high ratios for elastic scattering to total cross section and the high concentration in the fuel makes uranium-238 to the most important isotope contributing to effects caused by the new scattering approach in pressurized water reactor systems. With exception of oxygen all other isotopes including all plutonium isotopes do not change the neutron flux form significantly with the new formalism. For the deterministic approach in ULFISP oxygen plays an important role. Because of its high concentration in the UO<sub>2</sub> fuel and the absence of up scattering in the standard ULFISP scattering method, the application of potential scattering of oxygen leads to significant changes in the neutron flux form. This effect can not be investigated in Monte Carlo

approaches because there the up-scattering resulting from the potential scattering cross section is already taken into account.

To investigate the impact of the energy- and temperature dependent scattering method on a complete reactor core, part of an OECD/NEA - UO<sub>2</sub>/MOX - PWR reactor core benchmark was analyzed. For that purpose assembly burnup calculations have been performed for UO<sub>2</sub> and MOX fuel with different enrichments. The reactivity differences show very similar results compared to the investigated pin cell burnup simulations. Additional calculations utilizing the standard resonance shielding method (narrow resonance method) showed much higher reactivity discrepancies for the assembly burnup calculations than the two fine flux approaches.

The reactor core simulations were performed with the code system PARCS[36]. For this purpose, macroscopic cross sections had to be transformed from the KAPROS to the PARCS formats. This was realized by the new KAPROS module CRPAXS. Reactor core simulation analyses are performed for two core conditions. First a “hot zero power” simulation, at temperature T= 560 K for the complete core. Comparison with results from the OECD/NEA benchmark participants showed very good agreement. The reactivity differences between the different approaches in ULFISP are insignificant mainly because of the low fuel temperatures and because of the actual burnup values of the considered equilibrium core. As shown in chapter 3.3 compensating effects result in small over-all effects caused by the new scattering treatment because of changing fuel inventory during burnup. The effects of the energy- and temperature dependent scattering formalism are more important for safety related analysis, e.g. for the negative fuel Doppler reactivity coefficient which is increased by 7 % by the energy- and temperature dependent scattering method compared to the standard ULFISP scattering approach.

For a “hot full power” reactor core simulation a strongly simplified model is applied. Although an error estimation is provided, the results are very preliminary. The cross section transfer module CRPAXS is not yet capable to perform this task. Nevertheless this outlook shows the temperature dependence of the new scattering approach for PWR reactor core simulations. The negative Doppler coefficient is increased to 9% by the new approach at temperature T= 900 K which stresses the importance of the energy- and temperature dependent scattering method to safety analysis for PWR's.

# References

- [1] Abramowitz M.A., Stegun I.A.: *Handbook of Mathematical Functions*, Dover Publications, Inc., New York, 1965
- [2] Akimushkin S., Avvakumov A., Malofeev V., Roslyakov A.: *Validation of a Pin-by-pin Heterogeneous Method Against LWR MOX Benchmarks*, Proc. Of the International Conference on the New Frontiers of Nuclear Technology: Reactor Physics, Safety and High-performance Computin (PHYSOR 2002), Korea, October 2002
- [3] Askew J.R., Fayers F.J., Kemsell P.B.: *A General Description of the Lattice Code WIMS*, Journal of British Nuclear Energy Society, 5, 564 (1966)
- [4] Bachmann H., Buckel G., Hoebel W., Kleinheins S.: *The Modular System KAPROS for efficient Management of Complex Reactor Calculations*, Proc. Conf. Computational Methods in Nuclear Energy, Charleston, Conf-750413, 1975
- [5] Becker B., Dagan R., Broeders C.H.M., Lohnert G.: *On the Impact of the Resonance Dependent Scattering Kernel on Criticality, Doppler Reactivity Coefficient and Fuel Inventory*, Jahrestagung Kerntechnik 2008, Hamburg
- [6] Becker B., et al.: *Impact of the Resonance Scattering Kernel on HTR Calculations*, International Youth Nuclear Conference, 2008, Interlaken
- [7] Becker B., et al.: *Improvement of the Resonance Scattering Treatment in MCNP in View of HTR Calculations*, PHYSOR, 2008, Interlaken
- [8] Becker M., Broeders C.H.M.: *CRGIP – A modul to convert macroscopic cross sections from the GRUBA format in KAPROS/KARBUS to the GIP format used in the programs DORT/TORT and TDTORT*, FZK/IRS internal report, 2007
- [9] Bell G.I., Glasstone S.: *Nuclear Reactor Theory*, Van Nostrand Reinhold Company, 1970
- [10] Bell G.I.: *A Simple Treatment for Effective Resonance Absorption Cross Sections in Dense Lattices*, Nuclear Science and Engineering, Vol. 5, 138-139, 1959
- [11] Bell, M.J.: *ORIGEN – The ORNL Isotope Generation and Depletion Code*, ORNL.4628 UC-32, 1973
- [12] Blackshaw G.L., Murray R.L.: *Scattering functions for Low-Energy Neutron Collisions in a Maxwellian Monatomic Gas*, Nuclear Science and Engineering 27, 520, 1967

- [13] Bonalumi R.: *Neutron first collision probabilities in reactor physics*, Energia Nucleare, 8, 326, 1961
- [14] Bouland O., Kolesov V., Rowlands J.L.: *The Effect of Approximations in the Energy Distributions of Scattered Neutron on thermal Reactor Doppler Effects*. Proc. Int. Conf. on Nuclear Data for Science and Technology, Gatlinburg, USA, 1994, 1006-1008 (1994)
- [15] Broeders C.H.M., personal message
- [16] Broeders C.H.M.: *Entwicklungsarbeiten für die neutronenphysikalische Auslegung von fortschrittlichen Druckwasserreaktoren (FDWR) mit kompakten Dreiecksgittern in hexagonalen Brennelementen*, KFK 5072, 1992
- [17] Brown F., *Monte Carlo Advances and Challenges*, The 2005 Frédéric Joliot/Otto Hahn Summer School, Karlsruhe, August 2005
- [18] Brown H.D., John St., *Neutron Energy Spectrum in D<sub>2</sub>O*, ORNL report DP33, 1954
- [19] Carlvik I.: *Dancoff Correction in Square- and Hexagonal Lattices*, AE-257, 1966
- [20] Case K.M., de Hoffmann F., Placzek G.: *Introduction to the Theory of Neutron Diffusion, Vol. 1*, Los Alamos Scientific Library, 1953
- [21] *CENTRM: A One-Dimensional Neutron Transport Code for Computing Point wise Energy Spectra*, ORNL/TM-2005/39, Version 5.1, Vol. II, Book 4, Sect. F18, November 2006
- [22] Chao Y.A., Martinez A.S.: *On approximations to the Neutron Escape Probability from an Absorbing Body*, Nuclear Science and Engineering 66, 254-258, 1978
- [23] Courcelle A., Rowlands J.: *Approximate Model of Neutron Resonant Scattering in a Crystal*, International Conference on Nuclear Data for Science and Technology 2007, Nice, France
- [24] Cross Section Evaluation Group, *ENDF/B-VI Summary Documentation*, Report BNL-NCS-17541 (1991), edited by P.F.Rose, National Nuclear Data Center, Brookhaven National Laboratory, Upton, NY, USA
- [25] Cross Section Evaluation Working Group, NNDC Brookhaven National Laboratory: *ENDF-102 Data Formats and Procedures for the Evaluated Nuclear Data File ENDF-6*, Upton, N.Y. 11973-5000, April 2001
- [26] Dagan .R., Rothenstein W.: *The Contribution of Up scattering by Heavy Nuclides to the Doppler Effect*, Proceedings of the ICENES meeting - International Conference on Emerging Nuclear Energy Systems, Herzlia, Israel, June, 1998
- [27] Dagan R.: *Accurate Doppler Effect Calculations for Thermal Nuclear Power Reactors*, Research Thesis. Technion 1997 (partly translated version from Hebrew)

- [28] Dagan R.: *On the use of  $S(\alpha,\beta)$  tables for nuclides with well pronounced resonances*, Annals of Nuclear Energy, V. 32, 4, March 2005, p. 367-377
- [29] Dagan R., Rowlands J., Courcelle A., Lubitz C.R.: *On the treatment of neutron scattering in the resonance range*, International Conference on Nuclear Data for Science and Technology 2007, DOI: 10.1051
- [30] Dagan R.: *A consistent Formalism for the Neutron Scattering Source Term of the Boltzmann Transport Equation*, Habilitationsschrift, Universität Stuttgart, 2008
- [31] Dancoff S.M., Ginsburg M.: *Surface Resonance Absorption in a Closed Packed Lattice*, CP-2157, 1944
- [32] DeKruijf W.J.M., Jansen A.J.: *On the definition of the fuel temperature coefficient of reactivity for pin-cell calculations on an infinite lattice*, Annals of Nuclear Energy, V. 20, I. 9, p. 639-648, 1993
- [33] *DANTSYS 3.0: One-, Two- and Three-Dimensional, Multigroup, Discrete-Ordinates Transport Code System*, Los Alamos National Laboratory, Los Alamos, New Mexico
- [34] DeHart M.D., Pevey E., Parish T.A.: *An Extended Step Characteristic Method for Solving the Transport Equation in General Geometries*, Nuclear Science and Engineering, 118, 79-90, 1994
- [35] *DOORS 3.2: One-, Two- and Three Dimensional Discrete Ordinates Neutron/Photon Transport Code System*, Oak Ridge National Laboratory, Oak Ridge, Tennessee
- [36] Downar T., Lee D., Xu Y., Kozlowski T.: *PARCS v2.7 U.S. NRC Core Neutronics Simulator – User Manual*, Purdue University, School of Nuclear Engineering, 2006
- [37] Duderstadt J.J., Hamilton L.J.: *Nuclear Reactor Analysis*, Jon Wiley & Sons, 1976
- [38] Dunn M.E., Greene N.M.: *AMPX-2000: A Cross- Sections processing System for Generating Nuclear Data for Criticality Safety Applications*, Trans. Am. Nucl. Soc. 86, 118-119 (2002)
- [39] Eisenhart, L.D., et. al.: *CORETRAN-01: A Three-dimensional Program for Reactor Physics and Thermo-hydraulic Analysis*, EPRI Report WO-3574, Rev.3., November 2000
- [40] Emmendorfer D., Hoecker K.H.: *Theorie der Kernreaktoren Teil I/III*, B.I. Hochschultaschenbücher 412/412a, 1969
- [41] Fischer U., Wiese H.W.: *Verbesserte konsistente Berechnungen des nuklearen Inventars abgebrannter DWR-Brennstoffe auf der Basis von Zell-Abbrand\_Verfahren mit KORIGEN*, KFK3014, 1983
- [42] Goldstein R., Cohen E.R.: *Theory of Resonance Absorption of Neutrons*, Nuclear Science and Engineering, 13, 132-140. 1962

- [43] *HELIOS, 1.9 Methods*, Studsvik Scandpower, December 2005
- [44] Henry A.F.: *Nuclear-Reactor Analysis*, The MIT Press, 1975
- [45] Ivanov K.: *Coupled Thermo-hydraulics and Neutronics Simulations*, The Frédéric Joliot/Otto Hahn Summer School, Cadarache, France, 2006
- [46] Joo H.G., Cho J.Y., Kim Y.: *Dynamic Implementation of the Equivalence Theory in the Heterogeneous Whole Core Transport Calculation*, PHYSOR 2002, Seoul, Korea, 7-10 October 2002
- [47] Koning A.J., Bersillon O., Forrest R.A., Jacqmin R., Kellett M.A., Nouri A., and Rullhusen P.: *Status of the JEFF Nuclear Data Library*, Proceedings of the International Conference on Nuclear Data for Science and Technology, Santa Fe, 2004, p.177
- [48] Koning A.J., et al.: *The JEFF evaluated data project*, Proceedings of the International Conference on Nuclear Data for Science and Technology, Nice, 2007
- [49] Kozłowski T., Downar T.J.: *PWR MOX/ $UO_2$  Core Transient Benchmark, Final Report*, Purdue University, ISBN 92-64-02330-5, NEA/NSC/DOC (2006)20
- [50] Kuhnel K., Richter K., Seitz E.: *Einsatz von PANBOX zur Gewinnung einer zusätzlichen DNB-Marge in KKP2*, Framatome ANP, EnBW, Fachtagung Reaktorbetrieb und Kernüberwachung, Rossendorf, Germany, Februar 2003
- [51] Lamb W.E.: *Capture of Neutrons by Atoms in a Crystal*, Physical Review, Vol.55, 229, 1939
- [52] Lee D., Smith K., Rhodes J.: *The impact of U-238 resonance elastic scattering approximations on thermal reactor Doppler reactivity*, PHYSOR, 2008, Interlaken
- [53] Levine M.M.: *Resonance Integral Calculations for U-238 Lattices*, Nuclear Science and Engineering, Vol. 16, 271-279, 1963
- [54] Macfarlane R.E., Muir D.W.: *The NJOY Nuclear Data Processing System Version 91*, LA-12740-M, 1994
- [55] MacFarlane R.E., Weisbin C.R., Paik N.C.: *The Shielding Factor Method for Producing Effective Cross Sections*, RSIC Multigroup Cross Section Seminar, Oak Ridge, Tennessee, 1978
- [56] MacFarlane R.E.: *New Thermal Neutron Scattering Files of ENDF/B-VI, Release2*, LA-12639-MS (ENDF-356), March 2004
- [57] *MCNP4 – A General Monte Carlo N-Particle Transport Code Version 4C*, RSICC Computer Code Collection, ORNL, CCC-701, 2000
- [58] *MCNPX 2.4.0 – Monte Carlo N-Particle Transport Code System for Multiparticle and High Energy Applications*, ORNL, CCC-715, 2002

- [59] Mosteller, R.D.: *ENDF/B-V, ENDF/B-VI and ENDF/B VII.0 Results for the Doppler-defect Benchmark*, M&C+SNA 2007, Monterey, CA
- [60] Nakajima T., et. al.: *Analysis of the PWR MSLB Benchmark Using the Coupled 3-D Neutronics and Thermal-hydraulic Code Sketch-INS/TRAC-P*, NUTHOS-6, Nara, Japan, 4-8 October 2004
- [61] *NITAWL: SCALE System Module for Performing Resonance Shielding and Working Library Production*, ORNL/TM-2005/39, Version 5.1, Vol. II, Book 1, Sect. F2, November 2006
- [62] Nordheim L.W., Kuncir G. : *A Program of Research and Calculations of Resonance Absorption – Final Report*, GA-2527, 1961
- [63] Nordheim L.W.: *A New Calculation of Resonance Integrals*, Nuclear Science and Engineering, 12, 457-463, 1962
- [64] Oberle P., Broeders C.H.M., Dagan R.: *Comparison of PWR – burnup calculations with SCALE5.0/TRITON other burnup codes and experimental results*, PHYSOR 2006, Vancouver Canada
- [65] Oberle P., Broeders C.H.M.: *The Influence of calculation methods on burnup*, Jahrestagung Kerntechnik 2007, Karlsruhe, Germany
- [66] Oberle P., Broeders, C.H.M., Dagan R.: *Comparison of PWR – Pin Cell burnup calculations with SCALE5.0/TRITON – KAPROS/KARBUS – MONTEBURNS*, Jahrestagung Kerntechnik 2006, Aachen, Germany
- [67] Oberle P.: *Erstellung einer 78-Gruppenkonstanten Bibliothek mit Energien bis 150 MeV für KAPROS*, Diplom-Arbeit, Forschungszentrum Karlsruhe, Institut für Reaktorsicherheit, 2004
- [68] Oberle P.: *Neutronic Calculations using the Codes TRITON-TRANSFORMER-PARCS*, FZK/IRS internal report, 2008
- [69] Ouisloumen M., Sanchez R.: *A Model for Neutron Scattering Off Heavy Isotopes that Accounts for Thermal Agitation Effects*, Nuclear Science and Engineering, 107, 189-200 (1991)
- [70] *OZMA – A Code to Calculate Resonance Reaction Rates in Reactor Lattices Using Resonance Profile Tabulations*, EPRI NP-926, Project 709-1, Topical Report, 1981
- [71] Porsch D., at al.: *Spezifikationen eines DWR-Brennelementes, UO<sub>2</sub> (4 w/o U-235) 18x18 – 24, für Vergleichsrechnungen*, Framatome ANP GmbH Erlangen, Juli, 2004
- [72] Raghav .H.P.: *Polynomial Expression for the Neutron Escape Probability*, Nuclear Science and Engineering, 78, 91-96, 1980
- [73] *RELAP5-3D, Code Manual*, INEEL-EXT-00834-V1, Revision 2.3, Idaho National Laboratory, April 2005

- [74] Riik B., Rühle R.: *RESAB II, ein Programm zur Berechnung von Gruppenkonstanten im Resonanzbereich nach der Stosswahrscheinlichkeitsmethode*, IKE, University Stuttgart, Nr. 3.3-6.1209, 1972
- [75] Rhoades W.A., Childs R.L.: *The DORT Two-dimensional Discrete Ordinates Transport Code*, Nuclear Science and Engineering, 99, 1, pp. 88-89, (May 1988)
- [76] Rhodes J., Smith K., Lee D.: *CASMO-5 Development and Applications*, PHYSOR 2006, Vancouver, Canada
- [77] Rothenstein W., Barhen J., Taviv E.: *The Hammer Code System*, EPRI NP-565 Project 709, 1978
- [78] Rothenstein W.: *Proof of the formula for the ideal gas scattering kernel for nuclides with strongly energy dependent scattering cross sections*, Annuals of Nuclear Energy 31 (2004), 9-23
- [79] Rothenstein W., Dagan R.: *Ideal Gas Scattering Kernel for Energy Dependent Cross Sections*, Annuals of Nuclear Energy 25 (1998), p.209
- [80] Sauer A.: *Approximate Escape Probabilities*, Nuclear Science and Engineering, Vol. 16, 329-335, 1963
- [81] *SCALE: A Modular Code System for Performing Standardized Computer Analyses for Licensing Evaluation*, ORNL/TM-2005/39, Version 5.1, Vols. I-III, November 2006
- [82] Shamaoun A.I., Summerfield G.C.: *Chemical Binding Effects On Resonant Scattering of Neutrons*, Annuals of nuclear Energy, Vol. 17, No. 5, pp 229-237, 1990
- [83] Stacey W.M., *Nuclear Reactor Physics*, Georgia Institute of Technology, John Wiley & Sons, Inc., New York, 2001
- [84] Stamm'ler R.J.J., Abbate M.J.: *Methods of Steady-State Reactor Physics in Nuclear Design*, Academic Press, London, 1983
- [85] Tellier H., Coste M., Raepsaet C., Van der Gucht C.: *Heavy Nucleus Resonant Absorption Calculation Benchmarks*, Nuclear Science and Engineering, 113, 20-30, 1993
- [86] *TRACE V5.0 – Users Manual*, U.S. Nuclear Regulatory Commission, 2007
- [87] *TRITON: A Two-Dimensional Transport and Depletion Module for Characterization of Spent Nuclear Fuel*, ORNL/TM-2005/39, Version 5.1, Vol. I, Book 3, Sect. T1, November 2006
- [88] Trkov A., Mattes M.: *On the Thermal Scattering Law Data for Reactor Lattice Calculations*, Nuclear Energy for New Europe 2004, International Conference, Portoroz, Slovenia

- [89] Wigner E.P., et al.: *Resonance Absorption of Neutrons by Spheres*, Journal of Applied Physics, 26,260-270, 1955
- [90] Wigner E.P., Wilkins E.J., *Effect of the Temperature of the Moderator on the Velocity Distribution of Neutrons with Numerical Calculations for H as Moderator*, AECD-2275, Oak Ridge National Laboratory, 1944
- [91] Williams M.L., Gilai D.: *Incorporation of Clad Effects into Sauer's Method for Computing Dancoff Factors*, Annals of Nuclear Energy, Vol. 12, No 1, p. 1, 1965
- [92] Williams M.M.R.: *The Slowing Down And Thermalization of Neutrons*, North Holland Publishing Company, Amsterdam, 1966
- [93] Word R.E., Trammell G.T.: *Investigation of condensed matter via resonant neutron scattering. Correlation-function formalism with application to the study of the interatomic force density*, Physical Review B, Vol. 24, No 5, September 1981
- [94] Woll D.: *Introduction to the Use of the UNIX-Version of the Karlsruhe PROGRAM System KAPROS*, FZKA 6280, 2005
- [95] Woll D.: *GRUCAL, ein Programmsystem zur Berechnung makroskopischer Gruppenkonstanten*, KFK 2108, 1975
- [96] Woll D.: *Aufbau der Gruppenkonstantenbibliothek GRUBA und ihre Verwaltung durch das Programmsystem GRUMA*, KFK-3745, 1984
- [97] Xu Y., Downar T.: *GenPMAXS Code for Generating the PARCS Cross Section Interface File PMAXS*, Purdue University, School of Engineering, 2006
- [98] Yoo J.W., Jae Man Noh, Hyung Kook Joo: *Development of MOX Fuelled Core Analysis Code Based on the Refined Analytic Function Expansion Nodal Method*, Proceedings of Korean Nuclear Society Autumn Meeting, Yongpyong, Korea, October 2004

Institut für Kernenergetik und  
Energiesysteme

Universität Stuttgart

Pfaffenwaldring 31

D-70550 Stuttgart

